Path Diversity Schemes in OFDM Transmitter and Receiver

March 2012

NISHIMURA, Haruki

Path Diversity Schemes in OFDM Transmitter and Receiver

March 2012

A thesis submitted in partial fulfilment of the requirements for the degree of Doctor of Philosophy in Engineering

Keio University

Graduate School of Science and Technology
School of Integrated Design Engineering

NISHIMURA, Haruki

Contents

List of Figures

List of Tables

Acronyms

1G first generation

1xEV-DO 1x Evolution Data Only

2G second generation

3G third generation

3GPP third generation partnership project

ADC analogue-to-digital converter

AWGN additive white Gaussian noise

B3G beyond the third generation

BER bit error rate

BPSK binary phase shift keying

CCK complementary code keying

CE channel estimation

CDD cyclic delay diversity

CDMA code division multiple access

CP cyclic prefix

CSI channel state information

DD delay diversity

DFT discrete Fourier transform

DL down link

DS direct spread

DSP digital signal processor

FCC federal communications commission

FDM frequency division multiplexing

FEC forward error correction

FS fractional sampling

FIR finite impulse response

GFSK Gaussian filtered frequency shift keying

GI guard interval

GSM global system for mobile communications

HSPA high speed packet access

ICI intercarrier interference

IDFT inverse discrete Fourier transform

IEEE institute of electrical and electronics engineers

IFFT inverse fast Fourier transform

IMT international mobile telecommunication

IMT-A IMT-advanced

IPI inter-pulse interference

IR-UWB impulse-radio UWB

ISI intersymbol interference

ITU international telecommunication union

ITU-R ITU-radiocommunication sector

LAN local area network

LDD linear delay diversity

LNA low noise amplifier

LOS line-of-sight

LTE long term evolution

LTSP long training sequence preamble

MAC media access control

MB-OFDM multi-band OFDM

MIMO multiple-input multiple-output

MISO multiple-input single-output

MRC maximal ratio combining

MSE mean square error

NLOS non-line-of-sight

OFCDM orthogonal frequency and code division multiplexing

OFDM orthogonal frequency division multiplexing

OOK on/off keying

PA power amplifier

PAM pulse-amplitude modulation

PAPR peak to average power ratio

PHY physical layer

PPM pulse-position modulation

RAN radio access network

RF radio frequency

SC-FDMA single-carrier frequency-division multiple access

SDR software-defined radio

SIMO single-input multiple-output

SISO single-input single-output

SNR signal to noise ratio

SPS sampling point selection

SRS sampling rate selection

SS spread spectrum

STBC space time block code

STC space time code

STTC space time trellis code

TDD time division duplex

TDMA time division multiple access

UL uplink

UWB ultra wide band

W-CDMA wideband-CDMA

WLAN wireless local area network

WiMAX worldwide interoperability for microwave access

WG work group

WPAN wireless personal network

List of Notations

A_{max}	maximal permissible amplitude
$\alpha_l,\ \alpha_l(t)$	impulse response of lth path
$\boldsymbol{\alpha}$	multipath coefficient vector
b_n	nth information sequence
c_{k_c}	k_cth spreading code
$c(t),\ c(t,\ \tau)$	impulse response of physical channel
C_o	outage capacity
C_G	coefficient for oversampling ratio G
$\mathbf{C}_H$	channel correlation
d	delay sample
Δ	length of delay line
Δf	subcarrier space
$\delta(\cdot)$	delta function
Δ_g	normalized gth sampling point
Δ_t	cyclic delay at tth antenna
f_c	carrier frequency
f_D	maximum Doppler frequency
$\mathfrak{F}[\cdot]$	Fourier transform
ϕ_m	initial phase of mth clutter
g	fractional sampling index
G	oversampling ratio
G_d	diversity gain
G_r	multiplexing gain
$\tilde{G}$	average oversampling ratio
Γ	normalization factor for sampling point
γ_u	index for initial sampling point
γ_n	index for the combination of non-uniform sampling points
γ_{clip}	clipping ratio
$h(t),\ h(t,\ \tau)$	impulse response of channel
$h_g[n]$	sampled of $h(t)$ at $(nT_s + gT_s/G)$
$H(f)$	frequency response of channel
$H_g[k]$	frequency response of $h_g[n]$
$\mathbf{H}$	channel matrix

$\mathbf{I}$	identity matrix
j	imaginary unit
k_c	chip index
l	path index
L	number of multipaths
L_l	number of clutter of lth path
M_R	number of receive antenna
M_T	number of transmit antenna
n	time index
N_c	the length of the chip
N	number of subcarriers
N_{GI}	length of guard interval
N_{PRE}	number of preamble symbols in one packet
N_{SYM}	number of data symbols in one packet
$\nu_c,\ \nu_p$	power normalization factor
$p(t)$	impulse response of baseband filter
$p_2(t)$	pulse shaping filter
$P_2(f)$	power spectrum of $p_2(t)$
P_b	bit error probability
$P_G[k]$	power of received signal on kth subcarrier
θ_m	angle of arrival of the mth clutter
$r_{k_c}[n]$	received signal at k_cth chip of nth symbol duration
$\mathbf{R}[k]$	path correlation matrix of noise on kth subcarrier
$R_x(t)$	autocorrelation function of transmit signal
ρ	signal-to-noise ratio
$\mathbf{R}_w[k]$	covariance matrix of noise on kth subcarrier
$S[k]$	transmitted symbol on the kth subcarrier
$\mathbf{S}_p[k]$	precoded information symbol vector
σ_v^2	noise variance
t	antenna index
T_{SYM}	OFDM symbol duration
T_s	symbols duration equivalent to $\frac{T_{\mathrm{SYM}}}{N}$
τ_l	delay of lth path
$\mathrm{T}_1,\ \mathrm{T}_2$	LTSP period
$v(t)$	narrow band AWGN
$V(f)$	frequency response of $v(t)$
$v_g[n]$	sampled of $v(t)$ at $(nT_s + gT_s/G)$
$V_g[k]$	frequency response of $v_g[n]$

$w_{k_c}[n]$	noise sample at k_cth chip
W	bandwidth
$\mathbf{W}[k]$	weighting vector
$\mathbf{W}$	weighting matrix
$x(t)$	transmit signal
$\tilde{x}(t)$	clipped signal
$x[n]$	nth sample of $x(t)$
$x_{k_c}[n]$	transmit signal at k_cth chip of nth symbol duration
$x_k[n]$	kth fundamental subchannel signal
$x_p^m[n]$precoded transmit signal at mth antenna	
$X(f)$	transmit signal in frequency domain
$y(t)$	received signal
$y_g[n]$	sampled of $y(t)$ at $(nT_s + gT_s/G)$
$y_d[n]$ decision variable at nth symbol	
$Y(f)$	received signal in frequency domain
$Y_g[k]$	frequency response of $y_g[n]$
$\|\cdot\|$	absolute value
$\{\cdot\}^*$	complex conjugate
$\star$	convolution operator
$\approx$	approximately equal to
$\{\cdot\}^H$	Hermitian transpose matrix
$\{\cdot\}^H$	transpose matrix
$\{\cdot\}^\dagger$	pseudo inverse matrix
diag[·]	diagonalization operation
tr $\{\cdot\}$	trace operation
vec $(\cdot)$	vec-operator
$\otimes$	Kronecker product

Abstract

Orthogonal frequency division multiplexing (OFDM) is a very attractive modulation technique for reliable broadband wireless communications such as wireless local area network (WLAN), worldwide interoperability for microwave access (WiMAX), etc. In wireless communications, multipath fading distorts a received signal and causes bit errors at a receiver side. To overcome the effect of fading, diversity techniques have been proposed to improve the quality of the communication link. A fractional sampling (FS) scheme in OFDM has been proposed to achieve diversity with a single antenna. In the FS scheme, a received baseband signal is sampled with a rate higher than baud rate and combined to achieve path diversity on each subcarrier. Though the FS achieves diversity, it increases the power consumption of the receiver. In some channel conditions, the power of the received signal may be large enough to demodulate the information symbols with baud rate sampling. In this dissertation, the digital signal processing schemes for path diversity and the low power consumption of the receiver are proposed and investigated.

Chapter 1 introduces the background of the OFDM receivers and the motivation of the research.

In Chapter 2, path diversity schemes in receiver are investigated. In the first subchapter, a sampling rate selection scheme is proposed. The sampling rate is selected according to channel conditions. The path diversity can be achieved while the power consumption is still saved with the proposed sampling rate selection scheme. In the second subchapter, sampling point selection scheme is investigated to achieve higher power efficiency. It is necessary to improve the quality of the communication link with the same sampling rate to save the power consumption. This scheme selects the sampling points according to the frequency response of a channel. It also eliminates the specific sets of the sampling points and reduces the computational complexity for the sampling point selection.

Chapter 3 proposes precoded transmit path diversity schemes. The FS scheme still necessitates high oversampling ratio at a receiver and it causes large power consumption in a small mobile terminal. The proposed schemes make use of the impulse response

of the channel with the resolution of the FS interval and can achieve path diversity without oversampling the received signal. This chapter also introduces the procoding scheme on time invariant channels. The proposed scheme has designed the precoding matrix in order to minimize the mean square error (MSE) of received symbols. It can achieve intercarrier interference (ICI) suppression and path diversity without any additional signal processing at the receiver.

Chapter 4 summarizes the results of each chapter and concludes this dissertation.

Chapter 1

Introduction

Future wireless systems are expected to provide high data rates in the order of more than 1 Gbps. As well as ever-growing demand for high quality multimedia, human centric system, where human is connected wirelessly with any devices, is expected to require high speed, high reliability and real-time communication anytime anywhere.

In order to realize such a high data rate, antenna diversity has been implemented which provides diversity gain without increasing the transmission power and bandwidth [1]. There is a fundamental tradeoff between the multiplexing gain and the diversity gain [2]. In multiple-input multiple-output (MIMO)-OFDM systems, space-time code (STC), cyclic delay diversity (CDD), etc. have been proposed to improve the communication reliability. The space-time block code (STBC) utilizes the orthogonality property of the code to achieve full diversity. The space-time trellis code (STTC) uses trellis coding to provide full diversity. The CDD sends the same signal with cyclic delay at each transmit antenna to make a flat fading channel into a frequency selective channel to achieve frequency diversity. However, the STC can not achieve full-rate diversity transmission with the number of transmitters more than 2. The CDD also necessitates requires additional antennas at the transmitter. At the receiver side, it is hard to implement multiple antennas in a small terminal.

A FS scheme in OFDM has been proposed to achieve diversity with a single antenna. In the FS scheme, a received baseband signal is sampled with a rate higher than the baud rate and combined to achieve path diversity on each subcarrier. With FS, high data rate communication will be possible without increasing the number of antennas at the small terminal. In this thesis, path diversity schemes in receiver and transmitter have been introduced to improve the communication reliability with simple receiver/transmitter architectures.

In this chapter, wireless standards related to this thesis are introduced. Following the interdiction of the wireless standards, an OFDM modulation scheme is explained, which

is used in many wireless communication systems to achieve high data rate transmission. The motivation of the research is then presented.

1.1. Wireless Standards

1.1.1. Cellular Network

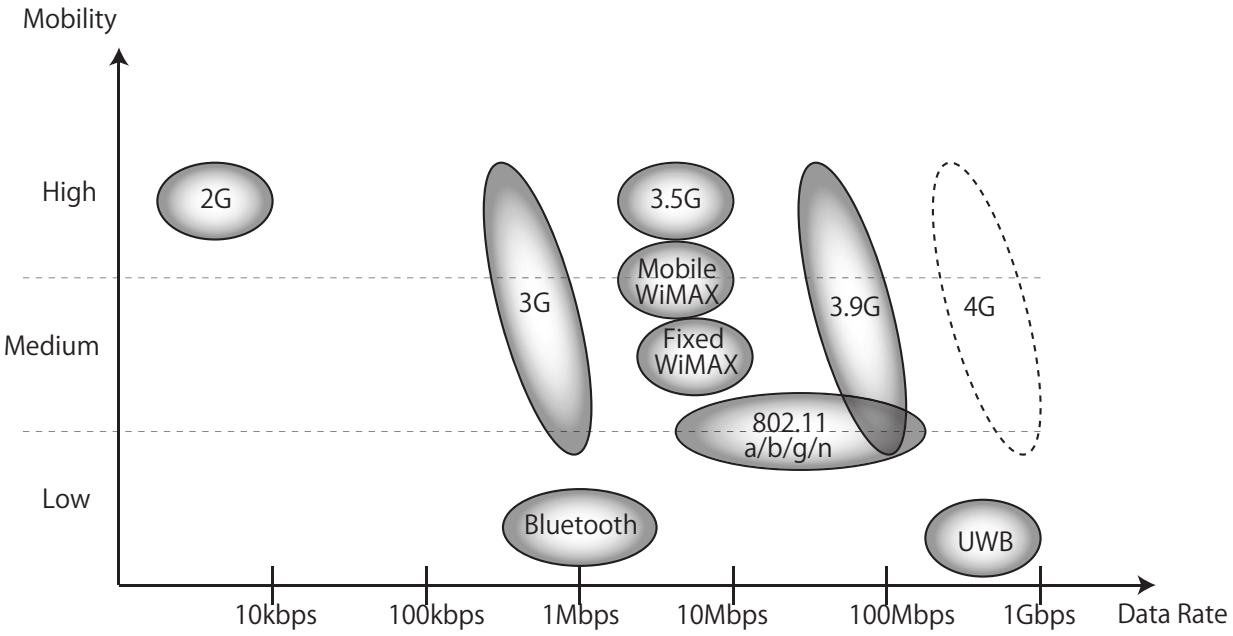

Figure 1.1: Wireless standards.

Table 1.1: Digital cellular communication systems.

Generation	2G	3G	3.5G	3.9G	4G
Name	GSM	IMT-2000		LTE	IMT-A
Frequency	900MHz	2GHz	2GHz	2GHz	3.4-3.6GHz
Rate	20kbps	2Mbps	14Mbps	100Mbps	1Gbps
Modulation	TDMA	W-CDMA	HSPA	DL:OFDM UL:SC-FDMA	OFDM, OFCDM

With the expansion of the wireless voice subscribers, the Internet users, and the portable computing devices, various wireless standards have been developed for realizing an anywhere/anytime access network as shown in Fig. 1.1. The specifications of the cellular systems are shown in Table 1.1. A mobile communication service started as auto mobile telephone service since the end of the 1970's. In the middle of 1980's,

cellular services have started because the size of the terminal reduces and it had become portable. This was the first generation (1G) cellular system and an analog modulation scheme was employed.

Since 1990's, a digital modulation scheme has been introduced as the second generation (2G) system. The most successful standard in the 2G has been the global system for mobile communications (GSM). The 2G was based on time division multiple access (TDMA). The GSM-based cellular mobile networks has been widely spread all over the world [3, 4].

International mobile telecommunications-2000 (IMT-2000), or the third generation (3G) system, has started with the demand of the Internet applications for the use of multimedia contents (eg. photo, movie, music, text and etc.) as well as voice communications. The modulation scheme of the 3G is code division multiple access (CDMA). Since 2001, NTT DoCoMo Corp. has launched the 3G service based on wideband-CDMA (W-CDMA). On the other hand, KDDI Corp. has started the service with CDMA2000 since 2002 [3]. Because many multimedia applications are packet-oriented, it is essential to optimize the 3G system effectively for variable bit rate and packet based transmission. These systems aim to support the wide range of services varying from low rate voice transmission to high rate video transmission of up to at least 144kbps in vehicular, 384kbps in outdoor-to-indoor, 2Mbps in indoor and picocell environments [5, 6].

With the demand for anytime-anywhere broadband wireless access, the 3.5th generation (3.5G) was introduced. KDDI Corp. has provided 1x evolution data only (1xEV-DO) since 2003. NTT DoCoMo Corp. and Softbank Corp. have provided the high speed downlink packet access (HSDPA) since 2006. 1xEV-DO and HSDPA have been developed from CDMA2000 and W-CDMA, respectively [3].

With the ever-growing demands for higher data rates, the technical requirements on the emerging "beyond 3G (B3G)" air-interface have been evolved. The first release of the long term evolution (LTE) standards was targeted to be completed in the third generation partnership project radio access network (3GPP RAN) by early 2009, and the commercial deployment was expected to start as early as 2009. During the initial roll-out of the LTE networks, it was anticipated that LTE would be deployed as an overlay of the operators' existing 2G/3G mobile networks. This is because currently there is no dedicated frequency spectrum allocated for the LTE use, and the operators would gradually migrate from the 2G/3G to the LTE on the same spectrum, in order to enhance the broadband data capacity of their networks while maintaining sufficient services on their networks. In the downlink (DL), OFDM is used due to its high spectral efficiency. In the uplink (UL), single-carrier frequency-division multiple access

(SC-FDMA) is employed because of its low peak to average power ratio (PAPR) characteristics and user orthogonality in frequency domain. The LTE supports the data rate up to 300Mbps in DL and up to 75Mbps in UL [7–9].

In September 2009 the 3GPP Partners made a formal submission to the international telecommunication union (ITU) and LTE Release 10 & beyond (LTE-Advanced) has been evaluated as a candidate for IMT-advanced (IMT-A). To support low to high user mobility and provide the communication links for high quality multimedia applications, the ITU - radiocommunication standardization sector (ITU-R) has set the IMT-A. The IMT-A system supports low to high mobility applications and a wide range of data rates in accordance with user and service demands in multiple user environments. The IMT-A also has capabilities for high-quality multimedia applications by providing significant improvement in the latency and the quality of the communication link. It is predicted that potential new radio interface(s) will need to support the data rates of up to approximately 100 Mbps for high mobility such as mobile access and up to approximately 1 Gbps for low mobility such as nomadic/local wireless access [10, 11].

1.1.2. WLAN

WLANs are being studied as a alternatives to the high installation and maintenance costs incurred by modifications of the network experienced in wired local area network (LAN) infrastructures [12]. WLANs have been standardized in the institute of electrical and electronics engineers (IEEE) 802.11 group such as IEEE 802.11a, 802.11b and 802.11g for the data rates of up to 54 Mbps, as shown in Table 1.2 [13, 14]. In the IEEE 802.11a/g system, OFDM is used as a modulation scheme.

In 2002 discussions began in the IEEE 802.11 working group (WG) to extend the data rates of the physical layer (PHY) beyond those of IEEE 802.11a/g in order to replace higher throughput wired applications that would benefit from the flexibility of wireless connectivity. Subsequently the IEEE 802.11n task group (TGn) began to develop an amendment to the IEEE 802.11 standard (i.e., IEEE 802.11n). Two basic concepts are employed in 802.11n to increase the PHY data rates: MIMO and 40 MHz bandwidth channels.

According to [15, 16], 40 MHz bandwidth channel operation is optional in the standard due to concerns regarding interoperability between 20 and 40 MHz bandwidth devices, the permissibility of the use of 40 MHz bandwidth channels in the various regulatory domains, and spectral efficiency. With the PHY data rate of 600 Mbps, a media access control (MAC) throughput of over 400 Mbps is now achievable with 802.11n MAC enhancements.

Table 1.2: WLAN Protocols

Protocol	IEEE 802.11a	IEEE 802.11g	IEEE 802.11b	IEEE802.11n
Frequency	5.2GHz	2.4GHz	2.4GHz	2.4GHz / 5GHz
Rate	54 Mbps	54 Mbps	11 Mpbs	600Mbps
Modulation	OFDM	OFDM	DS/CCK	OFDM

1.1.3. WPAN

Table 1.3: WPAN Protocols

Protocol	Bluetooth	IR-UWB	MB-OFDM
Frequency	2.4GHz	3.1-10.6GHz	
Rate	up to 3Mbps	up to 480Mps	
Modulation	GFSK	PPM/PAM/OOK/BPSK	OFDM

To realize seamless communications between mobile personal terminals and electronic devices in a short range (less than 10m), wireless personal area network (WPAN) has been developed. For example, file transfer between a video camera and a desktop PC, and real time services (e.g. between video server and personal terminal) can be realized without connecting any wired cable.

Bluetooth has been adopted as the first technology for WPAN. The standard is designed for low power consumption, low cost applications, and low data rate. The data rate is limited to 3Mbps and the modulation scheme is Gaussian frequency shift keying (GFSK) [17].

IEEE 802.15.3 has been launched to provide higher data rate for WPAN using an ultra-wide bandwidth (UWB) technology. The requirement of the data rates is 55, 80, 110, 160, 200, 320 and 480Mbps. The support of 55, 110 and 200Mbps is mandatory. The modulation technique in 802.15.3a was discussed between the two candidates, the impulse-radio UWB (IR-UWB) or the multiband-OFDM (MB-OFDM). However, IEEE 802.15.3a task group has dissolved in 2006 because it could not select one of them [18,19].

1.2. Multipath Fading

In a typical mobile radio propagation environment, received signals travel through many different paths and they experience reflection, diffraction, scattering, etc. due to obstacles surrounding a receiver [20]. The standing wave then occurs and the mobile terminal passes through it. The amplitude of the received signal is weakened or

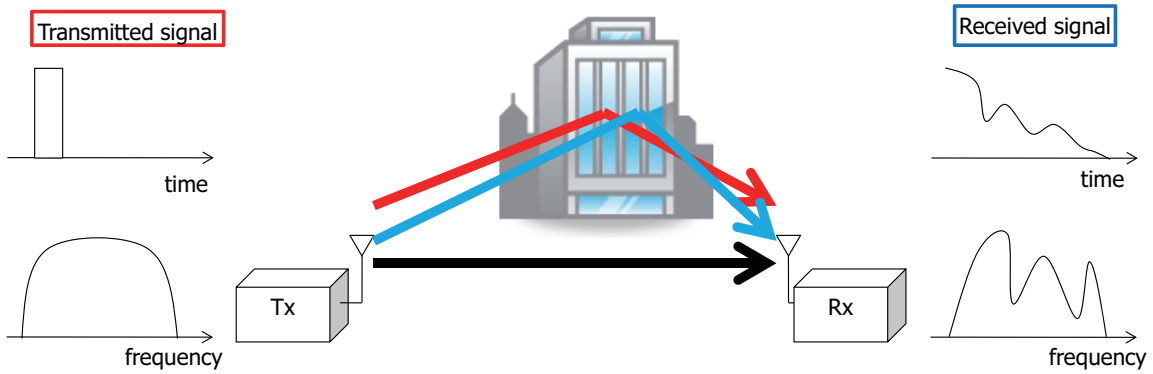

Figure 1.2: Multipath Fading.

strengthened according to the position of the terminal. This is called multipath fading, which is the cause of inter-symbol interference (ISI) and signal waveform distortion. Rayleigh fading is a statistical model of the fading channel and is recognized as the worst case model. It assumes that the power of a signal that has passed through such a transmission medium (also called a communication channel) will vary randomly, or fade, subject to Rayleigh distribution. Along with the evolution of the wireless standards, the transmission rate increases. This results in the shorter symbol duration and the larger amount of the distortion caused by the ISI appears more significantly. Therefore, direct sequence spread spectrum modulation (DS/SS) schemes and OFDM have been investigated because of their robustness to multipath fading.

1.2.1. Anti-multipath Schemes

1.2.1.1. Direct Sequence Spread Spectrum

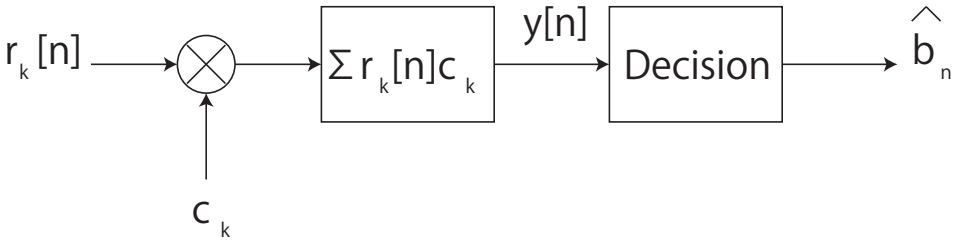

Figure 1.3: Basic spread spectrum correlation receiver.

In DS/SS systems, an nth information sequence, b_n is transformed to a transmit signal, which is given as

$$x_{k_c}[n] = b_n c_{k_c}, \ (k_c = 0, ..., N_c - 1) \tag{1.1}$$

where $\{c_{k_c}\}_{k_c=0}^{k_c=N_c-1} = \pm 1$ is the spreading code and N_c is the length of the chip. The spread-spectrum property arises from the fact that the spreading sequence, $\{c_{k_c}\}$, are known as binary source. The sequence of chips is called a spreading sequence. Now, we assume that the spreading sequence $\{c_{k_c}\}$ has the period of N_c, i.e.,

$$\frac{1}{N_c}\sum_{k_c=0}^{N_c-1} c_{k_c}c_{k_c+mN_c} = 1 \quad \text{for any } m. \tag{1.2}$$

The spreading sequence has the following two key properties:

1. Approximately zero mean value
2. Discrete-time periodic autocorrelation function

These two properties are idealy given by

$$\frac{1}{N_c}\sum_{k_c=0}^{N_c-1} c_{k_c} \approx 0 \tag{1.3}$$

$$\frac{1}{N_c}\sum_{k_c=0}^{N_c-1} c_{k_c}c_{k_c+k_c'} \approx \begin{cases} 1 & \left(k_c'=0\right) \\ 0 & \left(0<\left|k_c'\right|<N_c\right) \end{cases}. \tag{1.4}$$

The received signal of the nth data sequence on an additive white Gaussian noise (AWGN) channel is expressed as

$$\begin{aligned} r_{k_c}[n] &= x_{k_c}[n] + w_{k_c} \\ &= b_n c_{k_c} + w_{k_c} \end{aligned} \tag{1.5}$$

where w_{k_c} is the noise sample. The correlation receiver for the spread-spectrum signal is given in the block-diagram in Fig. 1.3. The receiver processes the following operation to obtain the decision variable, $y[n]$:

$$\begin{aligned} y_d[n] &= \sum_{k=0}^{N_c-1} r_{k_c}[n]c_{k_c} \\ &= \sum_{k=0}^{N_c-1} (b_n c_{k_c} + w_{k_c})c_{k_c}. \end{aligned} \tag{1.6}$$

Using Eq. (1.4), Eq. (1.6) becomes

$$\begin{aligned} y_d[n] &= \sum_{k_c=0}^{N_c-1} b_n c_{k_c}c_{k_c} + \sum_{k_c=0}^{N_c-1} w_{k_c}c_{k_c} \\ &= N_c b_n + \sum_{k_c=0}^{N_c-1} w_{k_c}c_{k_c}. \end{aligned} \tag{1.7}$$

The above mentioned signal recovery process requires that the receiver's own copy of the spreading sequence should be synchronized with the received version because of the second property of the spreading code described in Eq. (1.4).

Assume that the multipath channel consists of a direct path with the impulse response of α_0 and a d samples delayed path with the impulse response of α_1. The received signal $r_{k_c}[n]$ is expressed as

$$r_{k_c}[n] = \begin{cases} \alpha_0 b_n c_{k_c} + \alpha_1 b_{n-1} c_{N_c-d+k_c} + w_{k_c} & (0 \leqslant k < d) \\ \alpha_0 b_n c_{k_c} + \alpha_1 b_{n-1} c_{k_c-d} + w_{k_c} & (d \leqslant k_c < N_c) \end{cases}, \tag{1.8}$$

Then, the decision variable is obtained by

$$\begin{aligned} y_d[n] &= N_c\alpha_0 b_n + \alpha_1 b_{n-1} \sum_{k_c=0}^{d-1} c_{N_c-d+k_c} c_{k_c} + \alpha_1 b_n \sum_{k_c=d}^{N_c-1} c_{k_c-d} c_{k_c} + \sum_{k_c=0}^{N_c-1} w_{k_c} c_{k_c} \\ &\approx N_c\alpha_0 b_n + 0 + 0 + \sum_{k_c=0}^{N_c-1} w_{k_c} c_{k_c}. \end{aligned} \tag{1.9}$$

Therefore, the despreading operation resolves the multipaths and mitigates the ISI [21].

1.2.1.2. OFDM Modulation

OFDM has been adopted in many broadband wireless standards such as IEEE 802.11a/g/n, IEEE 802.16a, or ISDB-T. This is due to its robustness against multipath fading and its efficiency of spectrum usage.

OFDM began from a frequency-division multiplexing (FDM). FDM became the main multiplexing mechanism for telephone carrier systems. With the introduction of digital telephony, FDM carrier systems with individual subchannels for voice signals began, in the 1970s. However FDM, had drawbacks:

1. The waste of scarce wireless frequency spectrum in guard spaces
2. The large complexity of a multiplicity of separate modulators for the different subchannels

The first problem is illusrated in Fig. 1.4. In FDM systems, data streams are allocated to each subchannel. The guard band between the subchannels degrades spectrum efficiency. This problem was alleviated by the concept of OFDM as an FDM system with subchannel signals having overlapping but non-interfering frequency spectra as shown in Fig. 1.5. Harmonic sinusoids are used as an obvious choice, since they are orthogonal on a period T_{SYM} of the fundamental (lowest) subchannel signal. In an OFDM signal, the kth fundamental subchannel signal, $x_k(t)$, is

$$x_k(t) = S[k] \exp(j2\pi k \Delta f t), \tag{1.10}$$

$$\Delta f = \frac{1}{T_{\mathrm{SYM}}}, \tag{1.11}$$

These complex signals $\{x_k(t)\}$ are mutually orthogonal despite overlapping spectra. N, the number of subchannels, is arbitrary and varies among applications. An OFDM

signal block, on the interval T_{SYM}, can be defined as the sum of these subchannel signals, and, ideally, one block immediately follows another. In the absence of channel distortion, there is neither inter-subchannel nor intersymbol interference. It is easy to show in [22] that an N-point inverse DFT (IDFT) operating on the (possibly complex) data block $\{S[k]\}$,

$$x[n] = \sum_{k=0}^{N-1} S[k] \exp\left(j2\pi kn/N\right), \tag{1.12}$$

generates samples, at time intervals $\frac{T_{\mathrm{SYM}}}{N}$, of the OFDM signal that is the sum of the subchannel signals defined in Eq. (1.11). Operating on the received signal with the discrete Fourier transform (DFT), like Eq. (1.12) but with a negative exponent, recovers the data.

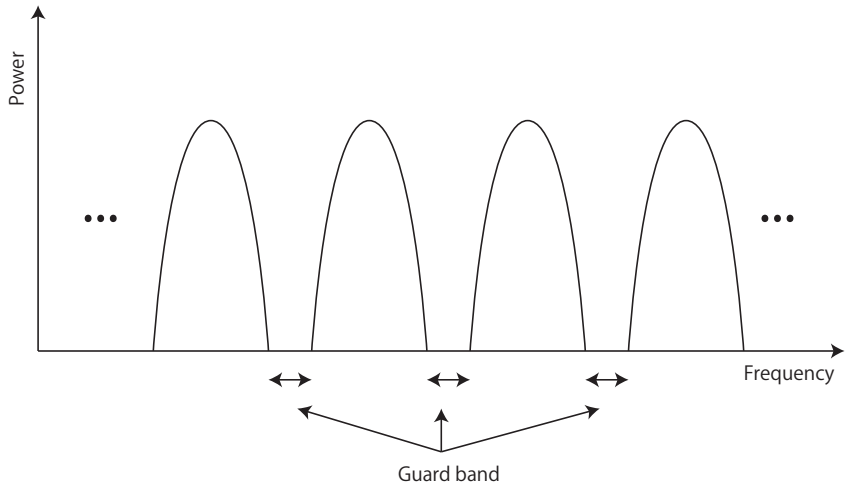

Figure 1.4: Power spectrum of FDM.

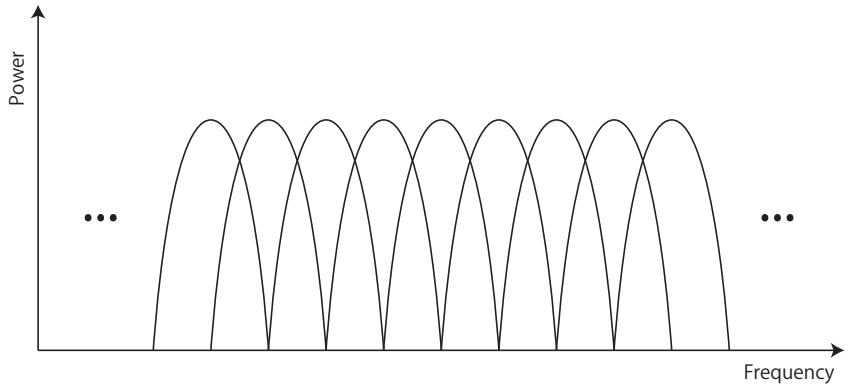

Figure 1.5: Power spectrum of OFDM.

In the modulation process of transmitted digital data, information is converted to

the phase or the amplitude of a radio-frequency carrier. In the modulation of multiple carriers such as OFDM, different information symbols are transmitted simultaneously and synchronously in different frequency subcarriers. The symbol rate on each of the subcarriers is selected to be equal to the frequency separation of adjacent subcarriers. Consequently, the subcarriers are orthogonal over the symbol duration, and independent of the relative phase relationship between any two subcarriers. An N-point IDFT operating on the (possibly complex) data block generates OFDM signal [22].

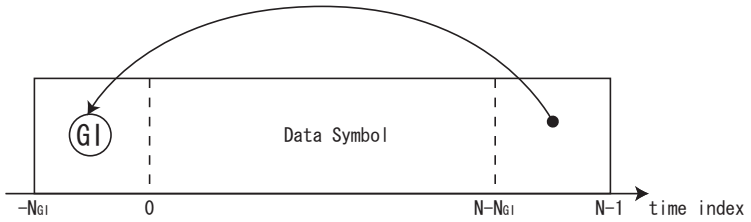

Figure 1.6: Cyclic Prefix.

The operation of cyclic prefix (CP) is a mean of avoiding ISI and preserving orthogonality between subcarriers. It copies the last N_{GI} samples of the body of the OFDM symbol and append them as a preamble to form the complete OFDM symbol as shown in Fig. 1.6 [23, 24]. The effective length of the OFDM symbol as transmitted is this cyclic prefix plus the body ($N + N_{\mathrm{GI}}$ samples long). The insertion of a cyclic prefix can be shown to result in an equivalent parallel orthogonal channel structure that allows for simple channel estimation and equalization [25]. In spite of the loss of transmission power and bandwidth associated with the cyclic prefix, these properties generally motivate its use [23, 24].

1.2.2. Anti-fading Schemes

1.2.2.1. RAKE and Pre-RAKE

RAKE receiver resolves multipaths and combines them to achieve path diversity. The RAKE technique was first published by R. Price and P. E. Green in 1958 [26]. Here, the principle of RAKE reception is explained with a simple detection receiver for simplicity [27]. Assume that the impulse response of the channel is expressed as

$$h(t) = \sum_{l=0}^{L-1} \alpha_l \delta(t - \tau_l) H(f) = \sum_{l=0}^{L-1} \alpha_l \exp(-j2\pi f \tau_l) \tag{1.13}$$

where α_l and τ_l are complex impulse response and delay of the lth path, respectively. The lowpass-equivalent impulse response of the transversal filter with a length of a

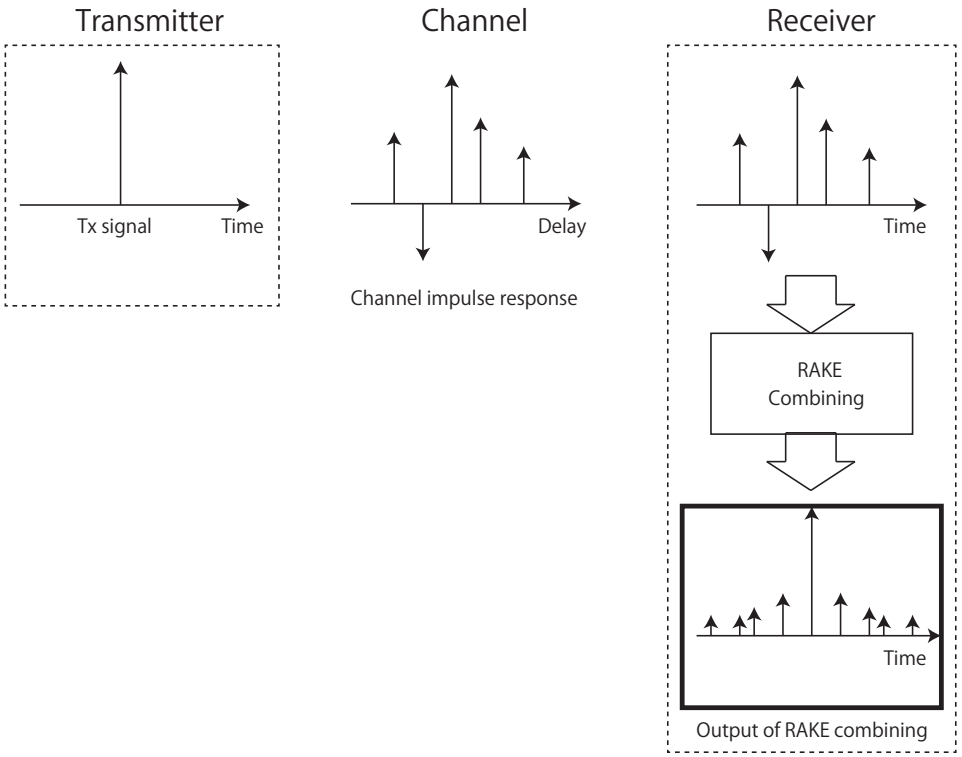

(a) RAKE combining.

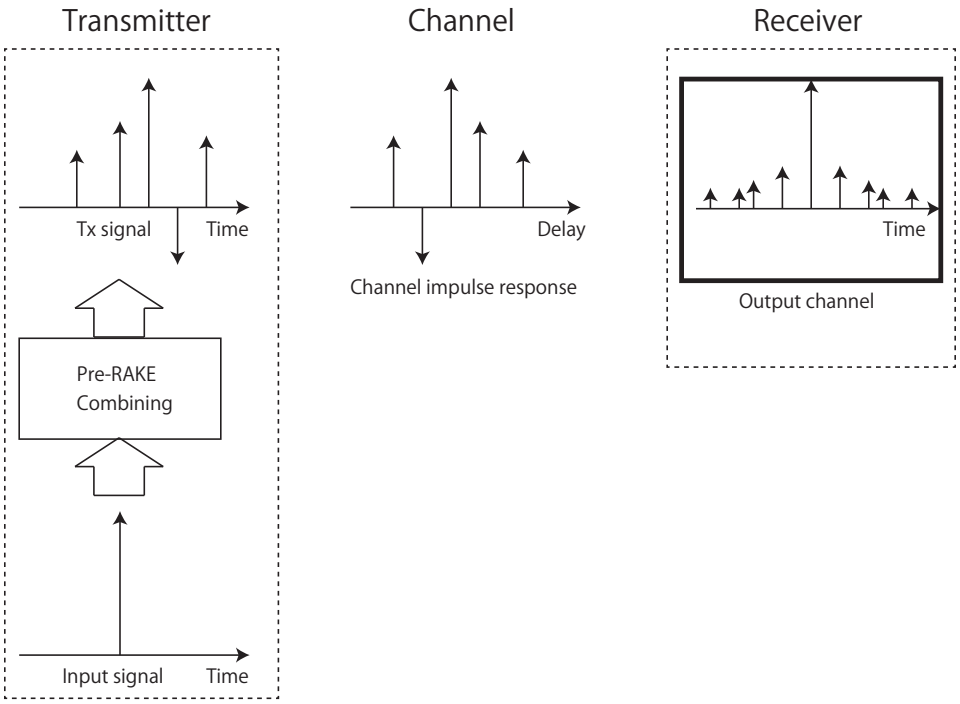

(b) Pre-RAKE combining.

Figure 1.7: RAKE & Pre-RAKE.

delay line, Δ, is

$$h(t) = \sum_{l=0}^{L-1} \alpha_l^* \delta(\Delta - t - \tau_l) \tag{1.14}$$

where $\{\cdot\}^*$ is complex conjugate. Its frequency response is

$$H(f) = \sum_{l=0}^{L-1} \alpha_l^* \exp(-j2\pi f(\Delta - \tau_l)). \tag{1.15}$$

Therefore, the output of the RAKE receiver has the following frequency response

$$\begin{aligned} Y(f) &= |X(f)|^2 H(f)H^*(f) \\ &= |X(f)|^2 \sum_{l=0}^{L-1}\sum_{m=0}^{L-1} \alpha_l \alpha_m^* \exp(-j2\pi f(\tau_l - \tau_m)) \exp(-j2\pi f(T+\Delta)) \end{aligned} \tag{1.16}$$

where $|\cdot|$ and T are absolute value and a time shift to obtain $\exp(-j2\pi f(T+\Delta)) = 1$, respectively. Then Eq. (1.16) becomes

$$Y(f) = |X(f)|^2 \sum_{l=0}^{L-1}\sum_{m=0}^{L-1} \alpha_l \alpha_m^* \exp(-j2\pi f(\tau_l - \tau_m)). \tag{1.17}$$

The output in time domain is

$$\mathfrak{F}[Y(f)] = \sum_{l=0}^{L-1}\sum_{m=0}^{L-1} \alpha_l \alpha_m^* R_x(t) \tag{1.18}$$

where $R_x(t)$ is

$$\begin{aligned} R_x(t) &= \mathfrak{F}[|X(f)|^2] \\ &= \int_0^T x^*(\tau)x(\tau - t)d\tau. \end{aligned}$$

The resolution of multipath is associated with the autocorrelation of the signal. In the case of a signal having a continuous spectrum whose bandwidth is W as shown in Fig. 1.8, the autocorrelation function has a single peak of width about $\frac{1}{W}$ seconds, centered at the origin, and disappearing toward zero elsewhere. When W is small, the central correlation peak is very wide, and path contributions will appear in the filter outputs for a wide variety of delays. When W is large, the correlation function narrows greatly, so that the RAKE receiver will make use of more echoes which arrive within $\frac{1}{W}$ of synchronization with the references. Thus, it is necessary to make W sufficiently wide to separate multipaths.

As mentioned above, RAKE combining scheme can improve the communication quality. However, the RAKE receiver necessitates some extra signal processing for setting the weighing factors and the combining functions. It causes more complexity and larger power consumption in the receiver. In mobile communications, it is desirable to reduce the power consumption, size and cost of a mobile terminal in DL. Pre-RAKE has been proposed to shift the signal processing burden from the receiver to a transmitter

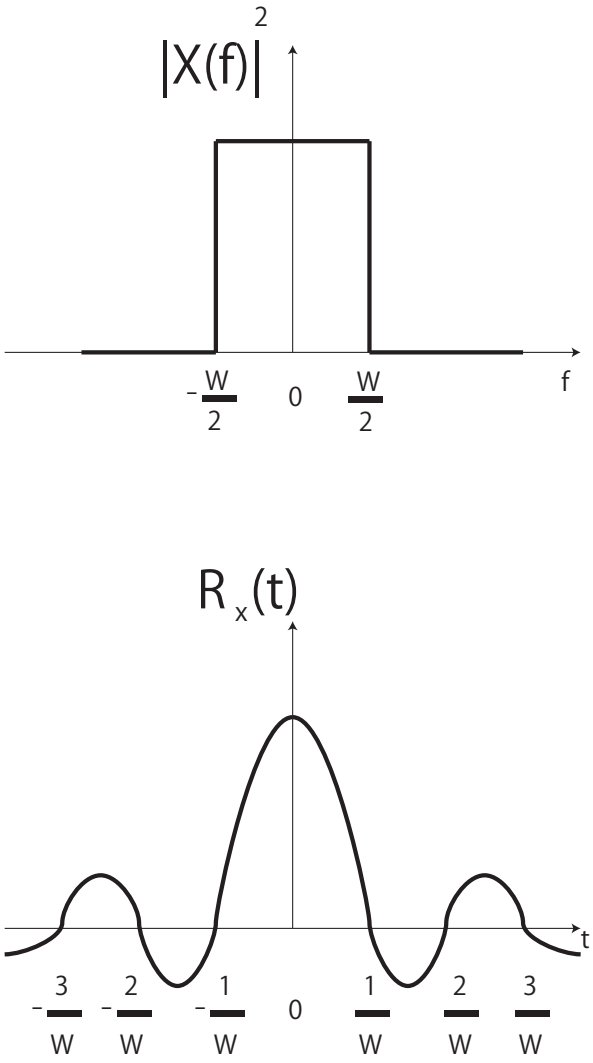

Figure 1.8: Relationship between the resollution of multipath and autocorrelation of the signal.

[28, 29]. In Pre-RAKE systems, the transversal filter in Eq. (1.14) is not used in the receiver. Instead, it is used for generating a transmit signal by convolution with an information signal as follow:

$$\begin{aligned} x_p(t) &= \sum_{l=0}^{L-1} \int x_s(\tau)\alpha_l^* \delta(t-(\Delta-\tau_l)-\tau)d\tau \\ &= \sum_{l=0}^{L-1} \alpha_l^* x_s(t-(\Delta-\tau_l)-\tau) \end{aligned} \tag{1.19}$$

where $x_s(t)$ is the information signal after DS/SS. In order to generate the Pre-RAKE transmit signal, channel state information (CSI) must be known at the transmitter. The estimation of the CSI is possible with preamble signals on uplink in the time division duplex (TDD) system.

1.2.2.2. Antenna Diversity and MIMO

The initial form of antenna system for improving the performance of wireless communication systems was antenna diversity; it reduces the amount of fluctuation in the received signal amplitude due to fading. Antenna diversity has been implemented in the base stations of the most of wireless communications for many years.

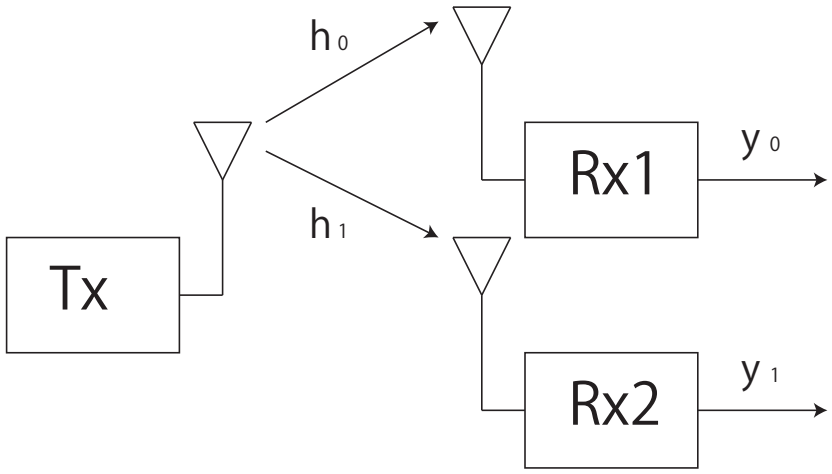

Figure 1.9: Antenna diversity in receiver.

The primary goal of the single-input multiple-output (SIMO) system is to reduce amplitude fluctuation due to fading. It makes use of the signals received by two or more antennas that are uncorrelated. Figure 1.9 shows an example of antenna diversity in the receiver. If one antenna is experiencing a faded signal, it is likely that the other antenna will not. Thus at least one good signal can be received. Typical methods for producing uncorrelated antenna signals are space, polarization, or pattern diversity. Three common processing techniques are used for diversity: switch diversity, equal gain, and maximum ratio combining (MRC). In switch diversity, the idea is to select the antenna with the best signal (usually the signal strength is taken as a measure of signal quality, but other measures can be used such as bit error rate, or signal quality). Equal gain combining seeks to improve on this by co-phasing the signals and adding them together. MRC is the optimum method in the presence of noise and weighting (and co-phasing) the signals before combining by their SNRs [30,31].

With the increasing demands for higher data rate, a MIMO system has been introduced as the key technology to improve spectral efficiency. The capacity of multi-antenna fading channels applying antenna arrays at both ends was first published by Winters in 1987 [1]. However, the theoretical background was later developed by Foschini and Gans [32,33], and Telatar [34]. If M_T transmit antennas and M_R receive antennas MIMO system is assumed, achievable multiplexing gain, G_r, and diversity

gain, G_d, are expressed as follows:

$$G_r \leqslant \min\{M_T M_R\} \tag{1.20}$$

$$G_d \leqslant M_T M_R \tag{1.21}$$

and they have the following relationship

$$G_d \leqslant (M_T - G_r)(M_R - G_r) \tag{1.22}$$

Hence there is a fundamental tradeoff between G_r and G_d [2]. An outage capacity in MIMO systems is given by

$$C_o = \log_2 \det\left(\mathbf{I} + \frac{\rho}{M_T}\mathbf{H}\mathbf{H}^H\right) \tag{1.23}$$

where ρ is signal-to-noise ratio (SNR) at each receive antenna. Therefore, it is required that the number of antennas at a transmitter and a receiver should be increased to enhance the reliability of communications [32].

1.2.2.3. Space-Time Coding

The use of multiple antennas is an important mean to improve the performance of wireless systems. It is widely understood that in MIMO systems, the spectral efficiency is much higher than that of the conventional single-input single-output (SISO) systems. Traditionally, multiple antennas have been used to increase diversity gain to alleviate the effect of channel fading.

Each pair of transmit and receive antennas provides a different signal path from the transmitter to the receiver. By sending signals that carry the same information through the different paths, multiple independently faded replicas of the data symbol can be obtained at the receive end. It is well known that maximum diversity gain can be achieved if fading is independent across antenna pairs [35]. More recent work has concentrated on using multiple transmit antennas to get diversity such as STC, which is categorized into STBC [36] and STTC [37, 38].

The STBC operates on a block of input symbols producing a matrix output whose columns represent time and rows represent antennas. Unlike traditional single antenna block codes for the AWGN channel, the most STBCs do not provide coding gain. Its key feature is the provision of full diversity with extremely low encode/decoder complexity. The STTC encodes the input symbol stream into an output vector symbol stream. Unlike the STBC, the STTC maps one input symbol at a time to an $M_t \times 1$ vector output. Since the encoder has memory, these vector codewords are correlated in time. Decoding is performed via maximum likelihood sequence estimation. The STTC provides coding gain and this is the key advantage over the STBC. The disadvantage

of the STTC is that it is extremely difficult to design and it requires a computationally intensive encoder and decoder [39].

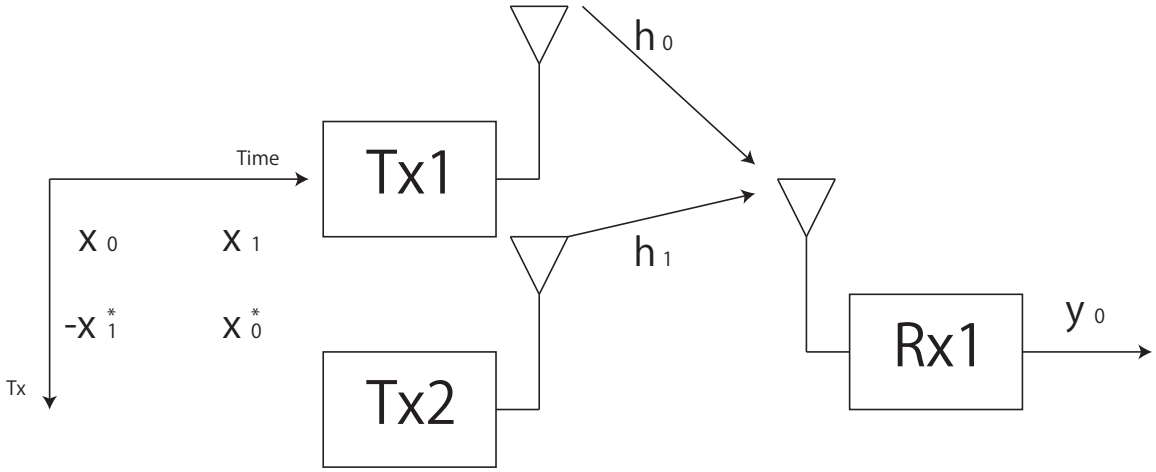

Figure 1.10: Antenna diversity in transmitter using STBC.

An effective and simple transmit diversity was introduced by S. M. Alamouti in 1998 [36]. Figure 1.9 shows the baseband representation of the two branch transmit diversity scheme. The scheme uses two transmit antennas and one receive antenna. At a given symbol period, two signals are simultaneously transmitted from the two antennas. The signal transmitted from antenna zero is denoted by x_0 and from antenna one by x_1. During the next symbol period signal $-x_1^*$ is transmitted from antenna zero, and signal x_0^* is transmitted from antenna one where $\{\cdot\}^*$ is the complex conjugate operation. Assuming that fading is constant across two consecutive symbols, the channel from the 0th and 1st transmitted antennas can be given as $\alpha_0,\ \alpha_1$, respectively. The received signals is expressed as

$$\begin{aligned} y_0 &= \alpha_0 x_0 + \alpha_1 x_1 + n_0 \\ y_1 &= -\alpha_0 x_1^* + \alpha_1 x_0^* + n_1 \end{aligned} \tag{1.24}$$

where y_0 and y_1 are the received signals at the 0th and 1st time slots and n_0 and n_1 are AWGN. The combiner builds the following MRC:

$$\begin{aligned} \tilde{x}_0 &= \alpha_0^* y_0 + \alpha_1 y_1^* \\ \tilde{x}_1 &= \alpha_1^* y_0 - \alpha_0 y_1^* \end{aligned} \tag{1.25}$$

The outputs of the combiner, $\tilde{x}_0,\ \tilde{x}_1$, are obtained by substituting Eq. (1.24) into Eq.

(1.25) as follows:

$$\begin{aligned}\tilde{x}_0 &= \alpha_0^*(\alpha_0 x_0 + \alpha_1 x_1 + n_0) + \alpha_1(-\alpha_0 x_1^* + \alpha_1 x_0^* + n_1)^* \\ &= (|\alpha_0|^2 + |\alpha_1|^2)x_0 + h_0^* n_0 + h_1 n_1^* \qquad (1.26)\\ \tilde{x}_1 &= \alpha_1^*(\alpha_0 x_0 + \alpha_1 x_1 + n_0) - \alpha_0(-\alpha_0 x_1^* + \alpha_1 x_0^* + n_1)^* \\ &= (|\alpha_0|^2 + |\alpha_1|^2)x_1 - h_0 n_1^* + h_1^* n_0. \qquad (1.27)\end{aligned}$$

It can achieve transmit diversity with full-rate data transmission when the number of transmit antennas is 2.

1.2.2.4. Cyclic Delay Diversity

The STBC and STTC can provide full spatial diversity for multiple-input single-output (MISO) systems. The STBC utilizes the orthogonal property of the code to achieve full diversity; however, it cannot realize full-rate transmission when the number of the transmit antennas is greater than two [40]. The STTC uses trellis coding to provide full diversity; but the decoding complexity increases exponentially with the number of the transmit antennas [37]. Moreover, both the STBC and the STTC lack scalability with the number of transmit antennas. As the number of the transmit antennas is changed, different space-time codes are needed. The STBC and the STTC were originally introduced for quasi-static flat fading channels. To apply these space-time codes to frequency selective fading channels, they must be used in conjunction with other techniques such as equalization or OFDM [41].

MIMO-OFDM arrangements have been suggested for frequency selective fading channels, where either the STBC or the STTC is used across the different antennas in conjunction with OFDM. Such approaches can provide very good performance on frequency-selective fading channels. However, the complexity can be very high, especially for MIMO systems having a large number of transmit antennas [41]. Furthermore, the STTC is not suitable for extending existing systems, because this would require non-standards compliant modifications to be made. Therefore, for standardized systems only additional spatial diversity techniques can be implemented to keep the system compatibility to the standard. Another approach uses delay diversity (DD) together with OFDM for flat-fading channels [41]. In linear delay diversity (LDD) systems, spatial diversity is obtained by sending the delayed versions of the same OFDM-modulated signal over different antennas. A similar effect can be obtained by CDD systems, where cyclic delays are used in place of linear delays. The use of cyclic delays is a very effective strategy that, differently from LDD, allows adding diversity without the need for a longer cyclic prefix [42].

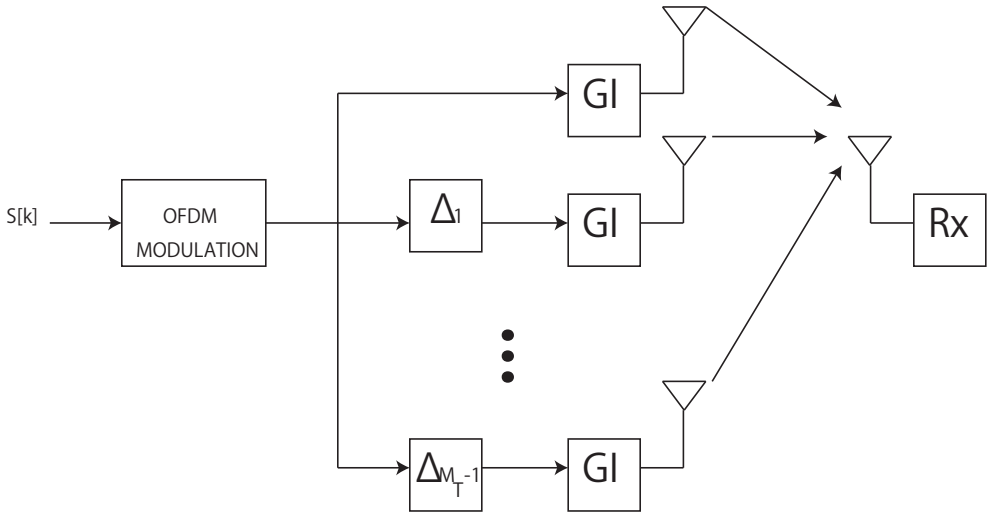

Figure 1.11: CDD in OFDM system.

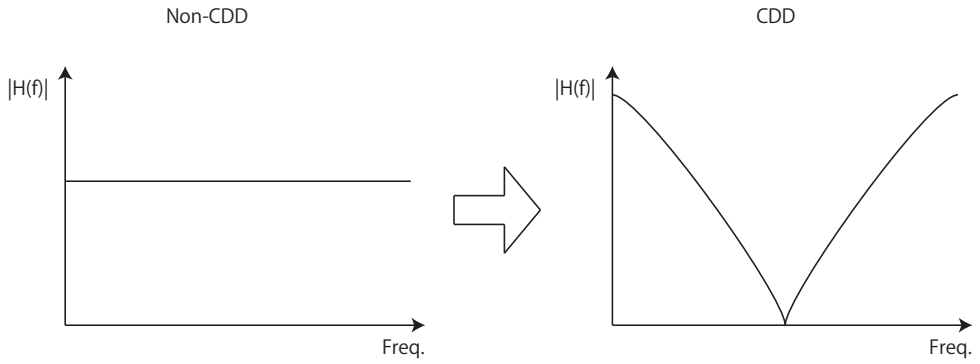

Figure 1.12: Transformation of frequency response of channel by CDD.

The principle of CDD is depicted in Fig. 1.11. The data is assumed to be encoded by a forward error coding (FEC) and interleaved. For simplicity, a flat fading channel is assumed. OFDM signal $x[n]$ is obtained by inverse fast Fourier transform (IFFT) of size N and introduced to each antenna with the cyclic delay of Δ_t, $(t = 1, ..., M_T)$. The transmit signal from the tth antenna, $x_t[n]$, is expressed as

$$x_t[n] = x_{(n-\Delta_t) \ mod \ N}. \tag{1.28}$$

Then, the CDD system is equivalent to the transmission of the sequence, $x_t[n]$, over a frequency selective channel with one transmit antenna. The transformation of the frequency response of the channel is illustrated in Fig. 1.12 [43]. Therefore, CDD can achieve frequency diversity because of low correlation between the subcarriers even on the flat fading channel.

1.2.2.5. Fractional Sampling

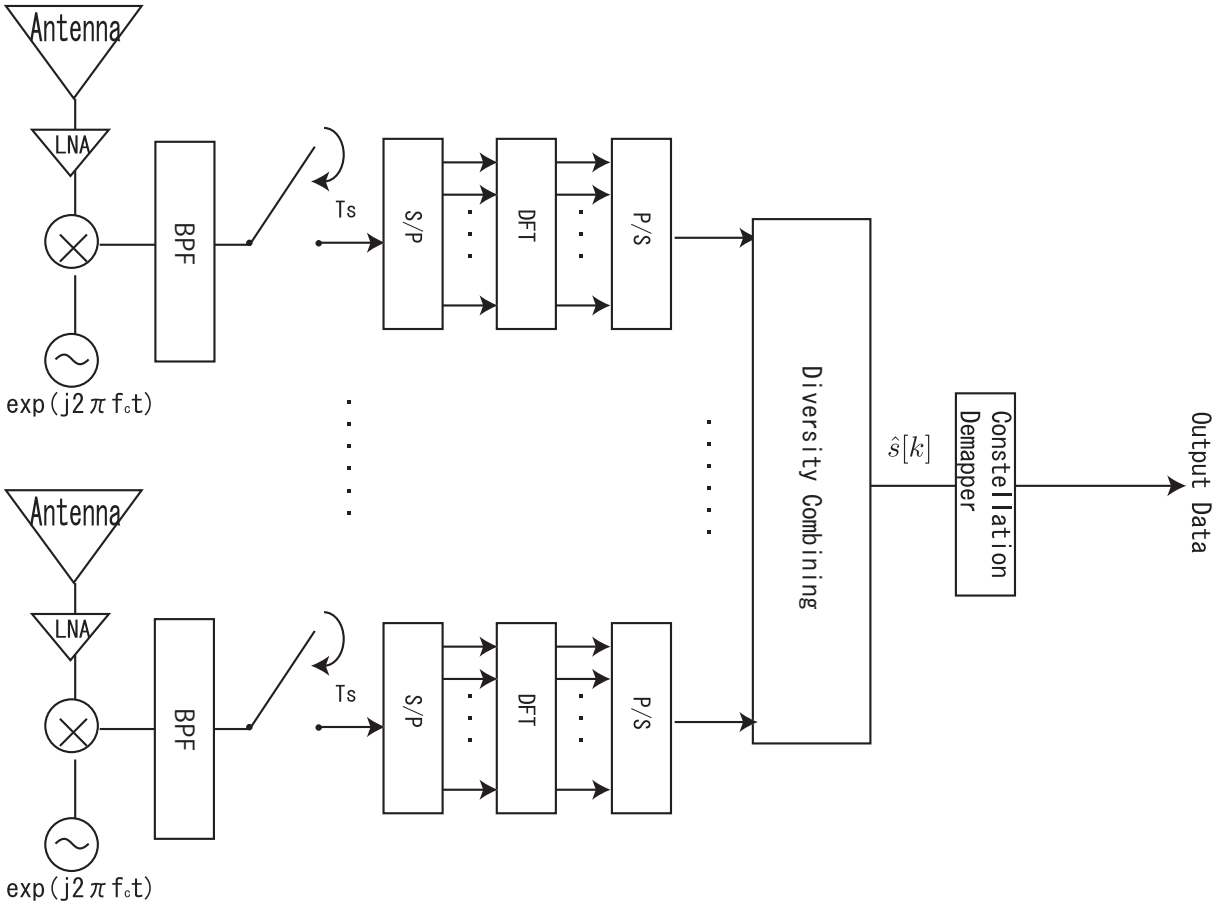

Figure 1.13: Block Diagram of Antenna Diversity.

To overcome the effect of signal fading in a multipath environment, multiple antennas are used at a receiver to achieve antenna diversity. The block diagram of the antenna diversity system is shown in Fig.1.13. A received signal is amplified by low noise amplifier (LNA) and sampled at the rate of $\frac{1}{T_S}$ at each antenna. These samples are demodulated and diversity combined. However, it may be difficult to implement multiple antenna elements in small terminals [44]. Therefore, to achieve diversity with a single antenna, a FS scheme in OFDM has been proposed [45].

FS at the receiver is used to obtain diversity gains over frequency fading channels. FS is known to covert a SISO channel into a SIMO channel. The block diagram of a receiver which uses FS is shown in Fig. 1.14. The received signal is downconverted to baseband and oversampled. The sampled signals are separated to G branches. The guard interval (GI) is removed on each branches. The samples are serial-to-parallel converted and put into a DFT block. The output of the DFT are parallel-to-serial converted. The signals on all G branches are put into the whitening filters as the oversampled noise components are correlated. The outputs of the whitening filter are

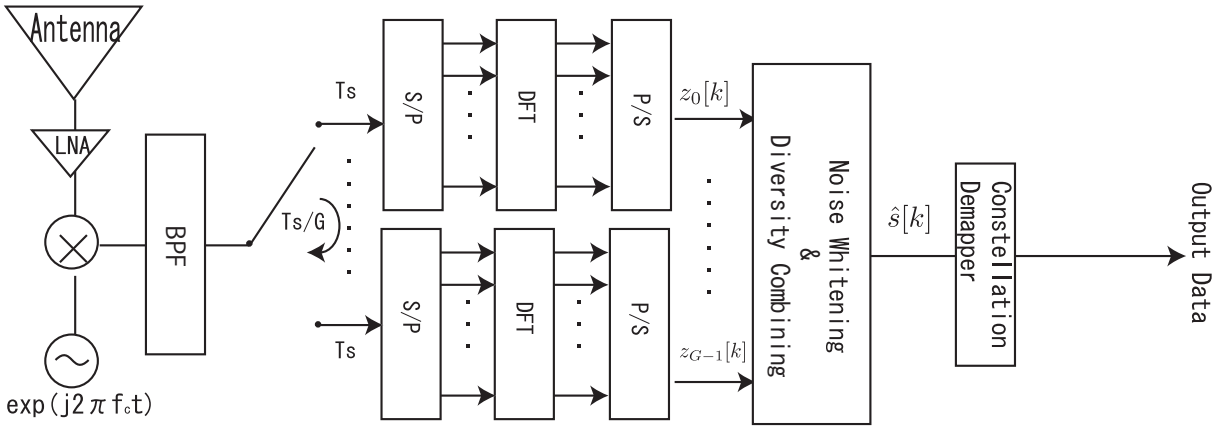

Figure 1.14: Block Diagram of Path Diversity.

then combined together and demodulated.

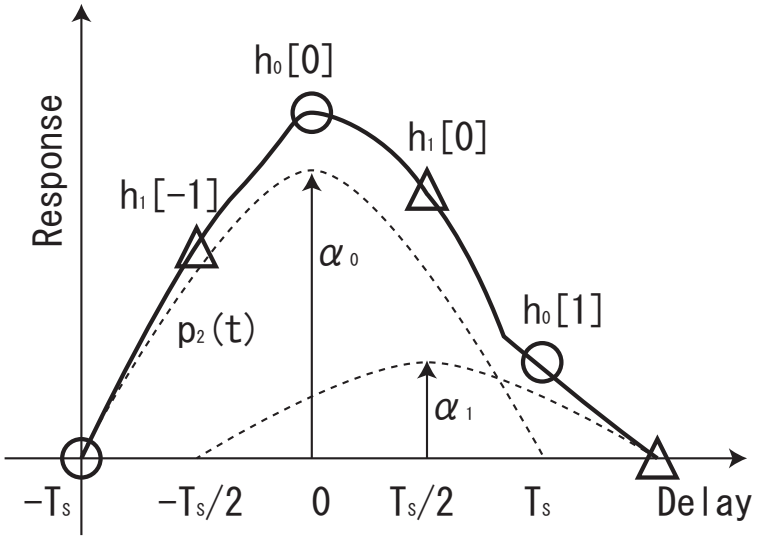

Figure 1.15: Impulse Response of Channel ($G = 2$).

To achieve path diversity through FS, channel correlation between neighboring samples needs to be low. An example of an impulse response of channel is shown in Fig.1.15. The impulse response of channel is expressed as

$$h(t) = \alpha_0 p_2(t) + \alpha_1 p_2\left(t - \frac{T_s}{2}\right) \tag{1.29}$$

where α_0 and α_1 are response of the complex amplitude of the path and T_S is symbol duration. In the figure, pulse shaping filter $p_2(t)$ is assumed to be a truncated sinc pulse of duration $2T_S$ and the oversampling ratio is $G = 2$. ◯ and △ indicate the samples of $h(t)$ at $g = 0$ and $g = 1$, respectively, that is expressed as $h_g[n]$ $(n = -1, 0, 1)$. These responses are converted with the DFT and the frequency responses on the kth

subcarrier, $H_g[k]$, are given by

$$H_0[k] = h_0[0] + h_0[1] \exp\left(-j\frac{2\pi k}{N}\right), \tag{1.30}$$

$$H_1[k] = h_1[-1] \exp\left(-j\frac{2\pi k(-1)}{N}\right) + h_1[0]. \tag{1.31}$$

As the frequency response on the kth subcarriers, $H_0[k]$ and $H_1[k]$, are not equivalent, path diversity can be achieved.

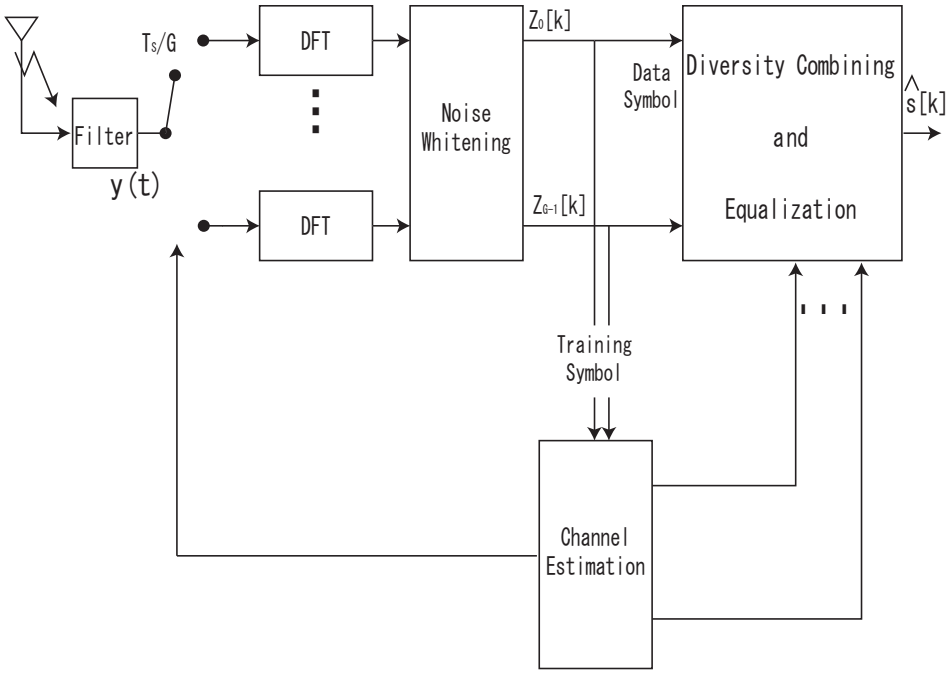

Figure 1.16: OFDM receiver using FS.

The block diagram of an OFDM system with FS is shown in Fig. 1.16 [45]. Suppose the information symbol on the kth subcarrier is $S[k]$ $(k = 0, ..., N-1)$, the OFDM symbol is then given by

$$x[n] = \frac{1}{\sqrt{N}} \sum_{k=0}^{N-1} S[k] e^{j\frac{2\pi nk}{N}} \tag{1.32}$$

where $n(n = 0, 1, ..., N-1)$ is the time index. A GI is appended before transmission. N_{GI} is the length of the GI.

The baseband signal at the output of the filter is given by

$$x(t) = \sum_{n=0}^{N+N_{\mathrm{GI}}-1} x[n] p(t - nT_s)$$

where $p(t)$ is the impulse response of the baseband filter and T_s is the symbol duration. This signal is upconverted and transmitted through a multipath channel with an impulse

response $c(t)$. The received signal after the down conversion is given by

$$y(t) = \sum_{n=0}^{N+N_{\mathrm{GI}}-1} x[n]h(t-nT_s) + v(t) \tag{1.33}$$

where $h(t)$ is the impulse response of the composite channel and is given by $h(t) := p(t) \star c(t) \star p(-t)$ and $v(t)$ is the additive Gaussian noise filtered at the receiver. $:=$ and $\star$ are definition symbol and convolution operator, respectively. For the multipath channel, $h(t)$ can be expressed in a baseband form as

$$h(t) = \sum_{l=0}^{L-1} \alpha_l p_2(t-\tau_l) \tag{1.34}$$

where $p_2(t) := p(t) \star p(-t)$ is the deterministic correlation of $p(t)$ and satisfies Nyquist's property. It is assumed that the channel in Eq. (1.34) has L path components, α_l is the amplitude that is time-invariant during one OFDM symbol (quasistatic channel model), and τ_l is the path delay. If $y(t)$ is sampled at the rate of T_s/G, where G is the oversampling rate, its polyphase components can be expressed as

$$y_g[n] = \sum_{m=0}^{N+N_{\mathrm{GI}}-1} x[m]h_g[n-m] + v_g[n]$$

where $y_g[n]$, $h_g[n]$, and $v_g[n]$ $(g = 0, ..., G-1)$ are polynomials of sampled $y(t)$, $h(t)$, and $v(t)$, respectively, and are expressed as

$$y_g[n] := y\left(nT_s + g\frac{T_s}{G}\right), \tag{1.35}$$

$$h_g[n] := h\left(nT_s + g\frac{T_s}{G}\right), \tag{1.36}$$

$$v_g[n] := v\left(nT_s + g\frac{T_s}{G}\right) \tag{1.37}$$

After removing the GI and taking DFT at each branch, the received symbol is given by

$$\mathbf{Y}[k] = \mathbf{H}[k]S[k] + \mathbf{V}[k] \tag{1.38}$$

where $\mathbf{Y}[k] = [Y_0[k]...Y_{G-1}[k]]^T, \mathbf{H}[k] = [H_0[k]...H_{G-1}[k]]^T$and $\mathbf{V}[k] = [V_0[k]...V_{G-1}[k]]^T$ are $G \times 1$ column vectors, each gth component representing

$$[\mathbf{Y}[k]]_g := Y_g[k] = \sum_{n=0}^{N-1} y_g[n]e^{-j\frac{2\pi kn}{N}}, \tag{1.39}$$

$$[\mathbf{H}[k]]_g := H_g[k] = \sum_{n=0}^{N-1} h_g[n]e^{-j\frac{2\pi kn}{N}}, \tag{1.40}$$

$$[\mathbf{V}[k]]_g := V_g[k] = \sum_{n=0}^{N-1} v_g[n]e^{-j\frac{2\pi kn}{N}}, \tag{1.41}$$

respectively.

When the bandlimited noise, $v(t)$, is sampled at the baud rate of $1/T_s$, the samples of $v(t)$ are independent of one another. However, when the sampling rate increases, the noise samples are correlated and noise-whitening is required to maximize the SNR [46]. The whitening filter equalizes the spectrum of the correlated noise samples [47]. In order to perform noise-whitening, it is necessary to calculate a $G \times G$ noise covariance matrix on the kth subcarrier, $\mathbf{R}_w[k]$. The (g_1, g_2)th element of the noise covariance matrix on the kth subcarrier is given as

$$\begin{aligned} &[\mathbf{R}_w[k]]_{g_1 g_2} \\ &= \sigma_v^2 \frac{1}{N} \sum_{n_1=0}^{N-1} \sum_{n_2=0}^{N-1} p_2((n_2 - n_1)T_s) e^{j\frac{2\pi k(n_2-n_1)}{N}}. \end{aligned} \tag{1.42}$$

and multiplying both sides of Eq. (1.38) by $\mathbf{R}_w^{-\frac{1}{2}}[k]$

$$\mathbf{R}_w^{-\frac{1}{2}}[k]\mathbf{Y}[k] = \mathbf{R}_w^{-\frac{1}{2}}[k](\mathbf{H}[k]\mathbf{S}[k] + \mathbf{V}[k]), \tag{1.43}$$

$$\mathbf{Y}^{'}[k] = \mathbf{H}^{'}[k]S[k] + \mathbf{V}^{'}[k], \tag{1.44}$$

where $\mathbf{Y}^{'}[k] = \mathbf{R}_w^{-\frac{1}{2}}[k]\mathbf{Y}[k]$, $\mathbf{H}^{'}[k] = \mathbf{R}_w^{-\frac{1}{2}}[k]\mathbf{H}[k]$, and $\mathbf{V}^{'}[k] = \mathbf{R}_w^{-\frac{1}{2}}[k]\mathbf{V}[k]$. Based on the frequency responses of the subcarriers estimated with the preamble symbols, those samples are combined to maximize the SNR expressed as the following equation [45],

$$\begin{aligned} \hat{S}[k] &= \frac{\mathbf{H}^{'H}[k]\mathbf{Y}^{'}[k]}{\mathbf{H}^{'H}[k]\mathbf{H}^{'}[k]} \\ &= \frac{(\mathbf{R}_w^{-\frac{1}{2}}[k]\mathbf{H}[k])^H(\mathbf{R}_w^{-\frac{1}{2}}[k]\mathbf{Y}[k])}{(\mathbf{R}_w^{-\frac{1}{2}}[k]\mathbf{H}[k])^H(\mathbf{R}_w^{-\frac{1}{2}}[k]\mathbf{H}[k])} \end{aligned} \tag{1.45}$$

where $\{\cdot\}^H$ is the Hermitian operator.

1.3. Motivation of Research

To overcome the effect of signal fading in a multipath environment, multiple antennas are used at a receiver to achieve antenna diversity [44, 48]. However, it may be difficult to implement multiple antenna elements in a small terminal [44]. Therefore, to achieve diversity with a single antenna, a FS scheme in OFDM has been proposed [45]. In the FS scheme, a received baseband signal is sampled with a rate higher than the baud rate and they are combined to achieve path diversity on each subcarrier [45]. With the FS, high data rate communication will be possible without increasing the number of antennas at the small terminal [49]. Further, the effect of the pulse shaping filter in FS

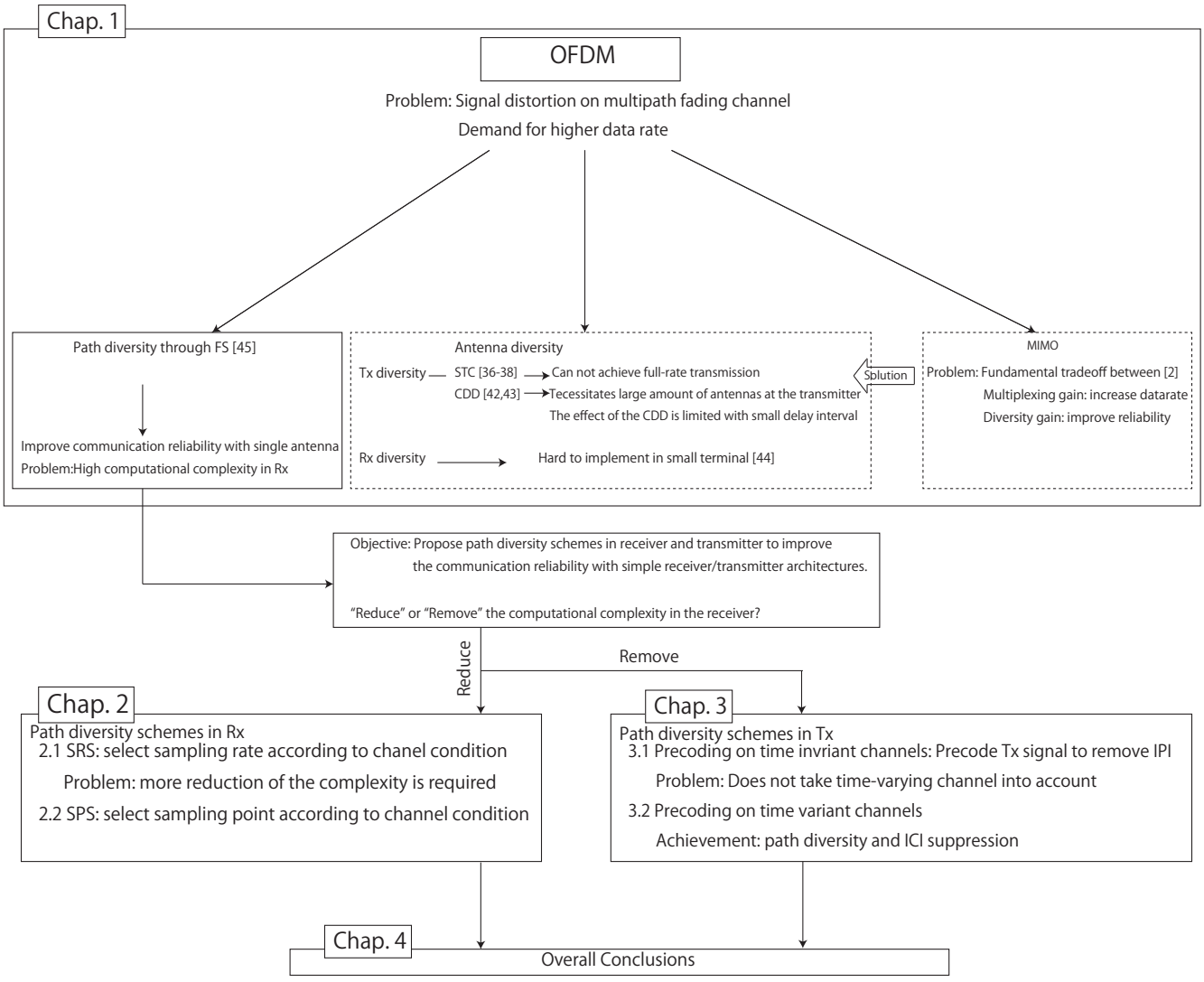

Figure 1.17: Overview of thesis.

has been investigated in [45, 50, 51]. It has been shown that the excessive bandwidth of the filter realizes path diversity in FS.

The problem of FS is that as the sampling rate increases, the power consumption grows due to the use of multiple demodulators. In this thesis, path diversity schemes in receiver and transmitter have been introduced to improve the communication reliability with simple receiver/transmitter architectures. The overall structure of the thesis is presented in Fig. 1.17. Table 1.4 summarizes the purpose, research issue, proposed scheme, and its achievement. In Chap. 2, the path diversity schemes in a receiver are introduced to reduce the complexity due to the FS. In Section 2.1, a sampling rate selection (SRS) scheme according to the frequency response of the channel is proposed [52]. The proposed scheme reduces the power consumption by decreasing the sampling

Table 1.4: Outline of the proposals.

Chapter 2	Purpose	Reduce the complexity due to the FS.
	Research issue	In the existing FS scheme, the oversampling ratio and the sampling points are always same in any channel conditions.
	Proposed scheme	Select sampling rate/point according to frequency response of the channel.
	Achievement	The proposed SRS and SPS have reduced the computational complexity for the FS in receiver while improving the BER performance.
Chapter 3	Purpose	Shift the signal processing burden for FS from receiver to transmitter.
	Research issue	SRS and SPS still require fast A/D converter and lots of OFDM demodulators.
	Proposed scheme	Precombine the transmitted OFDM signal in transmitter to achieve path diversity. Furthermore, generate the precoded symbols for not only the path diversity but also ICI suppression on time varying channel.
	Achievement	Path diversity and ICI suppression can be achieved without any specific signal processing in the receiver.

rate when the delay spread is small. In the second section, sampling point selection (SPS) scheme is investigated to achieve better power efficiency in the receiver. It is necessary to improve the communication quality with the same sampling rate to save the power consumption. This scheme selects the sampling points according to the frequency response of a channel. The problem of the path diversity schemes in receiver is that they still require fast A/D converter and lots of OFDM demodulators to select the sampling rate/point in the preamble period. In Chap. 3, a precoded transmit path diversity scheme in an OFDM system has been proposed to shift the signal processing burden for the FS from the receiver to the transmitter. In Section 3.1, a precoded transmit path diversity scheme on a time invariant channel in an OFDM system has been proposed [53]. [53] makes use of the impulse response of the channel with the resolution of the FS interval and can achieve path diversity without oversampling the received signal. On time varying channels, however, the precoded transmit path diversity scheme has not been proposed yet. On this channel, ICI deteriorates the BER performance of the system proposed in [54]. In Section 3.2, the precoding for both ICI suppression and path diversity combining at the transmitter has been proposed. The proposed scheme has designed the precoding matrix in order to minimize the MSE of received symbols. It can achieve ICI suppression and path diversity without any specific signal processing at the receiver. The advantages and disadvantages of Chap. 2 and Chap. 3

Table 1.5: Advantages/disadvantages and target systems

	Advantage	Disadvantage	Target system
Chap. 2 Path Diversity in Rx	Easy to implement Implementable in DL / UL	Large complexity in Rx	WLAN
Chap. 3 Path Diversity in Tx	Much lower complexity in Rx	Only for DL Large complexity in Tx	WPAN Centralized network

are listed in Table 1.5. The advantages of SRS and SPS, which are presented in Chap. 2, are "low computational complexity" and "easiness of implementation". By selecting the sampling rate/point, they can reduce the total amount of the computational complexity. They are implementable in both UL and DL. The disadvantages of them are that they still require fast A/D converter and a multiple of OFDM demodulators to select the sampling rate/point in the preamble period. Therefore, these schemes are not suitable in the WPAN, where small battery-powered nodes are used. The advantage of precoding schemes proposed in Chap. 3 is that the precoding scheme can achieve path diversity without any diversity combining in receiver side. The disadvantage of them is that the precoding is effective only in DL. CSI is essential for generating the precoded symbols and it can be estimated at the transmitter based on the preamble signal appended before the data period which is sent from the mobile terminal. Under the assumption of slow fading, both the uplink and the downlink have almost the same impulse response in the TDD system [29]. Therefore, the receiver in the mobile terminal does not need to estimate the impulse response and still path diversity is realized with a single demodulation branch. As mentioned above, the target system of SRS/SPS is WLAN using OFDM and the precoding scheme is focusing on UWB centralized network, which are shown in Fig. 1.18 as an example.

1.3.1. Overview of Chapter 2

Although the FS achieves diversity, it increases power consumption of the receiver. In some channel conditions, the energy of the received signal may be large enough with baud rate sampling. In this dissertation, the digital signal processing schemes for path diversity are proposed and investigated. Chapter 2 introduces the schemes to reduce the computational complexity at the receiver. In Section 2.1, SRS scheme has been proposed. The SRS scheme selects the oversampling ratio according to the frequency response of a channel to reduce the number of OFDM demodulators for signal detection. The most of the bit error occurs on the subcarrier with small frequency response. Thus,

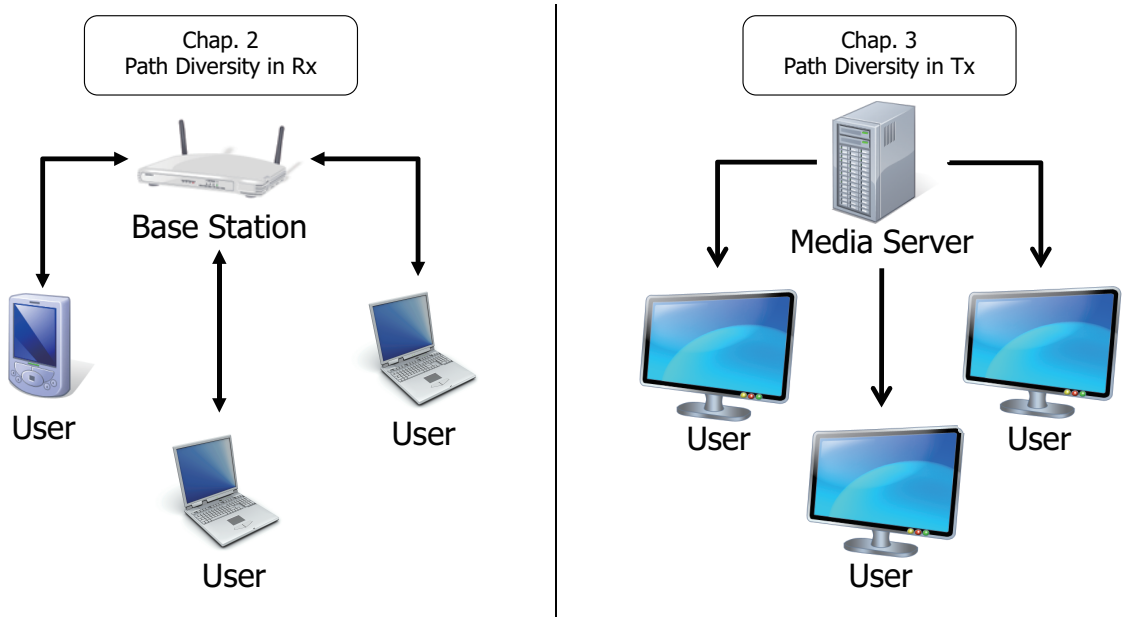

Figure 1.18: Target systems of the proposals.

the oversampling ratio, G, should be chosen in order to increase the power of the received signal on the subcarrier with the lowest frequency response. In the selection, there is a trade off between the bit error rate (BER) performance and the computational complexity. The selection of the coefficient for each oversampling ratio depends on the channel models and required performance in terms of BER and power consumption. With the proposed scheme, the power consumption can be reduced while improving the BER performance. To achieve more reduction of the computational complexity, section 2.1 has proposed SPS scheme. In [55], an initial phase of the sampling is selected according to the frequency response of the channel. In [56], the initial phase selection of the sampling has been evaluated through experiments. In these previous literatures for FS, the sampling interval is fixed to $\frac{T_S}{G}$ [45, 50–52, 55, 56] and the improvement of the power efficiency is not enough because it can not extract the multipaths which arrive non-uniformly in the delay domain. The selection of the sampling points makes the difference in the frequency response. It is then possible to achieve lower BER performance as compared to the conventional selection diversity schemes which are proposed in [52] or [55]. In other words, the number of demodulation branches in FS could be reduced for the same BER. In this section, non-uniform sampling point selection has been proposed. In this scheme, the interval between the sampling points is not fixed. As the oversampling rate increases, the complexity for the SPS grows exponentially. Therefore, this section has also proposed the low-complexity sampling point selection scheme to eliminate the specific sets of the sampling points which lead to large noise correlation.

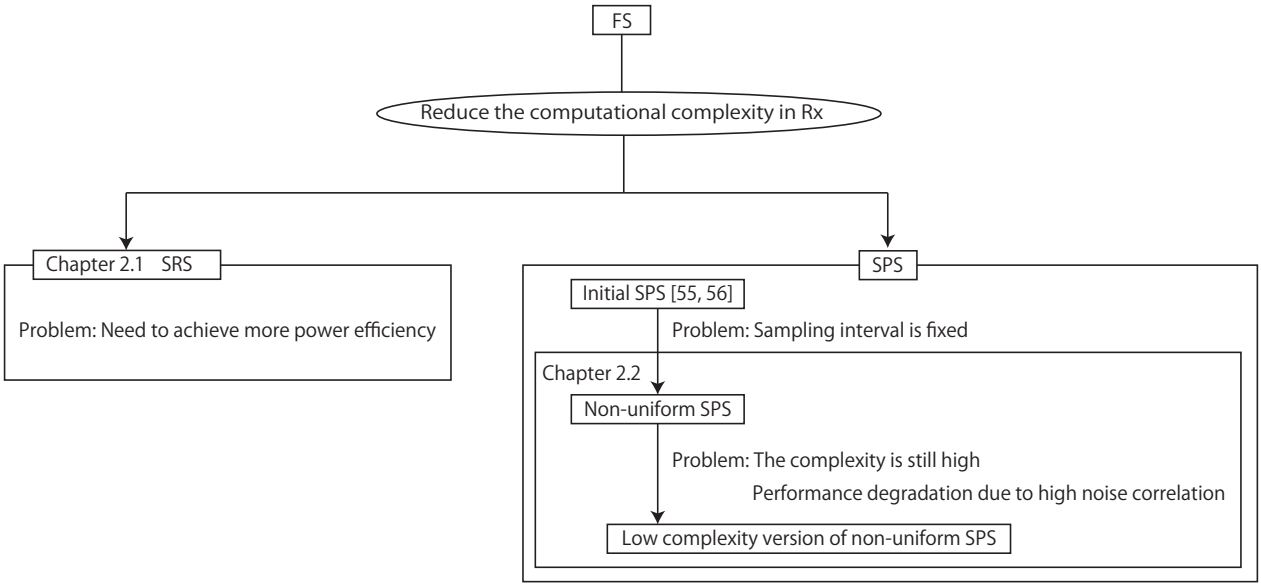

Figure 1.19: Overview of chapter 2.

1.3.2. Overview of Chapter 3

In DS/SS or IR-UWB communications, a rake receiver has been proposed to resolve multipath components and achieve path diversity [57–59]. In this scheme, the receiver needs to perform channel estimation and diversity combining, etc. These signal processing increases computational complexity in the receiver. Prerake has been proposed to shift these signal processing tasks from the mobile terminal to a receiver [29, 60–63]. In some circumstances the UWB transmitter has more signal processing capability than the receiver. In this case, the transmitter sends the signal generated by convolution between the transmit symbols and the FIR filter whose coefficients are generated through reverse and conjugate operations of the impulse response of the channel known at the transmitter side. The same as the rake scheme, prerake can achieve path diversity without combining at the receiver side. In [60], a prerake combining scheme is proposed when a pulse interval is smaller than a path interval and the impulse response of the channel is independent and Rayleigh distributed in an IR-UWB system. [61, 62] have proposed precombining schemes which tackle an inter-pulse interference (IPI) problem when the pulse interval is longer than the path interval. The precoding scheme on time varying channels has been proposed in [63]. However, it implements multiple antenna elements at the transmitter side and does not achieve path diversity. On the other hand, in an OFDM system, prerake has not been proposed while FS has been investigated to achieve path diversity with a single antenna [45, 50–52, 64–66]. However, in the FS-OFDM system, it is necessary to oversample a received signal and it leads to large

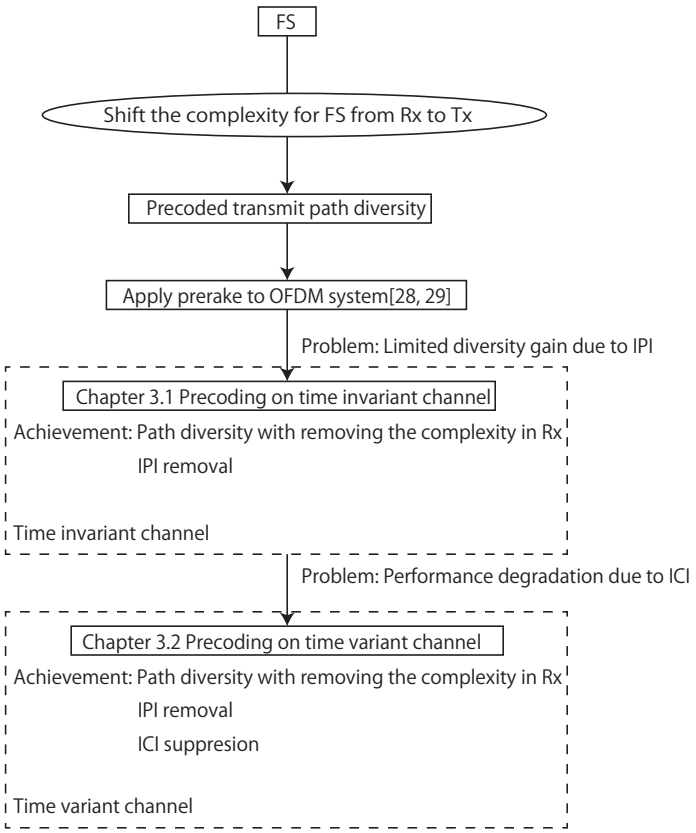

Figure 1.20: Overview of chapter 3.

power consumption in a small mobile terminal. Chapter 2 has proposed the SRS/SPS schemes and achieves the reduction of the computational complexity at receiver while obtaining the path diversity gain. However, they still require the high computational complexity and many OFDM demodulators. To realize low power consumption and small sized mobile terminal, the circuit size must be minimized. In this chapter, transmit path diversity schemes have been introduced to shift the signal processing burden from the receiver to the transmitter. Section 3.1 introduces the transmit path diversity scheme on time invariant channels. When the conventional prerake scheme [60–62] is applied to the OFDM system, effect of the path diversity is limited. This is because IPI within one OFDM symbol is generated at the receiver side. In the proposed scheme, the information symbols are precoded to remove the IPI by using the correlation matrix $\mathbf{R}[k]$ and can achieve path diversity without oversampling the received signal. Section 3.2 introduces the transmit path diversity scheme on time variant channels. In this paper, the precoding scheme for ICI suppression and path diversity in FS-OFDM has been proposed. In the conventional scheme, a precoded transmit path diversity scheme on time invariant channels has been proposed. On time varying channels, however, the precoded transmit path diversity scheme has not been proposed yet. On time variant

channels, Doppler spread causes ICI and it deteriorate the communication quality. The ICI due to the Doppler spread distorts the received signal in the conventional scheme. The proposed scheme has designed the precoding matrix in order to minimize the MSE of the received symbols to suppress the ICI.

Chapter 2

Fractional Sampling in OFDM Receiver

2.1. Sampling Rate Selection

2.1.1. Introduction

Nowadays, various wireless communications redsystems, including cellular systems, WLAN systems, etc., are widely employed. However, in conventional receivers, utilizing different frequency bands and modulation schemes necessitate different hardwares. Because of the various standards in different generations and regions, it is impossible to support all of those standards with one terminal. Therefore, to solve this problem, software-defined radio (SDR) techniques have been investigated. In the ideal SDR, the most of receiving process is carried out in reconfigurable devices such as digital signal processors (DSPs) or field programmable gate arrays (FPGAs). This will make it possible to use one terminal in any modulation schemes, generations, and regions [67].

The key component of the SDR is the devices from the radio frequency (RF) front-end to the analogue-to-digital converter (ADC). A variety of architectures has been proposed to realize the SDR. For example, an RF sampling reception scheme has also been proposed recently [68, 69]. In the RF sampling receiver architecture, the received signal is sampled at the radio frequency. Those samples are input to the averaging filter for decimation. Therefore, by selecting the decimation factor, it is possible to choose the oversampling ratio of the baseband signal.

On the other hand, a FS technique in OFDM has been proposed [45]. Through FS, the received baseband signal is sampled with the rate higher than the Nyquist rate in order to achieve diversity gain. However, as the sampling rate increases, the power consumption grows linearly [70].

In this chapter, a sampling rate selection scheme according to frequency response of

the channel is proposed. The proposed scheme reduces power consumption by decreasing the sampling rate when the delay spread is small.

2.1.2. Sampling Rate Selection

Though FS achieves diversity gain , it increases power consumption. In some channel conditions, the received signal may be large enough with Nyquist sampling. Therefore, in the proposed scheme, the sampling rate is selected in accordance with the frequency response of the channel. Also, the different sampling rate leads to the different response of the channel as indicated in Eq.(1.41). In the proposed scheme the sampling rate is selected as follows. Suppose the frequency response of the channel with the oversampling ratio of G at the kth subcarrier is expressed as follows.

$$P_G[k] = \mathbf{H}^{'H}[k]\mathbf{H}^{'}[k]. \tag{2.1}$$

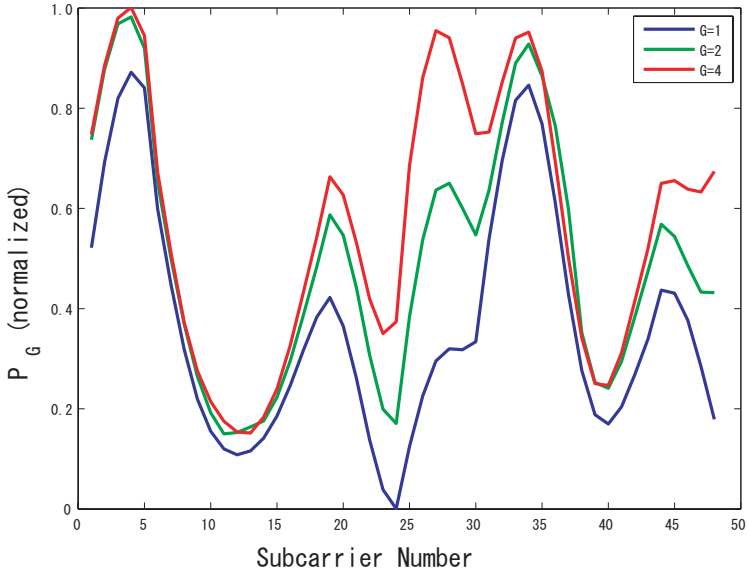

Figure 2.1: Example of the Frequency response of the channel.

Figure 2.1 shows the frequency response of the channel in terms of the subcarrier number. The most of the bit error occurs on the subcarrier with low frequency response. Thus, the oversampling ratio, G, should be chosen in order to increase the power of the received signal on the subcarrier with the lowest frequency response. Bit error increases in exponentially reverse proportion to SNR as given by the following equation [71]:

$$P_{b|H[k]}[k] = \frac{1}{2} erfc\left(\sqrt{\frac{|H[k]|^2 E_b}{N_0}}\right). \tag{2.2}$$

Thus, it is dominated by the lowest gain subcarrier. The oversampling ratio, G, is selected with the following criteria,

$$\max_{G}\{\min_{k} C_G P_G[k]\}, \tag{2.3}$$

where C_G is the coefficient for the oversampling ratio of G and

$$0 < C_G \leqslant 1.0.$$

2.1.3. Numerical Results

2.1.3.1. Simulation Conditions

Table 2.1: Simulation Conditions

Modulation scheme	1st:QPSK, 16QAM, 64QAM 2nd:OFDM
FFT size	64
Number of subcarriers	64
Number of data subcarriers	48
Number of OFDM packets per trial	10000
Number of OFDM symbols per packet	100
Bandwidth of subcarriers	312.5[kHz]
Preamble length (GI+Preamble)	$1.6 + 6.4[\mu s]$
OFDM symbol length (GI+Data)	$0.8 + 3.2[\mu s]$
Channel model	Rayleigh(16 path, equal gain), Indoor Residential A

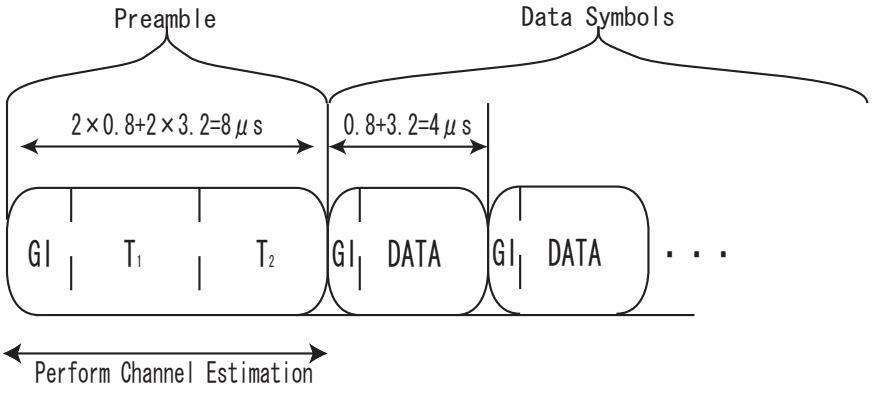

Figure 2.2: OFDM packet structure for simulation.

Simulation conditions are presented in Table.2.1. In this simulation, the oversampling ratio G is selected among $\{1, 2, 4\}$.

The response of the channel is assumed to be constant during one OFDM packet. The structure of the OFDM packet for computer simulation is shown in Fig. 2.2.

Relevant to IEEE802.11a/g standard, the number of subcarriers, N, is 64 (48 subcarriers are for data symbols, 4 subcarriers are for pilot symbols, and the rests are null subcarriers) [14, 72]. For channel estimation, two symbols, T_1 and T_2 are used. The ideal channel estimation is assumed here. The oversampling ratio in the preamble period is fixed to $G = 4$. In the data period, the oversampling ratio is selected according to the criteria in Eq. 2.3. Reconfigurable ADCs are assumed [73]. In Fig. 2.3, each stage performs sampling. the sampling rate can be reconfigured by letting the output of stage 2 and 4 being resampled by their preceding stages. By resampling one time, sampling rate is reduced to half the clock frequency, by resamplng twice, sampling rate twice, sampling rate is reduced to one third of the clock frequency. In this way, we can select sampling rate without switching clock rate.

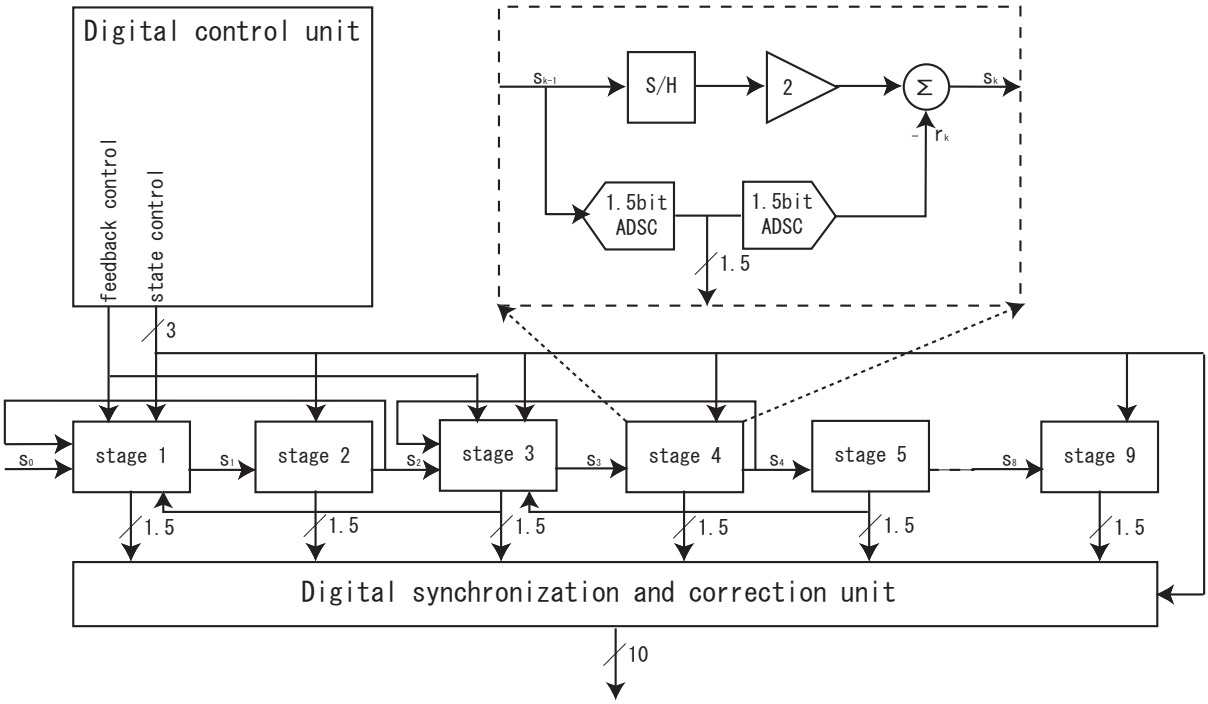

Figure 2.3: Pipelined ADC.

This chapter focuses on the average oversampling ratio in the data period as the length of the data period is 100 OFDM symbols which is much larger than the preamble length. The total response of the transmitter and receiver filters are also assumed to be truncated sinc pulses with the duration of $2T_s$ [45].

As the channel model, 16 path Rayleigh fading with uniform delay spread is assumed. Also, Indoor Residential A model in [74] is assumed, which has small delay spread.

2.1.3.2. 16 Path Rayleigh Fading

Figure 2.4 shows the relationship between the BER and the coefficients, C_2 and C_4 ($C_1 = 1.0$). Figure 2.5 shows the average oversampling ratio versus the coefficients. There is a tradeoff between BER performance and average oversampling ratio. As C_2 and C_4 increase, the BER reduces. However, as the BER performance improves, the average oversampling ratio, G, increases as shown in Fig.2.5. Figure 2.6(a) and (b) show the BER versus C_2 and the average of G versus C_2 when $0.3 \leqslant C_4 \leqslant 0.7$, respectively. It is clear that C_2 is relatively insensitive to the BER while it may reduce the average of G. In this thesis, the coefficients are selected so that the both the BER and the average of oversampling ratio can be reduced as C_2 increases. In Fig. 2.6(a), the BER performance is intensive to C_2 in the region of

$$0.3 \leqslant C_4 \leqslant 0.5. \tag{2.4}$$

Figure 2.6(b) shows that the average is intensive to C_2 in the region given by

$$0.4 \leqslant C_4 \leqslant 0.9. \tag{2.5}$$

Therefore, C_4 is selected to 0.5 to satisfy these equations and minimize BER as much as possible. Then, C_2 is selected to 1.0 so that both BER and the average can be minimized.

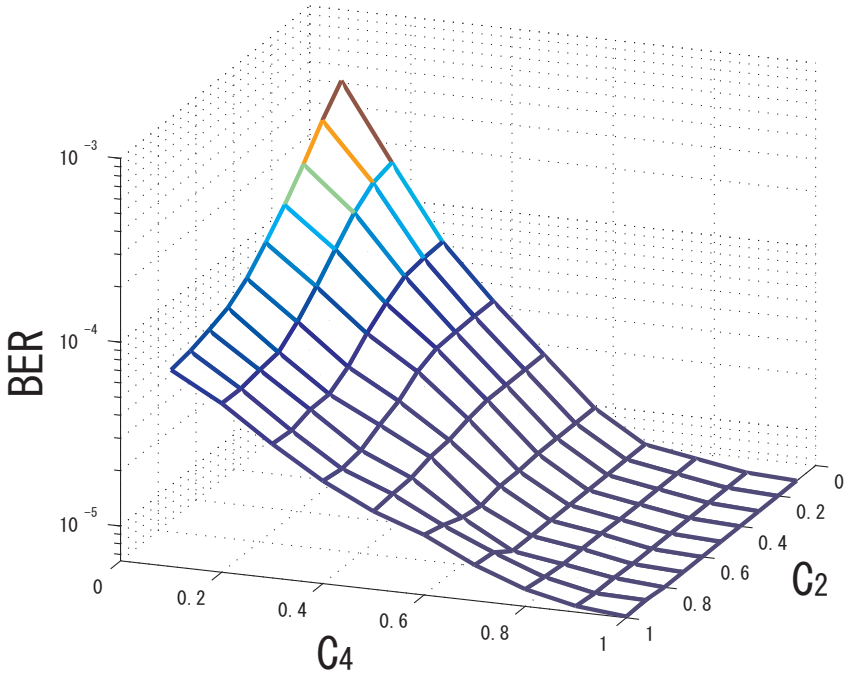

Figure 2.4: 16 path Rayleigh fading model($E_b/N_0 = 20$[dB]).

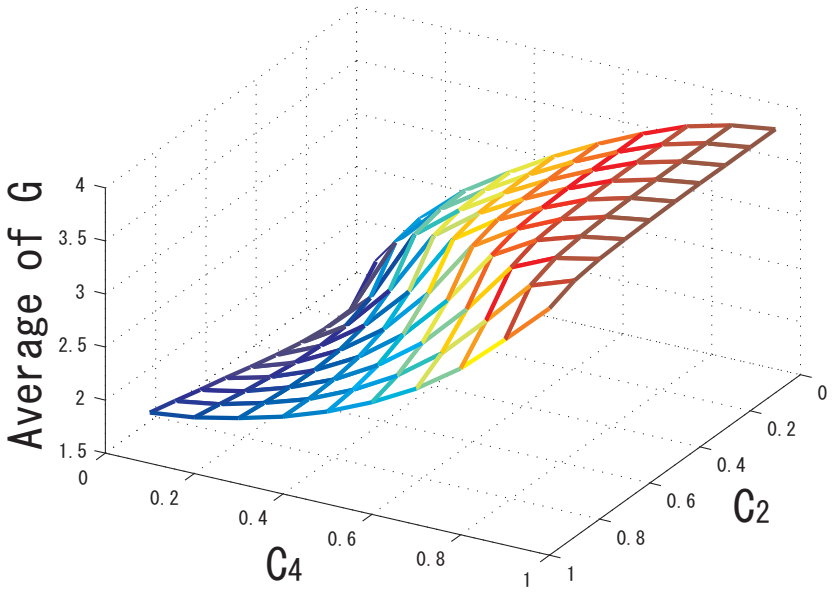

Figure 2.5: 16 path Rayleigh fading model($E_b/N_0 = 20$[dB]).

Table 2.2: 16 path Rayleigh fading model

E_b/N_0[dB]	Average of G
0	2.35
5	2.37
10	2.37
15	2.35
20	2.36
25	2.37
30	2.36

Figs. 2.7 (a) and (b) show the BER curves obtained through FS and the probability of sampling rate selection, respectively. Here, C_2 and C_4 are set to 1.0 and 0.5. From Fig.2.7(b), the probability of sampling rate selection is constant under different E_b/N_0 conditions. Table 2.2 shows the average oversampling ratio. From Fig.2.7(a) and Table 2.2, while the proposed scheme reduces the average oversampling ratio by 40%, the BER curve is still close to that with $G = 4$.

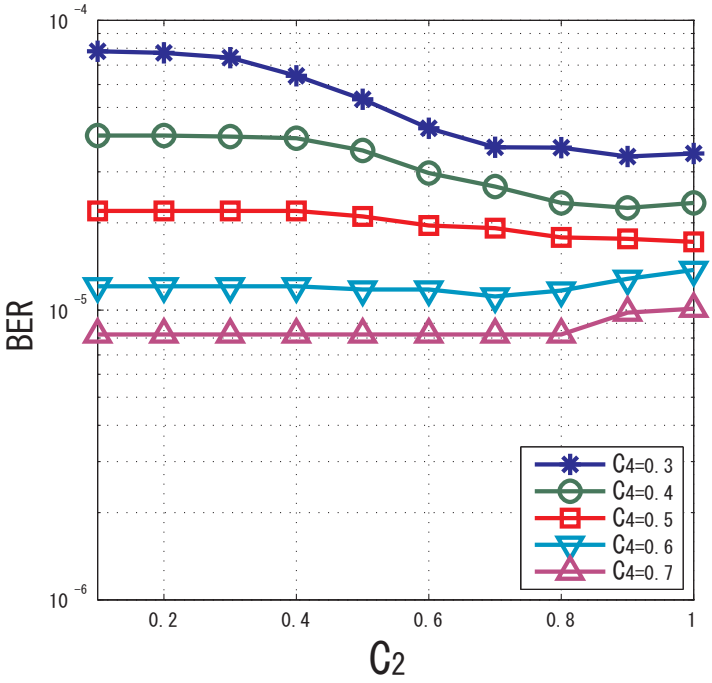

(a) BER

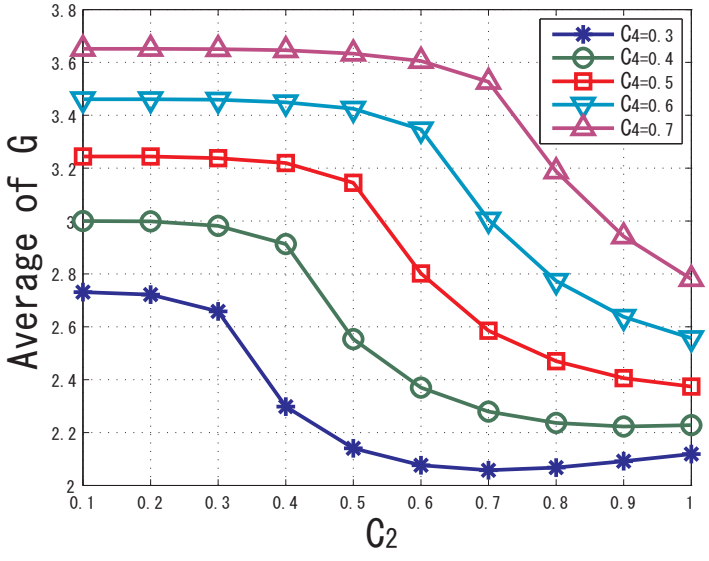

(b) Prob. of sampling rate selection

Figure 2.6: 16 path Rayleigh fading model($E_b/N_0 = 20$[dB]).

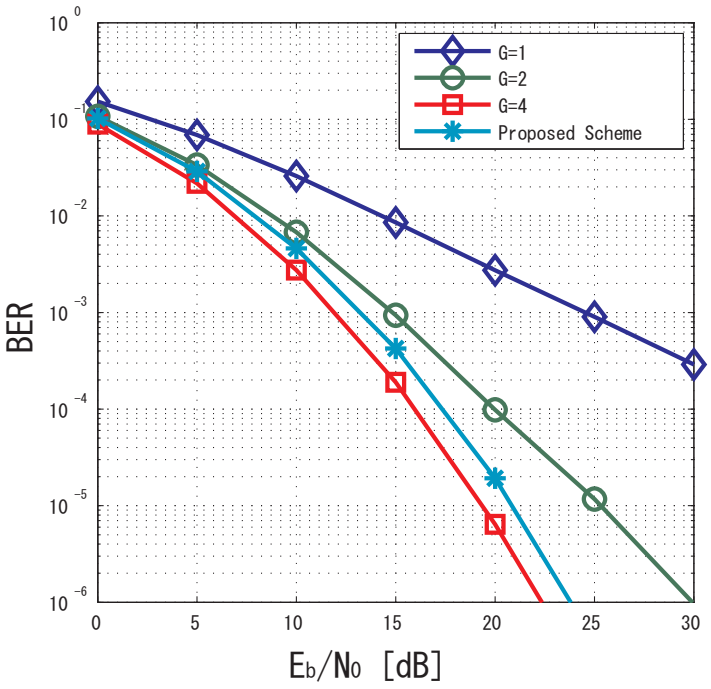

(a) BER

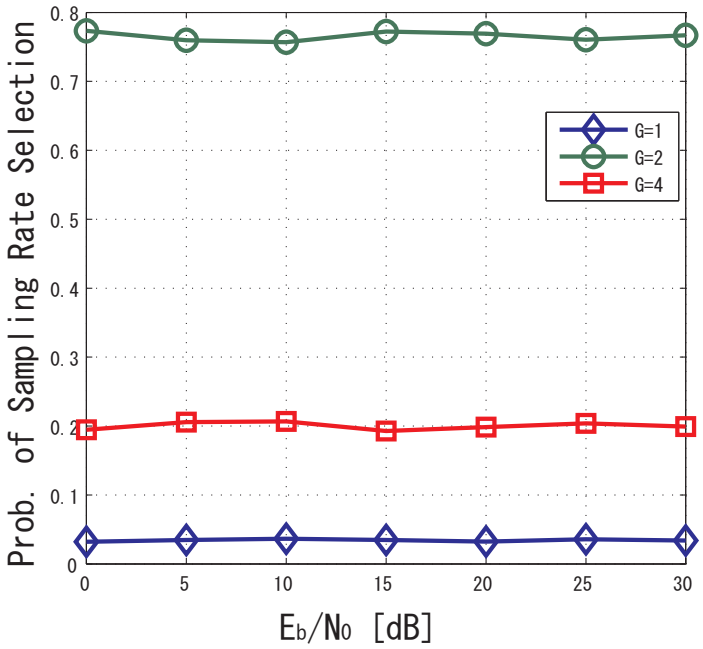

(b) Prob. of sampling rate selection

Figure 2.7: 16 path Rayleigh fading model($C_2 = 1.0, C_4 = 0.5$).

2.1.3.3. Indoor Residential A

Indoor Residential A model has exponential delay profile with the delay spread of 16 [ns]. Figure 2.8(a) and (b) show the BER versus E_b/N_0 and the probability of sampling rate versus E_b/N_0, respectively. Here, C_2 and C_4 are set to 0.7 and 0.5. The average oversampling ratio is about 1.74. From Fig. 2.8(a), it is clear that the BER improvement with FS is less significant because of small delay spread. The oversampling ratio of 4 is hardly selected and the average oversampling ratio is less than 1.8. Thus, power consumption is significantly reduced when the delay spread is small. This is because in Indoor Residential A model path diversity through FS is not effective since the power of the first arrival path is larger than the rest and the delay spread is small. On the same channel model, numerical results with higher modulation levels are shown in Figs. 2.9 (a) and (b). In the both figures, the BER with the proposed scheme is better than that with $G = 2$. The average oversampling ratio is about 1.74 and is constant in terms of the different $\mathrm{E_b/N_0}$.

2.1.3.4. Rician Channel

Figure 2.10 shows the BER performance on the Rician channel model which used in millimeter wave systems [75, 76]. The coefficients are set to $(C_2, C_4) = (0.8, 0.6)$ by the same way as in 16 path Rayleigh fading. As shown in this figure, the whole BER performance is better than that of 16 path Rayleigh fading. This because on the milliwave channel, there is a LOS component whose impulse response is constant value. Therefore, the received signal is demodulated properly with lower oversampling ratio and it leads to the reduction of power consumption in receiver. From the simulation results of the three channel models, the SRS can achieve

- Almost the same BER performance as $G = 4$ with $2 \leqslant \tilde{G} \leqslant 3$.
- Better BER performance than that of $G = 2$ with $\tilde{G} < 2$ on small delay spread channel or LOS channel.

2.1.3.5. Comparison of Computational Complexity

The total amount of the computational complexity is evaluated in terms of the number of multiplications here. The number of multiplications for each process such as DFT, noise-whitening, MRC, and SRS are shown in Table 2.3. DFT requires $N \log_2 N$ multiplications for FFT. Noise-whitening needs G^2 multiplications on each subcarrier by multiplication between a $G \times G$ matrix and a $G \times 1$ column vector as in Eq. (1.43).

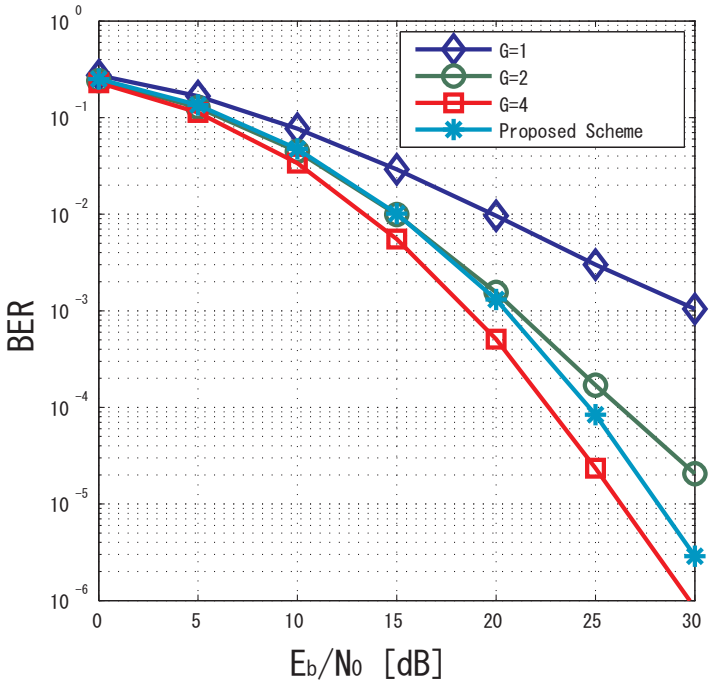

(a) BER

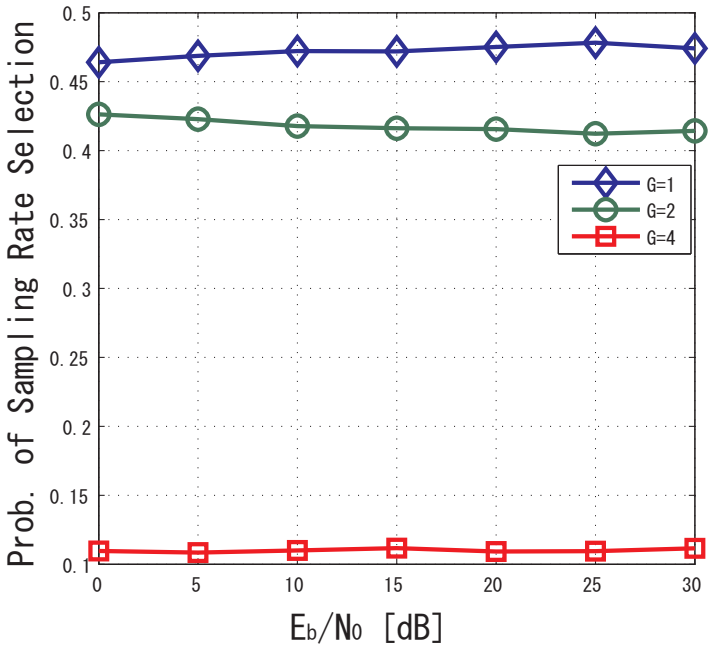

(b) Prob. of sampling rate selection

Figure 2.8: Indoor Residential A($C_2 = 0.7, C_4 = 0.5$).

In SRS, 7 ($= 1 + 2 + 4$) multiplications in Eq. (2.1) are required on each subcarrier because the inner product between $\mathbf{H}'^{H}[k]$ and $\mathbf{H}'[k]$ with the size of $G \times 1$ column vector requires G multiplications and this inner product is calculated for each G ($= 1, 2, 4$). Here, it is assumed that the oversampling rate is G during both the preamble period

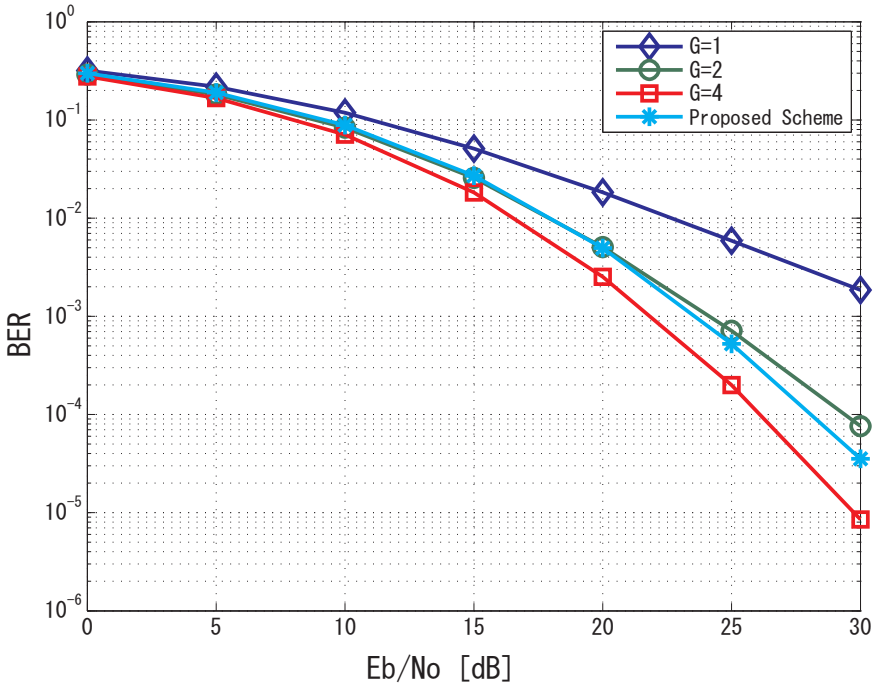

(a) 16QAM

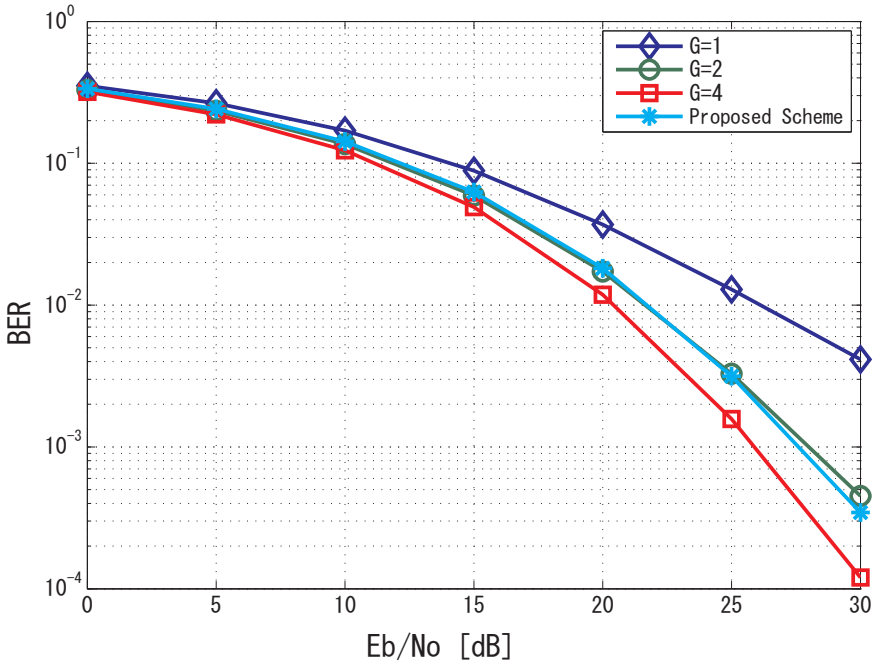

(b) 64QAM

Figure 2.9: Indoor Residential A($C_2 = 0.7, C_4 = 0.5$).

and the data period in the conventional FS (non-SRS). Thus, the total amount of the computational complexity in non-SRS is expressed as

$$\left(GN \log_2 N + G^2 N + GN\right) \cdot (N_{SYM} + N_{PRE}) \tag{2.6}$$

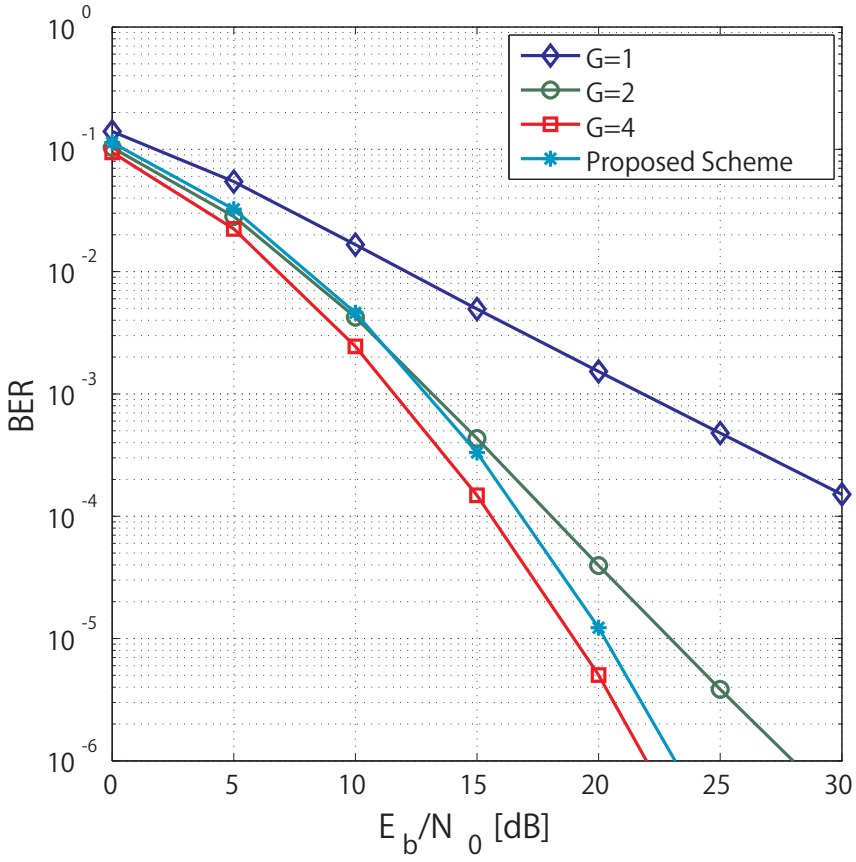

Figure 2.10: Rician Channel($C_2 = 0.8, C_4 = 0.6$).

whre N_{SYM} and N_{PRE} are the numbers of data symbols and preamble symbols in one packet. On the other hand, in the proposed scheme (SRS), the oversampling ratio is 4 during the preamble period and G during the data period. The total amount of the computational complexity is

$$\left(4N\log_2 N + 4^2N\right)\cdot N_{PRE} + 7N + \left(\tilde{G}N\log_2 N + \tilde{G}^2N + \tilde{G}N\right)\cdot N_{SYM} \qquad (2.7)$$

where $\tilde{G}$ is the average oversampling ratio. The total amount of computational complexity for the conventional FS schemes with oversampling ratio $G = 1, 2, 4$, and the proposed scheme per OFDM packet are shown in Table 2.4. From the table, the SRS realizes the more reduction of the complexity as the number of symbols increases.

2.1.4. Conclusions

In this subchapter, a sampling rate selection scheme for FS has been proposed for two typical channel models. The selection of the coefficient for each oversampling ratio depends on the channel models and required performance in terms of BER and

Table 2.3: Computational complexity of each processing

	No. of multiplications
DFT	$N \log_2 N$
Noise-whitening	$G^2 N$
MRC	GN
SRS	$7N$

Table 2.4: Total computational complexity

		10 symbols	100 symbols
Non-SRS	$G = 1$	6144	52224
	$G = 2$	13824	117504
	$G = 4$	33792	287232
SRS	16 path Rayleigh fading	19705	146940
	Indoor Residential A	15301	102900
	Rician channel	14746	97347

power consumption. With the proposed scheme, the power consumption can be reduced significantly if the delay spread is small. When the delay spread is large, the BER performance can be improved while the power consumption is still saved with the proposed sampling rate selection scheme.

2.2. Non-uniform Sampling Point Selection

2.2.1. Introduction

OFDM is a very attractive technique for reliable broadband wireless communications such as WLAN IEEE802.11a/g, WiMAX, etc [14,72,77]. This is due to the efficient use of frequency spectrum and robustness to multipath channels with the use of multiple subcarriers.

To overcome the effect of signal fading in a multipath environment, multiple antennas are used at a receiver to achieve antenna diversity [44,48]. However, it may be difficult to implement multiple antenna elements in a small terminal [44]. Therefore, to achieve diversity with a single antenna, a FS scheme in OFDM has been proposed [45]. In the FS scheme, a received baseband signal is sampled with a rate higher than the Nyquist rate and they are combined to achieve path diversity on each subcarrier [45]. Further, the effect of the pulse shaping filter in FS has been investigated in [45, 50, 51]. It has been shown that the excessive bandwidth of the filter realizes path diversity in FS.

In [52], a sampling rate selection algorithm for FS is proposed. In this scheme, the sampling rate is selected according to the frequency response of a channel. In [55], an initial phase of the sampling is selected according to the frequency response of the channel. In [56], the initial phase selection of the sampling has been evaluated by experiments. In these previous literatures for FS, the sampling interval is fixed [45, 50–52, 55, 56]. The selection of the sampling points makes the difference in the frequency response. It is then possible to achieve lower BER performance as compared to the conventional schemes in [52] or [55]. In other words, the number of demodulation branches in FS can be reduced for the same BER.

In this subchapter, a novel non-uniform sampling point selection scheme for FS based on the frequency response of the channel is proposed. The proposed scheme fixes neither the initial sampling point nor the sampling interval. The most of the bit errors occur on the subcarrier experiencing the deepest fade. The proposed scheme selects the sampling points so that the smallest frequency responses of the subcarriers is maximized to improve the average BER.

2.2.2. System Model

2.2.2.1. FS with SPS

The block diagram of an OFDM system with FS is shown in Fig. 2.11 [45]. Assume that the information symbol on the kth subcarrier is $S[k](k = 0, ..., N-1)$, the OFDM symbol is then given by

$$x[n] = \frac{1}{\sqrt{N}} \sum_{k=0}^{N-1} S[k] e^{j\frac{2\pi nk}{N}} \tag{2.8}$$

where $n(n = 0, 1, ..., N-1)$ is the time index. A GI is appended before transmission. N_{GI} is the length of the GI.

The baseband signal at the output of the filter is given by

$$x(t) = \sum_{n=0}^{N+N_{\mathrm{GI}}-1} x[n] p(t - nT_s)$$

where $p(t)$ is the impulse response of the baseband filter and T_s is the symbol duration. This signal is upconverted and transmitted through a multipath channel with an impulse response $c(t)$. The received signal after the down conversion is given by

$$y(t) = \sum_{n=0}^{N+N_{\mathrm{GI}}-1} x[n] h(t - nT_s) + v(t) \tag{2.9}$$

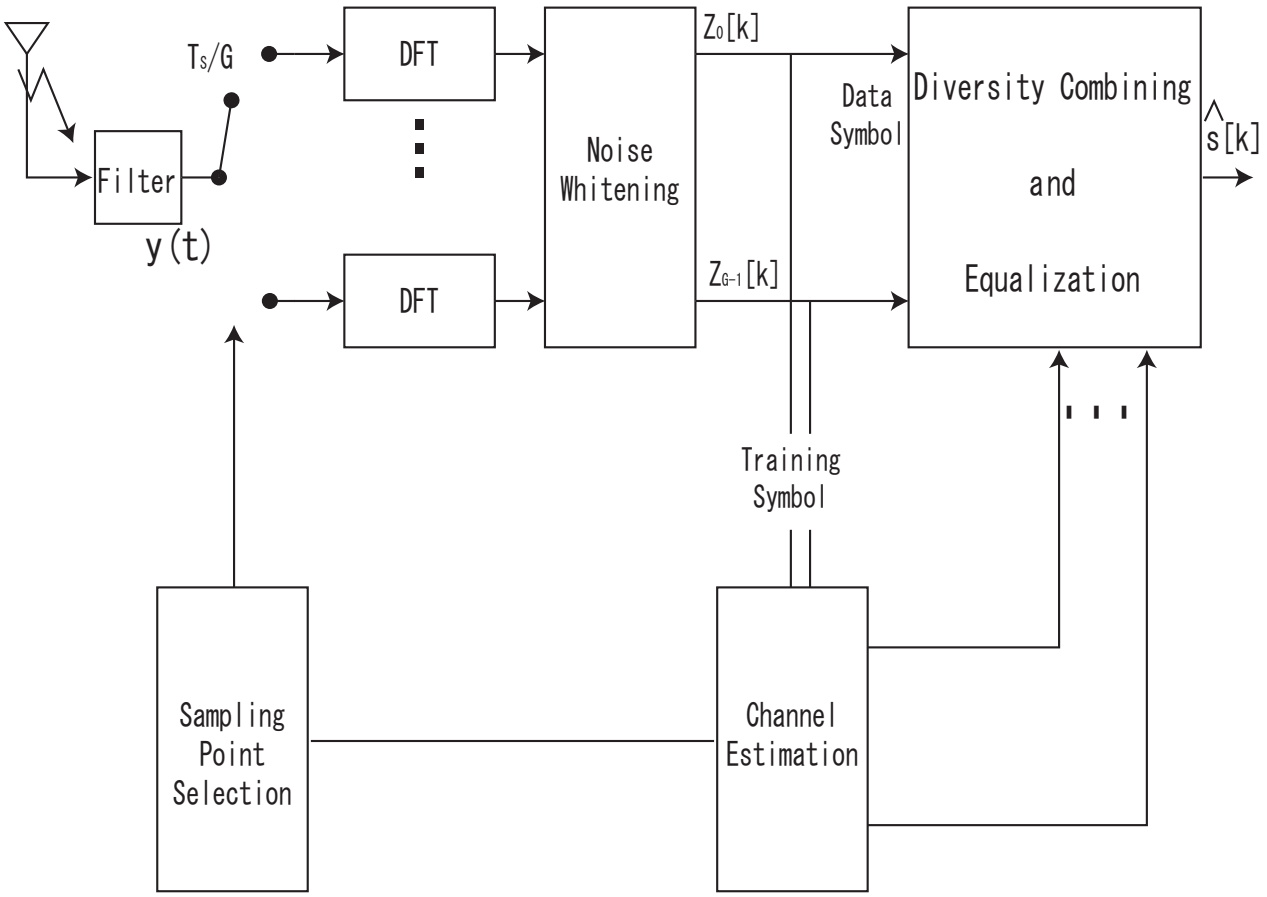

Figure 2.11: OFDM receiver using FS.

where $h(t)$ is the impulse response of the composite channel and is given by $h(t) := p(t) \star c(t) \star p(-t)$ and $v(t)$ is the additive Gaussian noise filtered at the receiver. For the multipath channel, $h(t)$ can be expressed in a baseband form as

$$h(t) = \sum_{l=0}^{N_m-1} \alpha_l p_2(t - \tau_l) \tag{2.10}$$

where $p_2(t) := p(t) \star p(-t)$ is the deterministic correlation of $p(t)$ and satisfies Nyquist's property. It is assumed that the channel in Eq. (2.10) has N_m path components, α_l is the amplitude that is time-invariant during one OFDM symbol (quasistatic channel model), and τ_l is the path delay. If $y(t)$ is sampled at the rate of T_s/G, where G is the oversampling rate, its polyphase components can be expressed as

$$y_g[n] = \sum_{m=0}^{N+N_{\mathrm{GI}}-1} u[m]h_g[n-m] + v_g[n]$$

where $y_g[n]$, $h_g[n]$, and $v_g[n]$ $(g = 0, ..., G-1)$ are polynomials of sampled $y(t)$, $h(t)$,

and $v(t)$, respectively, and are expressed as

$$\begin{aligned} y_g[n] &:= y(nT_s + \Delta_g T_s/\Gamma), && (2.11)\\ h_g[n] &:= h(nT_s + \Delta_g T_s/\Gamma), && (2.12)\\ v_g[n] &:= v(nT_s + \Delta_g T_s/\Gamma) && (2.13) \end{aligned}$$

where T_s/Γ is the step size of the initial timing and Δ_g is the normalized gth sampling point. Δ_g satisfies the following inequation,

$$0 \leqslant \Delta_0 < \Delta_1 < ... < \Delta_{G-1} \leqslant \Gamma - 1. \quad (2.14)$$

After removing the GI and taking DFT at each branch, the received symbol is given by

$$\mathbf{Y}[k] = \mathbf{H}[k]S[k] + \mathbf{V}[k] \quad (2.15)$$

where $\mathbf{Y}[k] = [Y_0[k]...Y_{G-1}[k]]^T, \mathbf{H}[k] = [H_0[k]...H_{G-1}[k]]^T$and $\mathbf{V}[k] = [V_0[k]...V_{G-1}[k]]^T$ are $G \times 1$ column vectors, each gth component representing

$$\begin{aligned} [\mathbf{Y}[k]]_g := Y_g[k] &= \sum_{n=0}^{N-1} y_g[n] e^{-j\frac{2\pi kn}{N}}, && (2.16)\\ [\mathbf{H}[k]]_g := H_g[k] &= \sum_{n=0}^{N-1} h_g[n] e^{-j\frac{2\pi kn}{N}}, && (2.17)\\ [\mathbf{V}[k]]_g := V_g[k] &= \sum_{n=0}^{N-1} v_g[n] e^{-j\frac{2\pi kn}{N}}, && (2.18) \end{aligned}$$

respectively.

As already stated, $v(t)$ in Eq. (2.9) is filtered by the pulse shaping filter in the receiver, $p(t)$. The power spectrum of the filter, $P_2(f)$, has the following relation.

$$p_2(t) = \int_{-\infty}^{\infty} P_2(f) e^{j2\pi ft} df. \quad (2.19)$$

Since the white noise is assumed to be input to the filter, the power spectrum of the filtered noise, $V(f)$, is expressed as

$$V(f) = \sigma_v^2 P_2(f), \quad (2.20)$$

and its autocorrelation is given as

$$\begin{aligned} R(\tau) &= E[v(t) v^*(t+\tau)] \\ &= \int_{-\infty}^{\infty} V(f) e^{j2\pi f\tau} df \\ &= \sigma_v^2 \int_{-\infty}^{\infty} P_2(f) e^{j2\pi f\tau} df \\ &= \sigma_v^2 p_2(\tau). && (2.21) \end{aligned}$$

Suppose $p_2(\tau)$ satisfies the following condition,

$$p_2(nT_s) = \begin{cases} 1 & (n=0) \\ 0 & (n \neq 0) \end{cases}, \tag{2.22}$$

and the bandlimited noise, $v(t)$, is sampled at the baud rate of $1/T_s$, the samples of $v(t)$ are independent of one another. However, when the sampling rate increases, the noise samples are correlated and noise-whitening is required to maximize the SNR [46]. The whitening filter equalizes the spectrum of the correlated noise samples [47]. In order to perform noise-whitening, it is necessary to calculate a $G \times G$ noise covariance matrix on the kth subcarrier, $\mathbf{R}_w[k]$. The (g_1, g_2)th element of the noise covariance matrix on the kth subcarrier is given as

$$\begin{aligned}
&[\mathbf{R}_w[k]]_{g_1 g_2} \\
&= E[V_{g_1}[k]V_{g_2}^*[k]] \\
&= \frac{1}{N} E\left[\left(\sum_{n_1=0}^{N-1} v\left(n_1 T_s + \Delta_{g_1}\frac{T_s}{\Gamma}\right) e^{-j\frac{2\pi k n_1}{N}}\right)\left(\sum_{n_2=0}^{N-1} v^*\left(n_2 T_s + \Delta_{g_2}\frac{T_s}{\Gamma}\right) e^{+j\frac{2\pi k n_2}{N}}\right)\right] \\
&= \frac{1}{N}\sum_{n_1=0}^{N-1}\sum_{n_2=0}^{N-1} E\left[v\left(n_1 T_s + \Delta_{g_1}\frac{T_s}{\Gamma}\right) v^*\left(n_2 T_s + \Delta_{g_2}\frac{T_s}{\Gamma}\right)\right] e^{j\frac{2\pi k(n_2-n_1)}{N}}.
\end{aligned} \tag{2.23}$$

Using Eq. (2.21),

$$\begin{aligned}
&E\left[v\left(n_1 T_s + \Delta_{g_1}\frac{T_s}{\Gamma}\right) v^*\left(n_2 T_s + \Delta_{g_2}\frac{T_s}{\Gamma}\right)\right] \\
&= \sigma_v^2 p_2\left(\left(n_2 T_s + \Delta_{g_2}\frac{T_s}{\Gamma}\right) - \left(n_1 T_s + \Delta_{g_1}\frac{T_s}{\Gamma}\right)\right) \\
&= \sigma_v^2 p_2\left(\left(n_2 - n_1 + \left(\Delta_{g_2} - \Delta_{g_1}\right)/\Gamma\right) T_s\right).
\end{aligned} \tag{2.24}$$

Thus, Eq. (2.23) is expressed as

$$\begin{aligned}
&[\mathbf{R}_w[k]]_{g_1 g_2} \\
&= \sigma_v^2 \frac{1}{N}\sum_{n_1=0}^{N-1}\sum_{n_2=0}^{N-1} p_2((n_2 - n_1 + (\Delta_{g_2} - \Delta_{g_1})/\Gamma)T_s) e^{j\frac{2\pi k(n_2-n_1)}{N}}.
\end{aligned} \tag{2.25}$$

and multiplying both sides of Eq. (2.15) by $\mathbf{R}_w^{-\frac{1}{2}}[k]$

$$\mathbf{R}_w^{-\frac{1}{2}}[k]\mathbf{Y}[k] = \mathbf{R}_w^{-\frac{1}{2}}[k](\mathbf{H}[k]\mathbf{S}[k] + \mathbf{V}[k]), \tag{2.26}$$

$$\mathbf{Y}'[k] = \mathbf{H}'[k]S[k] + \mathbf{V}'[k], \tag{2.27}$$

where $\mathbf{Y}'[k] = \mathbf{R}_w^{-\frac{1}{2}}[k]\mathbf{Y}[k]$, $\mathbf{H}'[k] = \mathbf{R}_w^{-\frac{1}{2}}[k]\mathbf{H}[k]$, and $\mathbf{V}'[k] = \mathbf{R}_w^{-\frac{1}{2}}[k]\mathbf{V}[k]$. Since $\mathbf{R}_w[k]$ is a Hermitian matrix, the covariance of the noise vector after noise-whitening, $\mathbf{V}'[k]$, is

$$
\begin{aligned}
& E\left[\mathbf{V}^{'}[k]\mathbf{V}^{'H}[k]\right] \\
&= \mathbf{R}_w^{-\frac{1}{2}}[k] E\left[\mathbf{V}[k]\mathbf{V}[k]\right] \mathbf{R}_w^{-\frac{H}{2}} \\
&= \mathbf{R}_w^{-\frac{1}{2}} \mathbf{R}_w[k] \mathbf{R}_w^{-\frac{H}{2}} \\
&= \mathbf{I}
\end{aligned} \tag{2.28}
$$

where $\mathbf{I}$ is the $G \times G$ identity matrix. From Eq. (2.28), the noise samples are whitened. After whitening, multiple outputs on each subcarrier are obtained through FS. Based on the frequency responses of the subcarriers estimated with the preamble symbols, those samples are combined to maximize the SNR expressed as the following equation [45],

$$
\begin{aligned}
\hat{S}[k] &= \frac{\mathbf{H}^{'H}[k]\mathbf{Y}^{'}[k]}{\mathbf{H}^{'H}[k]\mathbf{H}^{'}[k]} \\
&= \frac{(\mathbf{R}_w^{-\frac{1}{2}}[k]\mathbf{H}[k])^H (\mathbf{R}_w^{-\frac{1}{2}}[k]\mathbf{Y}[k])}{(\mathbf{R}_w^{-\frac{1}{2}}[k]\mathbf{H}[k])^H (\mathbf{R}_w^{-\frac{1}{2}}[k]\mathbf{H}[k])}
\end{aligned} \tag{2.29}
$$

where $\{\cdot\}^H$ is the Hermitian operator.

2.2.2.2. Sampling Point Selection

In the preamble period, the received signal is sampled at the rate of Γ times higher than the Nyquist rate. $G(\leqslant \Gamma)$ sampling points out of Γ are selected according to the frequency response of a channel, which is estimated with the preamble symbols of a packet. In the data period, the received signal is sampled at the timing selected by the sampling point selection schemes. In this chapter, two sampling point selection schemes are evaluated.

In the preamble period, the received preamble on the kth subcarrier is expressed as

$$
\mathbf{Y}^p[k] = \mathbf{H}^p[k] S^p[k] + \mathbf{V}^p[k] \tag{2.30}
$$

where $\mathbf{Y}^p[k]$ is $\Gamma \times 1$ vector of the received preamble, $\mathbf{H}^p[k]$ is $\Gamma \times 1$ vector of the frequency response of the channel, $S^p[k]$ is the preamble symbol that is known at the receiver side, and $\mathbf{V}^p[k]$ is the $\Gamma \times 1$ noise vector. In this chapter, the frequency response of the channel, $\hat{\mathbf{H}}[k]$, is estimated as follows.

$$
\hat{\mathbf{H}}^p[k] = \begin{bmatrix} \hat{H}_0^p[k] \\ \hat{H}_1^p[k] \\ \vdots \\ \hat{H}_{\Gamma-1}^p[k] \end{bmatrix} = \frac{\mathbf{Y}^p[k]}{S^p[k]} = \mathbf{H}^p[k] + \frac{\mathbf{V}^p[k]}{S^p[k]}. \tag{2.31}
$$

In WLAN, for example, the estimation is carried out in two long preamble symbols [14, 72], and they are averaged together. After the sampling point selection, the frequency response of the channel with the selected sampling points during the data period, $\mathbf{H}[k]$, is expressed as

$$\mathbf{H}[k] = \begin{bmatrix} H_0[k] \\ H_1[k] \\ \vdots \\ H_{G-1}[k] \end{bmatrix} = \begin{bmatrix} \hat{H}^p_{\Delta_0}[k] \\ \hat{H}^p_{\Delta_1}[k] \\ \vdots \\ \hat{H}^p_{\Delta_{G-1}}[k] \end{bmatrix} \tag{2.32}$$

where $\Delta_g (g = 0, 1, \ldots, G-1)$ indicates the gth sampling point defined in Eq. (2.14).

In the conventional scheme, uniform sampling interval is assumed and the initial phase of the sampling is selected. The sampling point in Eq. (2.12) is given as

$$\Delta_g(\gamma_u) = \Delta_0(\gamma_u) + g\frac{\Gamma}{G} \tag{2.33}$$

where $\Delta_0(\gamma_u) = \gamma_u \frac{\Gamma}{G}$ indicates the initial phase of the sampling and $\gamma_u (0 \leqslant \gamma_u \leqslant \frac{\Gamma}{G} - 1)$ is the corresponding index. Since the received signal is sampled at the oversampling rate of G in the data period, there are Γ/G candidates of the initial phase. Figure 2.12(a) shows the candidates of the initial phase when $G = 2$ as an example. In the figure, $\bigcirc$ and $\triangle$ represent the samples corresponding to $g = 0$ and $g = 1$, respectively. As shown in Fig. 2.12(a), the number of possible initial phase of the sampling is $\Gamma/G = 4$. The most of the bit errors occur on the subcarrier experiencing the deepest fade. In the conventional scheme, the index, γ_u, for the initial phase is selected based on the frequency responses of the subcarriers according to the following expression.

$$\underset{\gamma_u}{\text{argmax}}\{\min_k P_G[k, \gamma_u]\} \tag{2.34}$$

where $P_G[k, \gamma_u] = \mathbf{H}'^H[k, \gamma_u]\mathbf{H}'[k, \gamma_u]$ and $\mathbf{H}'[k, \gamma_u]$ is the frequency response on the kth subcarrier when the index of the initial phase is γ_u [55].

In the conventional schemes, the interval between the sampling points is fixed. The proposed scheme employs non-uniform sampling point interval. In the data period, the number of the possible combinations of the sampling points is ${}_\Gamma C_G = \frac{\Gamma!}{G!(\Gamma-G)!}$. Figure 2.12(b) shows the candidates of the sampling points when $G = 2$ as an example. In the figure, $\bigcirc$ and $\triangle$ represent the samples corresponding to $g = 0$ and $g = 1$, respectively. As shown in Fig. 2.12(b), the number of the possible combinations of sampling points is ${}_\Gamma C_G = 28$. In the figure, γ_n is the index for the combination of the sampling points, $\mathbf{S}_G(\gamma_n) = \{\Delta_g\} (g = 0, 1, ..., G-1)$, and

$$0 \leqslant \gamma_n \leqslant {}_\Gamma C_G - 1. \tag{2.35}$$

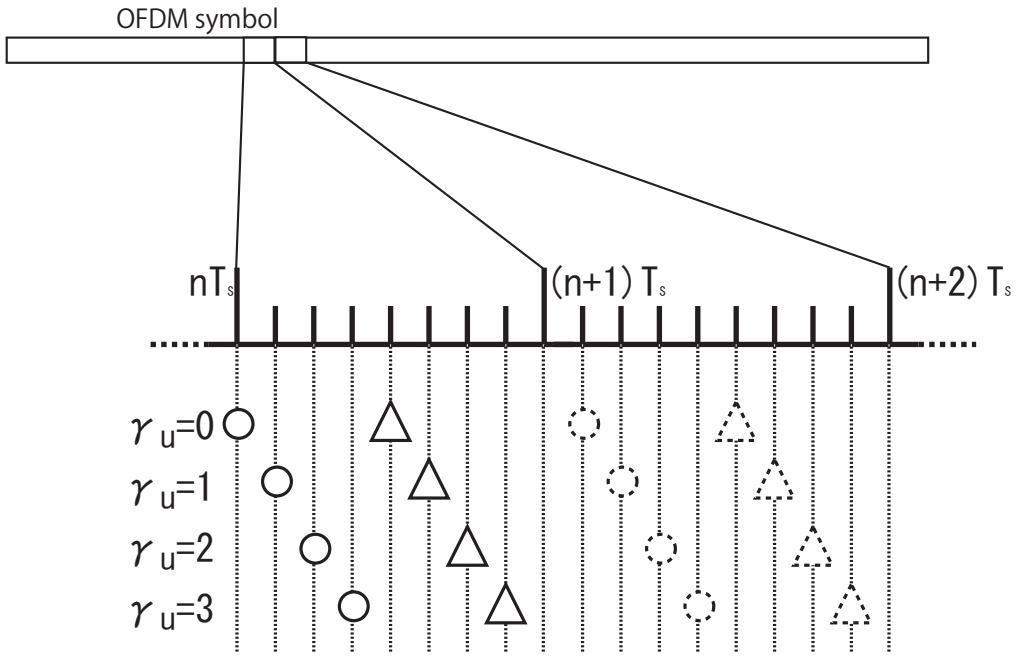

(a) Uniform sampling.

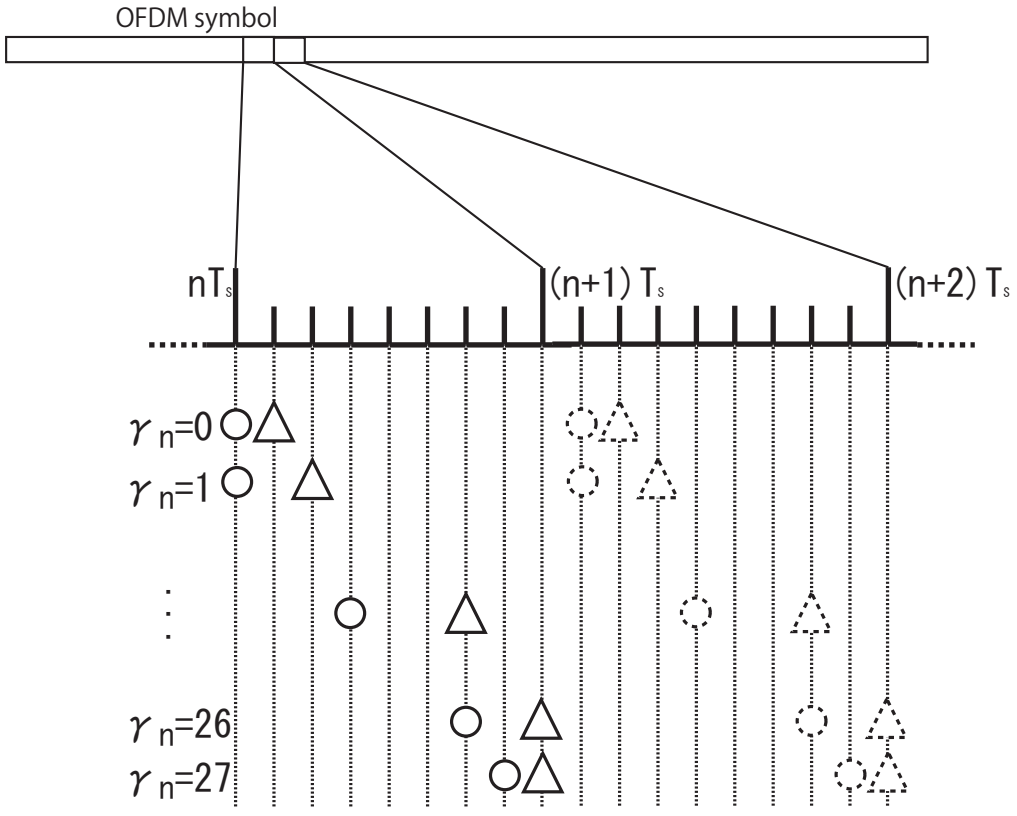

(b) Non-uniform sampling.

Figure 2.12: Candidates of sampling point ($\Gamma = 8, G = 2$).

The most of the bit errors occur on the subcarrier experiencing the deepest fade. In the proposed scheme, the index, γ_n, for the combination of the sampling points is selected

based on the frequency responses according to the following evaluation function.

$$\underset{\gamma_n}{\text{argmax}}\{\min_{k} P_G[k,\gamma_n]\} \tag{2.36}$$

where $P_G[k,\gamma_n] = \mathbf{H}'^{H}[k,\gamma_n]\mathbf{H}'[k,\gamma_n]$ and $\mathbf{H}'[k,\gamma_n]$ is the frequency response on the kth subcarrier for γ_n.

2.2.2.3. Complexity Reduction in Non-uniform Sampling Point Selection

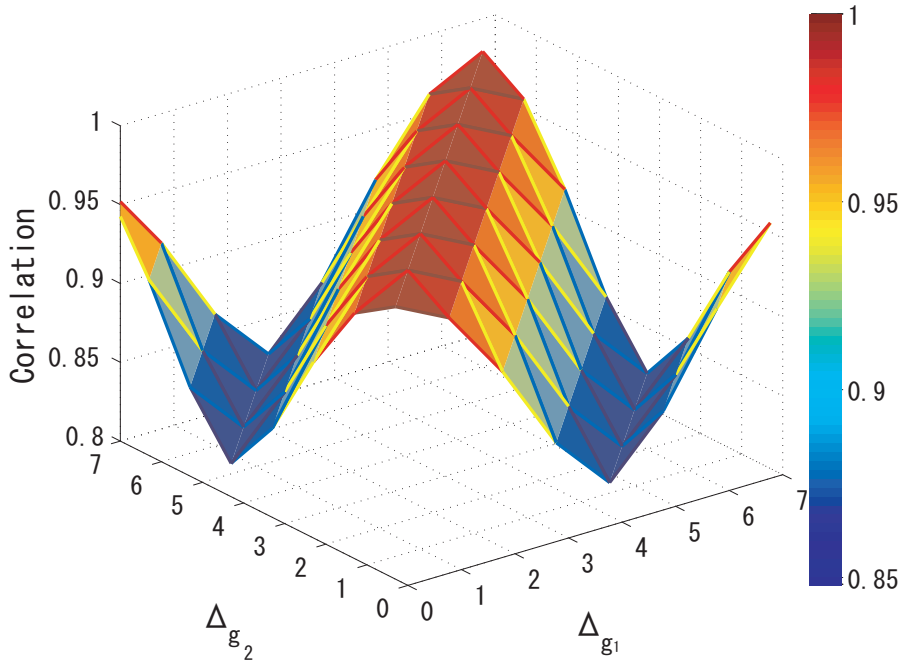

Figure 2.13: Correlation between samples (32 path Rayleigh).

The complexity of the non-uniform sampling point selection scheme is relatively large. To select the sampling point, it needs to calculate ${}_8C_2 = 28$ or ${}_8C_4 = 70$ frequency responses for $G = 2$ or 4, respectively. To reduce the amount of computational complexity, it is desirable to eliminate the combinations of the sampling points which can not achieve path diversity. Correlation between subcarrier responses is shown in Fig. 2.13, which is obtained by

$$\begin{aligned}&[\mathbf{C}_H[k]]_{\Delta_{g_1},\Delta_{g_2}} \\ &= \left| \frac{\mathrm{E}[H_{g_1}[k]H^*_{g_2}[k]]}{\sqrt{\mathrm{E}[H_{g_1}[k]H^*_{g_1}[k]]}\sqrt{\mathrm{E}[H_{g_2}[k]H^*_{g_2}[k]]}} \right|.\end{aligned} \tag{2.37}$$

From Eq. (2.37), when two given sampling points are next to each other, which means $|\Delta_{g_1} - \Delta_{g_2}| = 1$ or 7, the correlation is quite high. In this case, diversity gain is

relatively small. The sampling point indices that include the highly correlated samples are eliminated from the candidates in the proposed sampling point selection scheme. The number of the candidates reduces from ${}_8C_2 = 28$ to 20 for $G = 2$ and from ${}_8C_4 = 70$ to 2(=conventional scheme) for $G = 4$.

2.2.3. Numerical Results

2.2.3.1. Simulation Conditions

Table 2.5: Simulation Conditions

Modulation scheme	1st:QPSK 2nd:OFDM
FFT size	64
Number of subcarriers	64
Number of data subcarriers	48
Number of OFDM packets per trial	100000
Number of OFDM symbols per packet	10
Bandwidth of subcarriers	312.5[kHz]
Preamble length (GI+Preamble)	$1.6 + 6.4[\mu s]$
OFDM symbol length (GI+Data)	$0.8 + 3.2[\mu s]$
Channel estimation	Perfect
	Imperfect (Estimated by T_1 and T_2)

Simulation conditions are presented in Table 2.5. The parameters in the table are based on the IEEE802.11a/g standard [14,72]. The frequency response of the channel is assumed to be constant during one OFDM packet. The structure of the OFDM packet is shown in Fig. 2.14.

Relevant to the IEEE802.11a/g standard, the number of subcarriers, N, is 64 (48 subcarriers are for data symbols, 4 subcarriers are for pilot symbols, and the rests are null subcarriers) [14, 72]. For channel estimation, two symbols, T_1 and T_2 are used as shown in Fig. 2.14 and averaged together. In the simulation, perfect and imperfect channel estimations (CEs) for equalization are investigated, respectively. For the imperfect channel estimation, the frequency responses are estimated with the preamble

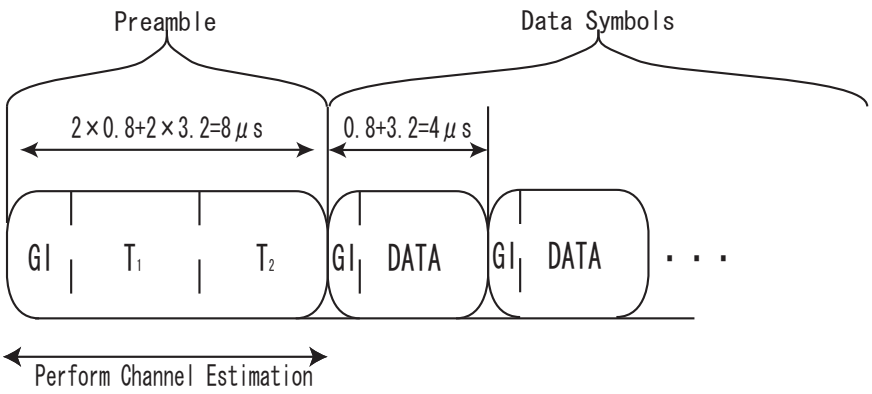

Figure 2.14: OFDM packet structure for simulation.

symbols, T_1 and T_2. Ideal carrier recovery is assumed here. The total response of the transmitter and receiver filters is assumed to be truncated sinc pulse with the duration of $2T_s$ [45]. The oversampling rate in the preamble period is fixed to $\Gamma = 8$. In the data period, γ_u and γ_n are selected according to the evaluation functions in Eqs. (2.34) and (2.36). In this simulation, the oversampling ratio at the data period, G, is selected among $\{1, 2, 4\}$. As channel models, 32 path Rayleigh fading with uniform delay profile and Indoor Residential A are assumed [74].

Figures 2.15, 2.19 and 2.21 show the BER performance for the above channel models with perfect CE. The BER curves with imperfect CE are shown in Fig. 2.20. In the figures, 'Fixed' means the BER curves with the fixed initial sampling point ($n_0 = 0, \gamma_u = 0$). 'Conv.' denotes the BER curves for the conventional scheme in Eq. (2.34). 'Pro.' indicates the BER curves with the proposed scheme in Eq. (2.36). The low complexity version of the proposed scheme is indicated as 'Low-Comp.'.

2.2.3.2. Uniform Sampling Point Selection and Non-uniform Sampling Point Selection

Figure 2.15 shows the BER performance on the 32 path Rayleigh fading channel with perfect CE. The conventional uniform sampling scheme improves the BER when $G = 1$ while the improvement is less significant when $G = 2$. The BER curve of the proposed scheme with $G = 2$ is slightly better as compared to that of the fixed sampling point scheme with $G = 4$. On the other hand, the BER curve of the proposed scheme with $G = 4$ is worse than that with $G = 2$. This is because the noise generated from the other subcarriers through noise-whitening in Eq. (2.26) deteriorates the BER performance.

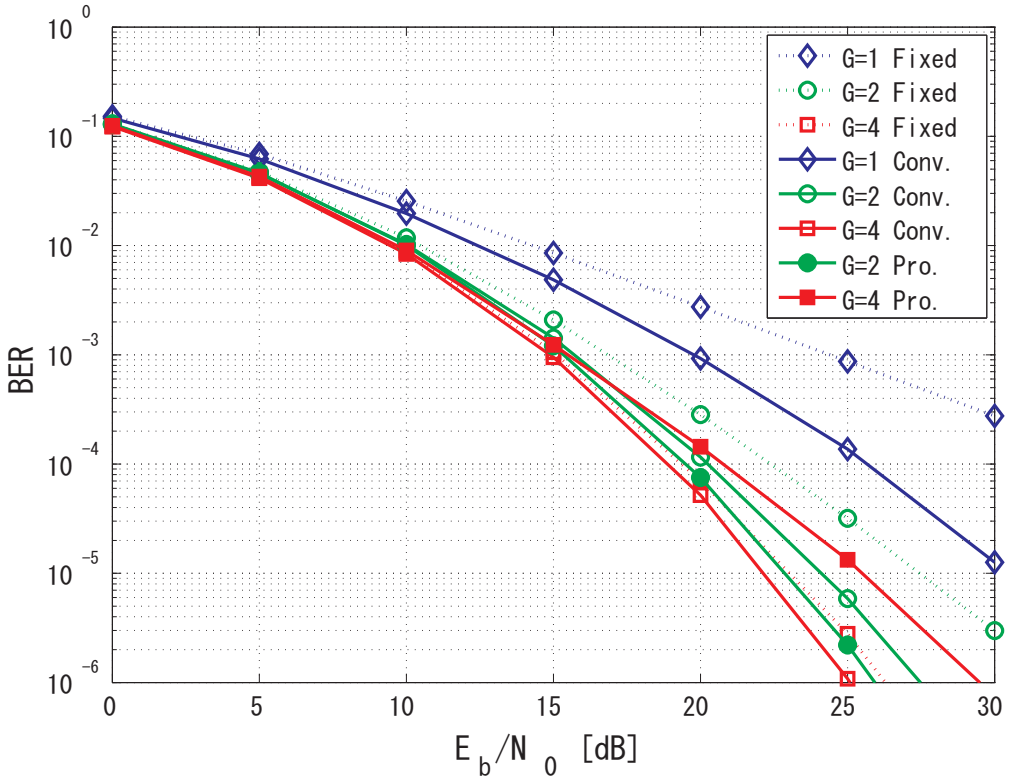

Figure 2.15: 32 path Rayleigh fading model.

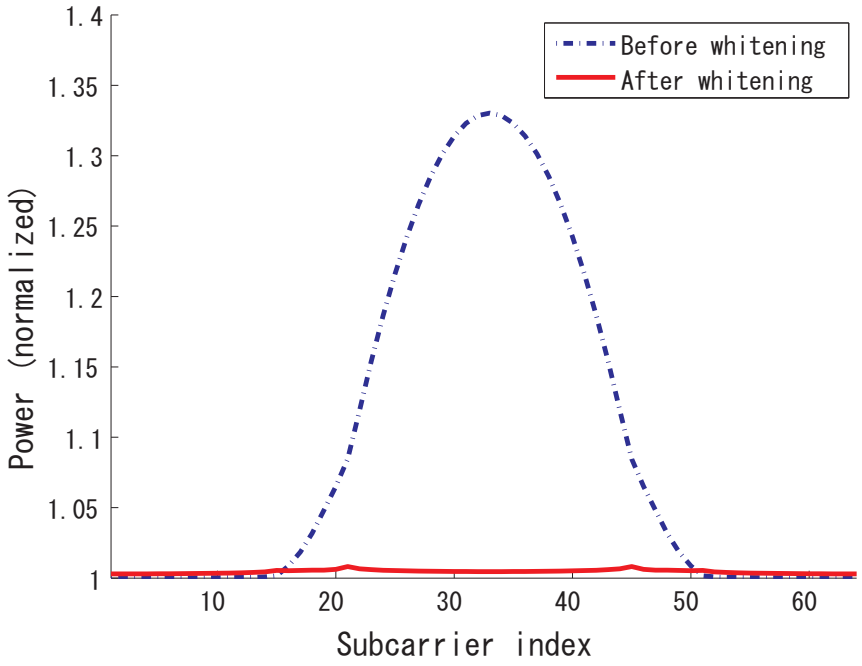

(a) $\gamma_n = \gamma_{ns}$

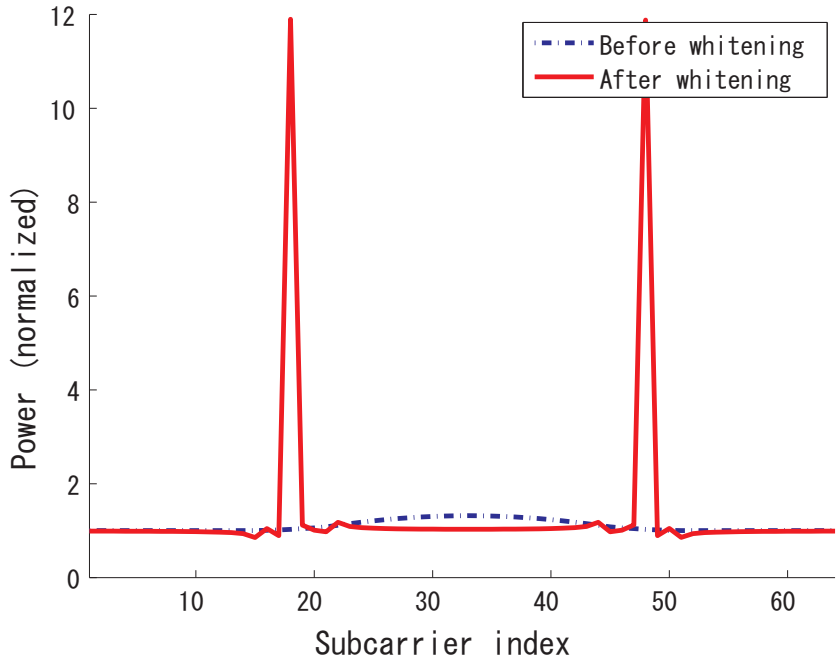

(b) $\gamma_n = \gamma_{nl}$

Figure 2.16: Noise power spectrum.

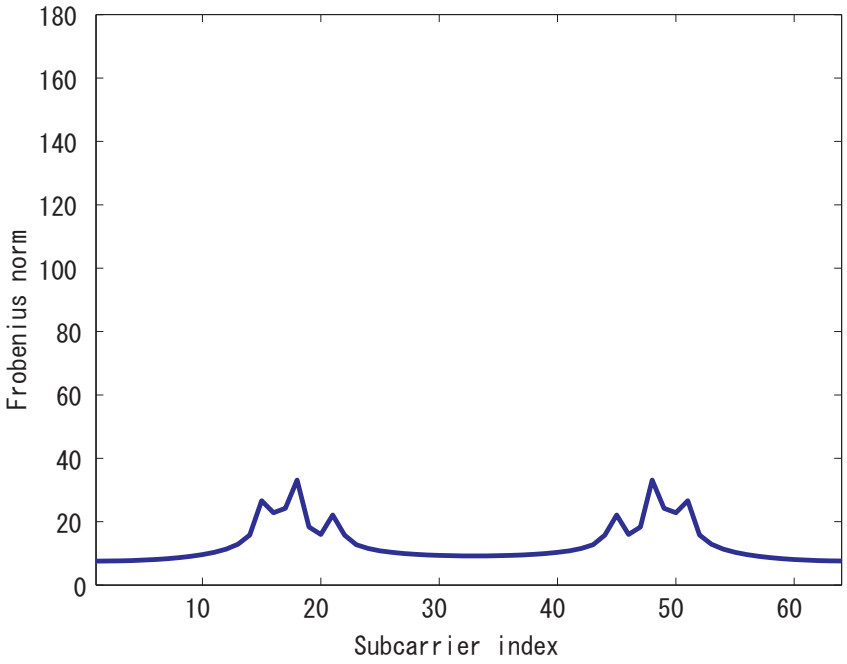

(a) $\gamma_n = \gamma_{ns}$

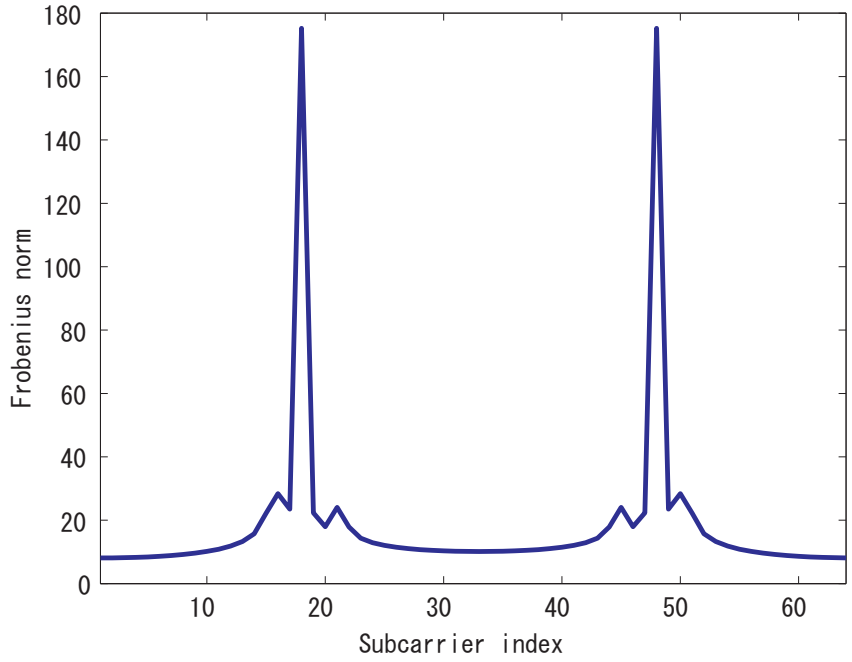

(b) $\gamma_n = \gamma_{nl}$

Figure 2.17: Frobenius norm of $\mathbf{R}_w^{-\frac{1}{2}}[k]$.

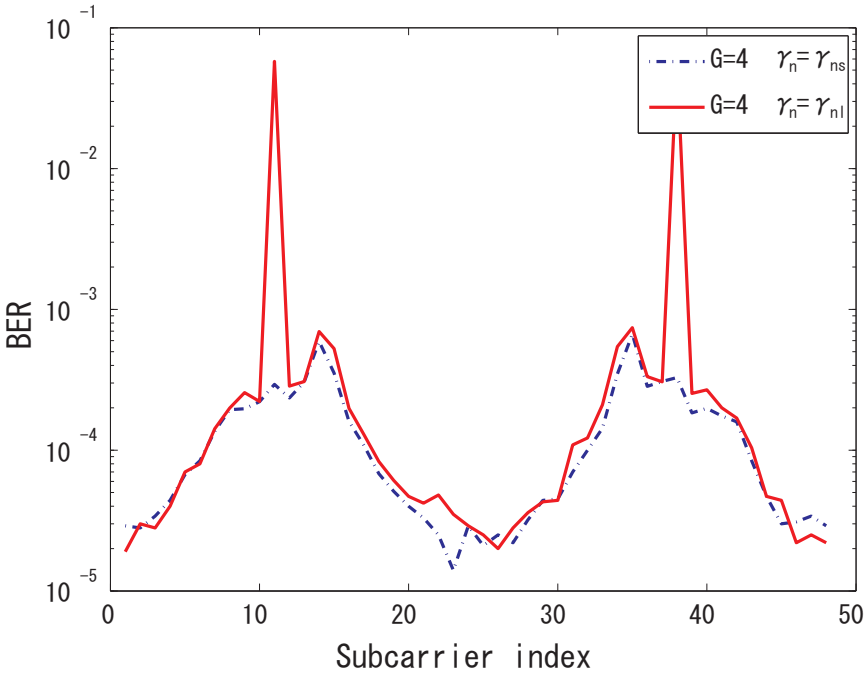

(a) BER vs. data subcarrier$E_b/N_0 = 20$[dB].

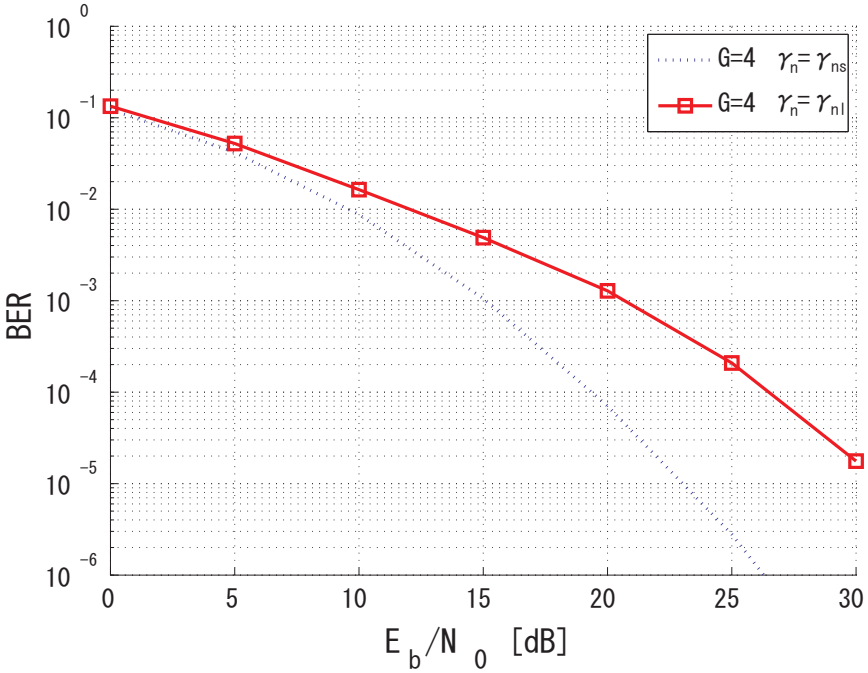

(b) BER vs. E_b/N_0.

Figure 2.18: BER comparison of $\gamma_n = \gamma_{ns}$ and γ_{nl}.

In Figs.2.16 (a) and (b), the power spectrum of the noise before and after whitening by Eq. (2.26) is shown when $G = 4$ and $\gamma_n = \gamma_{ns}$ or γ_{nl}, respectively. Those two sets of the sampling points, γ_{ns} and γ_{nl}, presented in Figs.2.17 (a) and (b) have the smallest and largest average Frobenius norms of $\mathbf{R}_w^{-\frac{1}{2}}[k]$. From Fig. 2.16(a), The whitening filter equalizes the spectrum of the correlated noise samples when $\gamma_n = \gamma_{ns}$. On the other hand, when $\gamma_n = \gamma_{nl}$, the noise power grows on the 18th and 48th subcarriers. On these subcarriers, the Frobenius norm of $\mathbf{R}_w^{-\frac{1}{2}}[k]$ is also large as shown in Fig. 2.17(b). The BER curves between $\gamma_n = \gamma_{ns}$ and γ_{nl} when $G = 4$ are compared in Figs.2.18 (a) and (b). In the Fig. 2.18(a), E_b/N_0 is fixed to 20[dB]. As exploited in the Fig. 2.18(a), if the Frobenius norm of $\mathbf{R}_w^{-\frac{1}{2}}[k]$ is large, the BER also increases as shown in Fig. 2.18(b). As given in Appendix A, this is due to the correlated noise component after noise-whitening [78].

2.2.3.3. Complexity Reduction in Non-uniform Sampling Point Selection

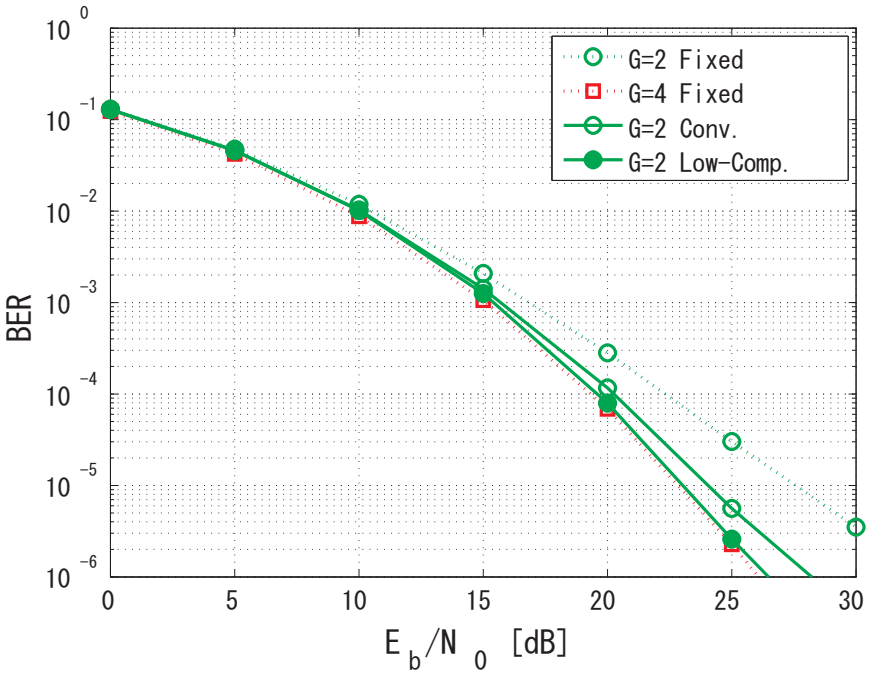

Figure 2.19: 32 path Rayleigh fading model (perfect CE).

Figure 2.19 shows the numerical results on the 32 path Rayleigh fading channel with perfect CE. The low-complexity scheme, '$G = 2$ Low-Comp.', achieves almost the same BER as that of '$G = 4$ Fixed'. Channel correlation and noise correlation from the other subcarriers increase with G. In this channel model, delay paths have the same average power. However, for a certain instance, it is possible that strong paths arrive

non-uniformly in terms of their delays. Therefore, '$G = 2$ Low-Comp.' can extract the stronger paths and less correlated noise than '$G = 4$ Fixed'. This is the reason why '$G = 2$ Low-Comp.' achieves the same performance as '$G = 4$ Fixed'. From Figs.2.15 and 2.19, this means that the low complexity version of the proposed scheme achieves almost the same performance as the original proposed scheme.

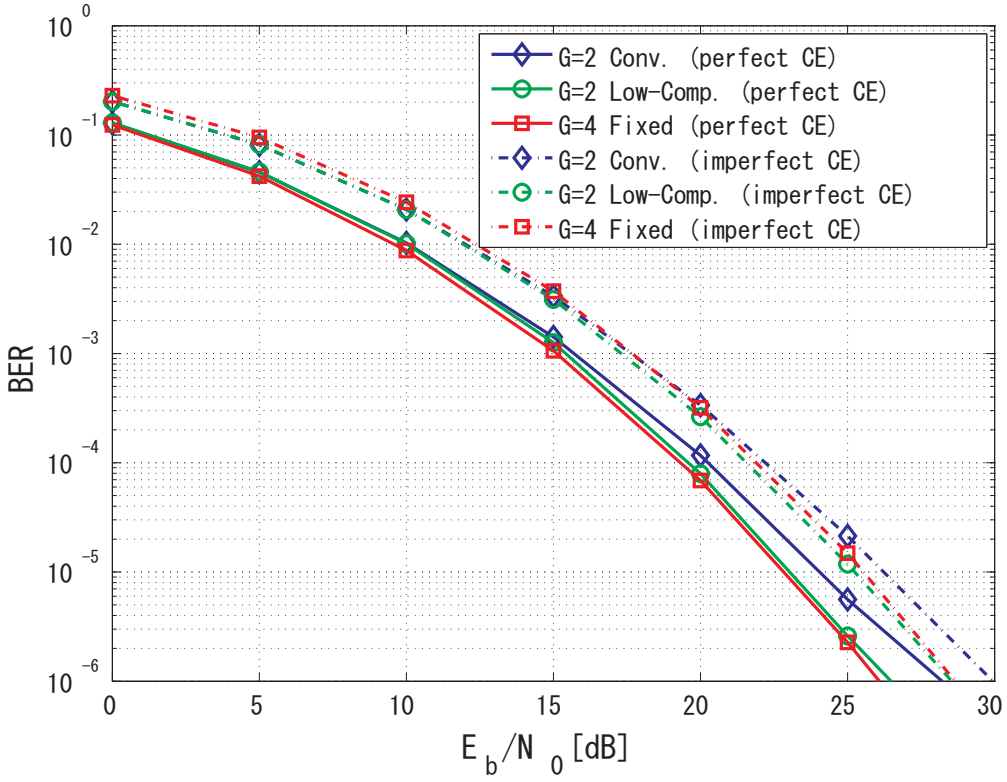

Figure 2.20: 32 path Rayleigh fading model (perfect and imperfect CE).

Figure 2.20 shows the BER curves with perfect and imperfect CEs. For the imperfect CE, the BER performance is deteriorated by about 2[dB] because of estimation error due to the noise. However, the same as Fig. 2.19, the proposed low complexity scheme with $G = 2$ achieves almost the equivalent performance with the conventional scheme with $G = 4$. In the imperfect CE case, the BER performance of the proposed low complexity version of '$G = 2$' is slightly better than that of '$G = 4$ Fixed'. It is because '$G = 2$ Low-Comp.' has less noise effect than '$G = 4$ Fixed' in both preamble and data period.

The BER performance on the Indoor Residential A is evaluated in Fig. 2.21. On Indoor Residential A, which has the smallest delay spread of the four, the improvement of the BER curves for '$G = 2$' is relatively insignificant as compared to the 32 path

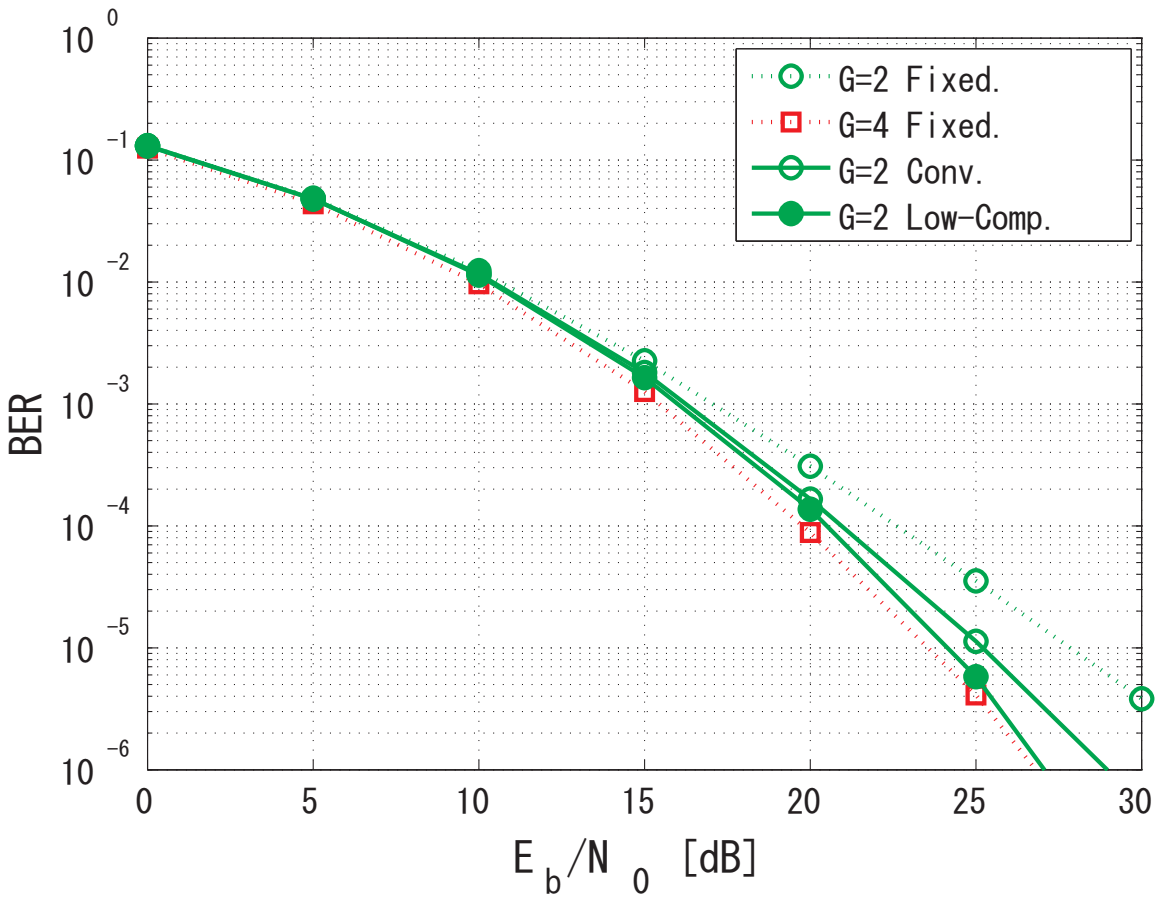

Figure 2.21: Indoor Residential A (perfect CE).

Rayleigh fading model. Therefore, if the delay spread is not large enough, path diversity through FS and sampling point selection are less effective with both perfect and imperfect CEs. In Fig. 2.19 the 32 path Rayleigh fading model has enough delay spread to improve the BER performance through FS and sampling point selection. The BER performance of '$G = 2$ Low-Comp.' is slightly better than that of '$G = 4$ Fixed'. On the other hand, on Indoor Residential A the BER improvement is relatively insignificant as compared to the other channel model as shown in Fig. 2.21. The relationship between the BER and the delay spread is investigated as shown in Fig. 2.22. The BER curves with perfect CE are investigated in Fig. 2.22. When the delay spread, τ_{RMS}, is smaller than 60 [ns], the BER of '$G = 4$ Fixed' is lower than that of '$G = 2$ Low-Comp.'. When τ_{RMS} is larger than 90 [ns], the BER of '$G = 2$ Low-Comp.' is slightly better than that of '$G = 4$ Fixed'. It is the same for imperfect CE when τ_{RMS} is more than 40 [ns] as the inaccuracy of the channel estimation diminishes the difference. From Fig. 2.22, the oversampling rate is required to be higher as the delay spread is small. On the other

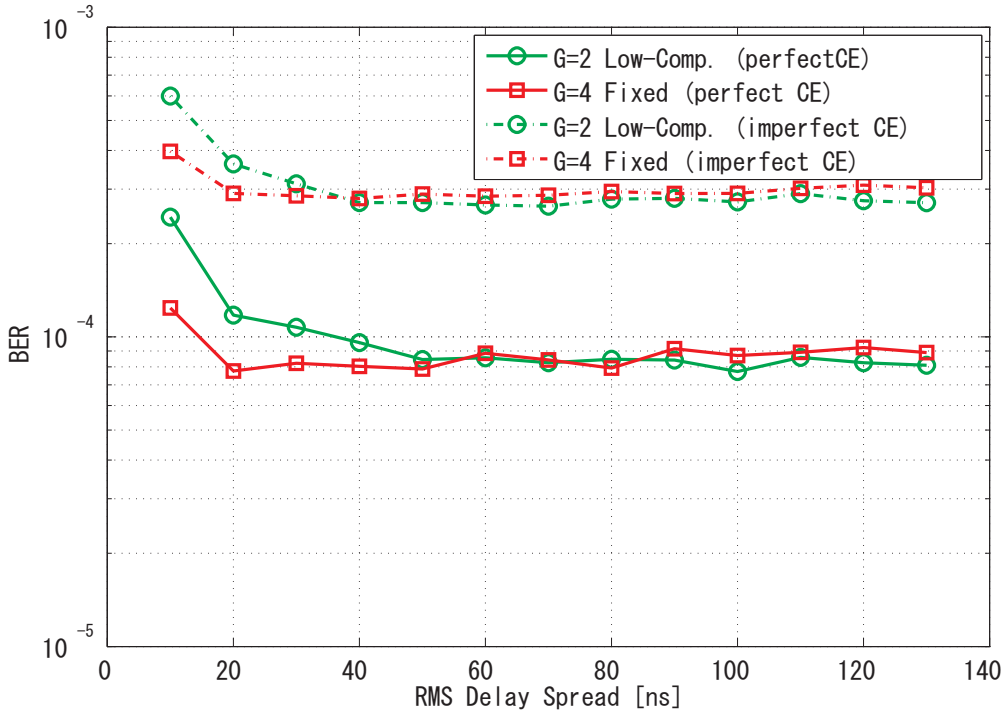

Figure 2.22: BER vs. Delay Spread.

hand, when τ_{RMS} is large, the oversampling rate can be kept small.

In this subsection, the computational complexity of the proposed low complexity scheme is evaluated as compared to that of '$G = 4$ Fixed' in terms of the number of multiplications. The number of multiplications for each process such as DFT, noise-whitening, MRC, and sampling point selection in Eqs. (2.34) or (2.36) are shown in Table 2.6. The total amount of computational complexity for the fixed sampling point scheme with $G = 4$ ('$G = 4$ Fixed'), the proposed non-uniform sampling point selection scheme with $G = 2$ ('$G = 2$ SPS'), and the proposed low complexity scheme with $G = 2$ ('$G = 2$ Low-Comp.') per OFDM packet are shown in Table 2.7. Here, it is assumed that the oversampling rate is 4 during both the preamble period and the data period in '$G = 4$ Fixed' while it is 8 during the preamble period and 2 during the data period in the proposed schemes. In the table, '10 symbols' and '100 symbols' represent the number of OFDM symbols per packet transmitted. As compared with '$G = 4$ Fixed' in Table 2.7, '$G = 2$ Low-Comp.' reduces the computational complexity by a factor of 2 when the number of symbols per packet is 100. This difference is because the fixed sampling point scheme requires 4 DFT processes per symbol while the proposed scheme requires only 2 in the data period. Thus, even though the selection of the sampling point requires additional 28 DFT processes per preamble symbol, the total amount of

complexity decreases. Compared with '$G = 2$ SPS', '$G = 2$ Low-Comp.' can reduce 2304 multiplications per packet in the SPS.

Table 2.6: Computational Complexity

	Number of Multiplications
DFT	$N \log_2 N$
Noise-whitening	G^2
MRC	G
Sampling Point Selection	G

Table 2.7: Total Computational Complexity

	10 symbols	100 symbols
'$G = 4$ Fixed'	33792	287232
'$G = 2$ SPS'	21696	116736
'$G = 2$ Low-Comp.'	19392	114432

2.2.4. Conclusions

In this subchapter, the sampling point selection schemes for the FS OFDM receiver have been proposed. In the conventional scheme, the interval between the sampling points is fixed to $\frac{T_S}{G}$ and it cannot extract the multipaths which arrive non-uniformly in the delay domain. In this chapter non-uniform sampling point selection has been proposed. In this scheme, the interval between the sampling points is not fixed. It then improves diversity gain by about 2 [dB] when the oversampling rate is 2. However, it actually deteriorates the performance when the oversampling rate is 4. This is due to the correlation of the noise samples. In addition, as the oversampling rate increases, the complexity for the sampling point selection grows exponentially. Therefore, this chapter has also proposed the low-complexity sampling point selection scheme to eliminate the specific sets of the sampling points which lead to large noise correlation. In the low-complexity non-uniform sampling point selection scheme, the complexity for the sampling point selection with $G = 2$ has been reduced by about 70% of the original one while it maintains the equivalent BER. As compared to the fixed sampling point selection scheme, the total complexity including the demodulation of 100 symbols decreases by a factor of 2. The proposed scheme with $G = 2$ achieves slightly better BER than the fixed sampling point scheme with $G = 4$ when the RMS delay spread is larger

than 40 [ns] for imperfect CE. Therefore, both path diversity and complexity reduction have been achieved with the proposed scheme.

Chapter 3

Precoded Transmit Path Diversity in FS-OFDM on UWB Channels

3.1. Precoding on Time Invariant Channels

3.1.1. Introduction

In DS/SS or Impulse radio (IR) UWB communications, a rake receiver has been proposed to resolve multipath components and achieve path diversity [57–59]. In this scheme, the receiver needs to perform channel estimation and diversity combining, etc. These signal processing increases computational complexity in a mobile terminal.

Prerake has been proposed to shift these signal processing tasks from the mobile terminal to a receiver [29, 60–62]. In this system, the receiver transmits the signal generated by convolution between the transmit symbols and the finite impulse response (FIR) filter whose coefficients are generated through reverse and conjugate operations of the impulse response of the channel known at the transmitter side. The same as the rake scheme, prerake can achieve path diversity without combining at the receiver side. In [60], a prerake combining scheme is proposed when a pulse interval is smaller than a path interval and the coefficients of the impulse response of the channel are independent and Rayleigh distributed in an IR-UWB system. [61, 62] have proposed precombining schemes which tackle an IPI problem when the pulse interval is longer than the path interval.

On the other hand, in an OFDM system, prerake has not been proposed while FS has been investigated to achieve path diversity with a single antenna [45, 50–52, 64–66]. However, in the FS-OFDM system, it is necessary to oversample a received signal and it leads to large power consumption in a small mobile terminal.

In this subchapter, a precoded transmit path diversity scheme in an OFDM system has been proposed. The proposed scheme makes use of the impulse response of the

channel with the resolution of the FS interval and can achieve path diversity without oversampling the received signal.

3.1.2. System Model

3.1.2.1. OFDM System

Suppose the information symbol on the kth subcarrier is $S[k]$ $(k = 0, ..., N-1)$, the OFDM symbol is then given as

$$x[n] = \frac{1}{\sqrt{N}} \sum_{k=0}^{N-1} S[k] e^{j\frac{2\pi nk}{N}} \tag{3.1}$$

where $n(n = 0, 1, ..., N-1)$ is the time index. A GI is appended before transmission. N_{GI} is the length of the GI.

The baseband signal at the output of the filter is given by

$$x(t) = \sum_{n=-N_{\mathrm{GI}}}^{N-1} x[n] p(t - nT_s) \tag{3.2}$$

where $p(t)$ is the impulse response of the baseband filter, T_s is the symbol duration, and NT_s is the duration of the OFDM symbol. This signal is upconverted and transmitted through a multipath channel with the impulse response of a physical channel $c(t)$. The received signal after the down conversion is given as

$$y(t) = \sum_{n=-N_{\mathrm{GI}}}^{N-1} x[n] h(t - nT_s) + v(t) \tag{3.3}$$

where $h(t)$ is the impulse response of the composite channel and is given by $h(t) := p(t) \star c(t) \star p(-t)$ and $\star$ is convolutional operation. $v(t)$ is the additive Gaussian noise generated at the receiver. For the multipath channel, $c(t)$ and $h(t)$ can be expressed as follows.

$$c(t) = \sum_{l=0}^{L-1} \alpha_l \delta(t - \tau_l) \tag{3.4}$$

$$h(t) = \sum_{l=0}^{L-1} \alpha_l p_2(t - \tau_l) \tag{3.5}$$

where $p_2(t) := p(t) \star p(-t)$is the deterministic correlation of $p(t)$ and normalized as $p_2(0) = 1$. L is the number of multipath, and α_l and τ_l are the amplitude and delay of the lth path, respectively.

If $y(t)$ is sampled at T_s, its polyphase components can be expressed as

$$y[n] = \sum_{m=-N_{\mathrm{GI}}}^{N-1} x[m] h_g[n - m] + v[n]$$

where $y[n]$, $h[n]$, $v[n]$ are the sampled versions of $y(t)$, $h(t)$, $v(t)$ and expressed as follows, respectively.

$$y[n] := y(nT_s), \tag{3.6}$$

$$h[n] := h(nT_s), \tag{3.7}$$

$$v[n] := v(nT_s). \tag{3.8}$$

After removing the GI and taking DFT at each branch, the received symbol is given by

$$Y[k] = H[k]S[k] + V[k] \tag{3.9}$$

where $Y[k]$, $H[k]$, $V[k]$ are the DFT outputs of $y[n]$, $h[n]$,$v[n]$, respectively.

3.1.2.2. Transmit Path Diversity

In this subsection, the conventional prerake scheme is applied to the OFDM system [60–62]. The transmitted prerake signal, $x_c(t)$, is given as

$$\begin{aligned} x_c(t) &= \sqrt{\frac{1}{\nu_c}} c^*(-t) \star x(t) \\ &= \sqrt{\frac{1}{\nu_c}} \left(\sum_{m=0}^{L-1} \alpha_m^* \delta(t+\tau_m) \right) \star x(t) \\ &= \sqrt{\frac{1}{\nu_c}} \sum_{m=0}^{L-1} \alpha_m^* x(t+\tau_m) \end{aligned} \tag{3.10}$$

where ν_c is a power normalization factor that normalizes the received signal power to that without the prerake scheme. Therefore, the total impulse response of the channel including the prerake combining is expressed as

$$\begin{aligned} h_c(t) &= \sqrt{\frac{1}{\nu_c}} c^*(-t) \star p(t) \star c(t) \star p(-t) \\ &= \sqrt{\frac{1}{\nu_c}} \sum_{m=0}^{L-1} \sum_{l=0}^{L-1} \alpha_m^* \alpha_l p_2(t+\tau_m-\tau_l). \end{aligned} \tag{3.11}$$

With the sampled version of $h_c(t)$, $h_c[n] = h_c(nT_s)$, the frequency response of the channel, $H_c[k]$, is given as

$$\begin{aligned} H_c[k] &= \mathrm{DFT}\left[h_c[n]\right] \\ &= \sqrt{\frac{1}{\nu_c}} \sum_{m=0}^{L-1} \sum_{l=0}^{L-1} \sum_{n=0}^{N-1} \alpha_m^* \alpha_l p_2(nT_s+\tau_m-\tau_l) e^{-j\frac{2\pi kn}{N}}. \end{aligned} \tag{3.12}$$

By using multipath coefficient vector, $\boldsymbol{\alpha} = [\alpha_0 \cdots \alpha_{L-1}]^T$, Eq. (3.12) is expressed as

$$H_c[k] = \sqrt{\frac{1}{\nu_c}} \boldsymbol{\alpha}^H \mathbf{R}[k] \boldsymbol{\alpha} \tag{3.13}$$

where $\mathbf{R}[k]$ is the path correlation matrix of size $L \times L$ and it's (m,l)th component is expressed as

$$[\mathbf{R}[k]]_{m,l} = \sum_{n=0}^{N-1} p_2(nT_s + \tau_m - \tau_l) e^{-j\frac{2\pi kn}{N}}. \tag{3.14}$$

The argument of the received signal, $\arg\{\boldsymbol{\alpha}^H \mathbf{R}[k]\boldsymbol{\alpha}\}$, is estimated at the receiver. However, $|\,\boldsymbol{\alpha}^H \mathbf{R}[k]\boldsymbol{\alpha}\,|$ is degraded on certain subcarriers. Different from DS/SS of IR-UWB systems, the IPI within one OFDM symbol expressed in Eq. (3.14) is generated as shown in Fig. 3.1. Therefore, the diversity gain of the conventional prerake combining scheme is limited. The block diagram of the proposed scheme is shown in Fig. 3.2.

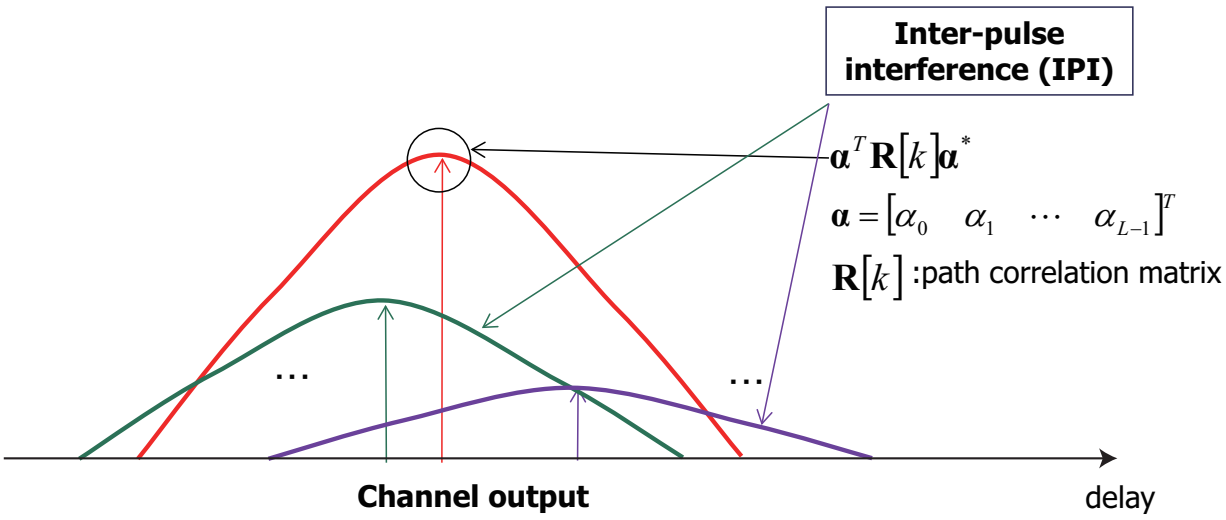

Figure 3.1: IPI induced by using existing prerake.

The proposed scheme precodes the information symbols on the kth subcarrier that is expressed as $S[k](k = 0, ..., N-1)$. The precoded information symbol vector of size $L \times 1$, $\mathbf{S}_p[k](k = 0, ..., N-1)$, is given as the following equation:

$$\mathbf{S}_p[k] = \begin{bmatrix} S_p^0[k] \\ S_p^1[k] \\ \vdots \\ S_p^{L-1}[k] \end{bmatrix} = \begin{bmatrix} W_0[k] \\ W_1[k] \\ \vdots \\ W_{L-1}[k] \end{bmatrix} S[k] \tag{3.15}$$

where $\mathbf{W} = [W_0[k] \cdots W_{L-1}[k]]^T$ is the weighting vector of size $L \times 1$ given as

$$\mathbf{W}[k] = \mathbf{R}^{-1}[k]\boldsymbol{\alpha}^*. \tag{3.16}$$

The precoded information symbols $\mathbf{S}_p[k]$ are input to the OFDM demodulators in parallel. The mth OFDM symbol $(m = 0, ..., L-1)$, $x_p^m[n]$, and the baseband signal, $x_p^m(t)$,

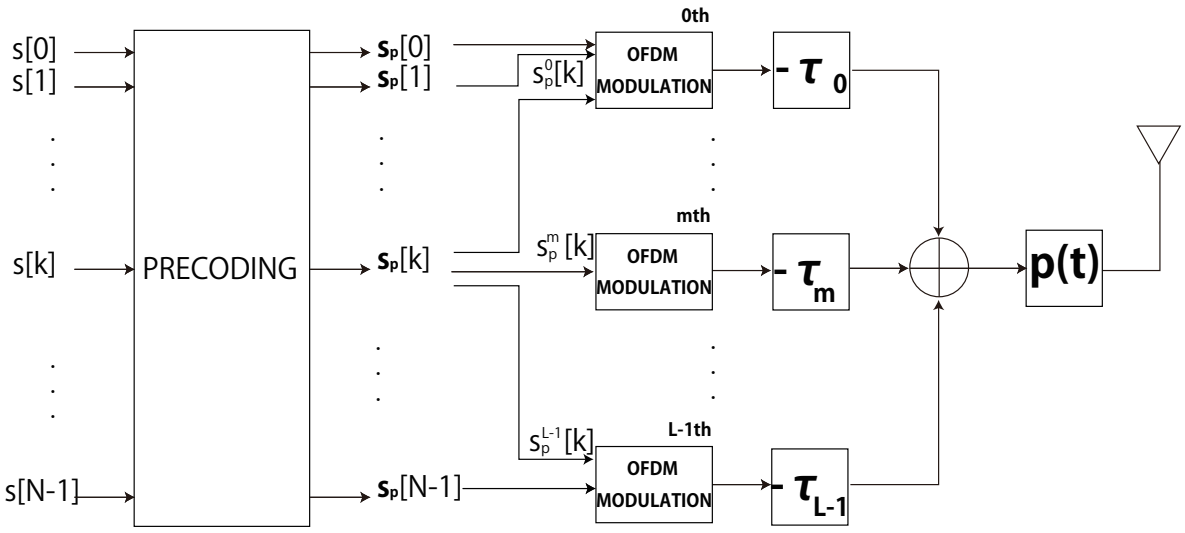

Figure 3.2: Block diagram of the precoded transmit diversity scheme.

are expressed as following equations, respectively.

$$x_p^m[n] = \sqrt{\frac{1}{N}} \sum_{k=0}^{N-1} S_p^m[k] e^{j\frac{2\pi nk}{N}} = \sqrt{\frac{1}{N}} \sum_{k=0}^{N-1} w_m[k] S[k] e^{j\frac{2\pi nk}{N}}. \tag{3.17}$$

$$\begin{aligned} x_p^m(t) &= \sum_{n=-N_{\mathrm{GI}}}^{N-1} x_p^m[n] p(t - nT_s) \\ &= \sqrt{\frac{1}{N}} \sum_{n=-N_{\mathrm{GI}}}^{N-1} \sum_{k=0}^{N-1} w_m[k] S[k] e^{j\frac{2\pi nk}{N}} p(t - nT_s). \end{aligned} \tag{3.18}$$

The transmitted signal is generated by

$$\begin{aligned} x_p(t) &= \sqrt{\frac{1}{\nu_p}} \sum_{m=0}^{L-1} x_p^m(t + \tau_m) \\ &= \sqrt{\frac{1}{\nu_p N}} \sum_{m=0}^{L-1} \sum_{n=-N_{\mathrm{GI}}}^{N-1} \sum_{k=0}^{N-1} w_m[k] S[k] e^{j\frac{2\pi nk}{N}} p(t - nT_s + \tau_m) \end{aligned} \tag{3.19}$$

where ν_p is the power normalization factor. Suppose $g(t)$ is obtained by convolution between the impulse response of the channel $c(t)$, and the impulse response of the filter at the receiver side $p(-t)$. Then, $g(t)$ is expressed as

$$g(t) = c(t) \star p(-t) = \sum_{l=0}^{L-1} \alpha_l p(-t - \tau_l). \tag{3.20}$$

The received signal is obtained by the following equations:

$$\begin{aligned} y_p(t) &= x_p(t) \star g(t) + v(t) = \int x_p(t - \xi) g(\xi) d\xi + v(t) \\ &= \sqrt{\frac{1}{\nu_p N}} \sum_{m=0}^{L-1} \sum_{l=0}^{L-1} \sum_{n=-N_{\mathrm{GI}}}^{N-1} \sum_{k=0}^{N-1} w_m[k] \alpha_l S[k] e^{j\frac{2\pi nk}{N}} p_2(t - nT_s + \tau_m - \tau_l) + v(t). \end{aligned} \tag{3.21}$$

As shown in Eq. (3.13), the frequency response of the total precoded channel is expressed as

$$\begin{aligned} \mathbf{w}^T\mathbf{R}[k]\boldsymbol{\alpha} &= \left(\mathbf{R}^{-1}[k]\boldsymbol{\alpha}^*\right)^T \mathbf{R[k]}\boldsymbol{\alpha} = \boldsymbol{\alpha}^H\mathbf{R}^{-1}[k]\mathbf{R}[k]\boldsymbol{\alpha} \\ &= \boldsymbol{\alpha}^H\boldsymbol{\alpha} = \sum_{l=0}^{L-1} \mid \alpha_l \mid^2 . \end{aligned} \tag{3.22}$$

By precoding the information symbols, the IPI is removed and path diversity is achieved in the proposed scheme.

3.1.3. Numerical Results

3.1.3.1. Simulation Conditions

Table 3.1: Simulation conditions.

Modulation	1st: QPSK 2nd: OFDM
Channel	Two path Rayleigh Fading IEEE802.15.3a CM1-4
Channel Estimation	Ideal
Coding	Convolutional coding
Coding rate	1/2
Constraint length(K)	7
Points of FFT	128
Number of subcarriers	128
OFDM Symbol Duration	312.5 [ns]
Cyclic Prefix	60.61 [ns]
Decoder	Soft decision Viterbi

Simulation conditions are presented in Table 3.1. Modulation parameters are following MB-OFDM system [79]. Convolutional code with the coding rate of 1/2 and the constraint length of 7 is used for forward error correction. QPSK and OFDM are used for the first and second modulations. The number of subcarriers, N, is 128. The OFDM symbol duration is 312.5 nsec and the cyclic prefix is 60.61 nsec. At the receiver side, soft decision Viterbi decoder is employed. The impulse response of a channel is assumed to be constant during one OFDM packet and known at the transmitter side. The total response of the transmitter and receiver filters is assumed to be truncated sinc pulse with the duration of T_s. Assumed channel models are two path Rayleigh fading with uniform delay profile and CM1 $-$ 4. Regarding the two path Rayleigh fading model, BER performance is evaluated with the delay between the paths, $\tau_d = \mid \tau_0 - \tau_1 \mid$. CM1

is a line-of-sight (LOS) channel within a distance between 0m and 4m. CM2 is a non-line-of-sight (NLOS) channel within a distance between 0m and 4m. CM3 is a NLOS channel within a distance between 4m and 10m. CM4 is a dense multipath NLOS channel. For each channel model, 100 impulse responses are generated. It is expected that all impulse responses are tested. Then, the best 90 BERs are averaged [79, 80]. In the transmitter, all of the path components are used for the precoding transmit diversity. In the figures, "No precoding" means the BER curves without diversity combining at either the transmitter or the receiver. "Conventional scheme" is the BER curves of the conventional precoding scheme which is expressed in Eq. (3.10). "Proposed scheme" indicates the BER curves of the proposed precoding scheme in which the precoded information symbols are generated by Eq. (3.15).

3.1.3.2. Simulation Results

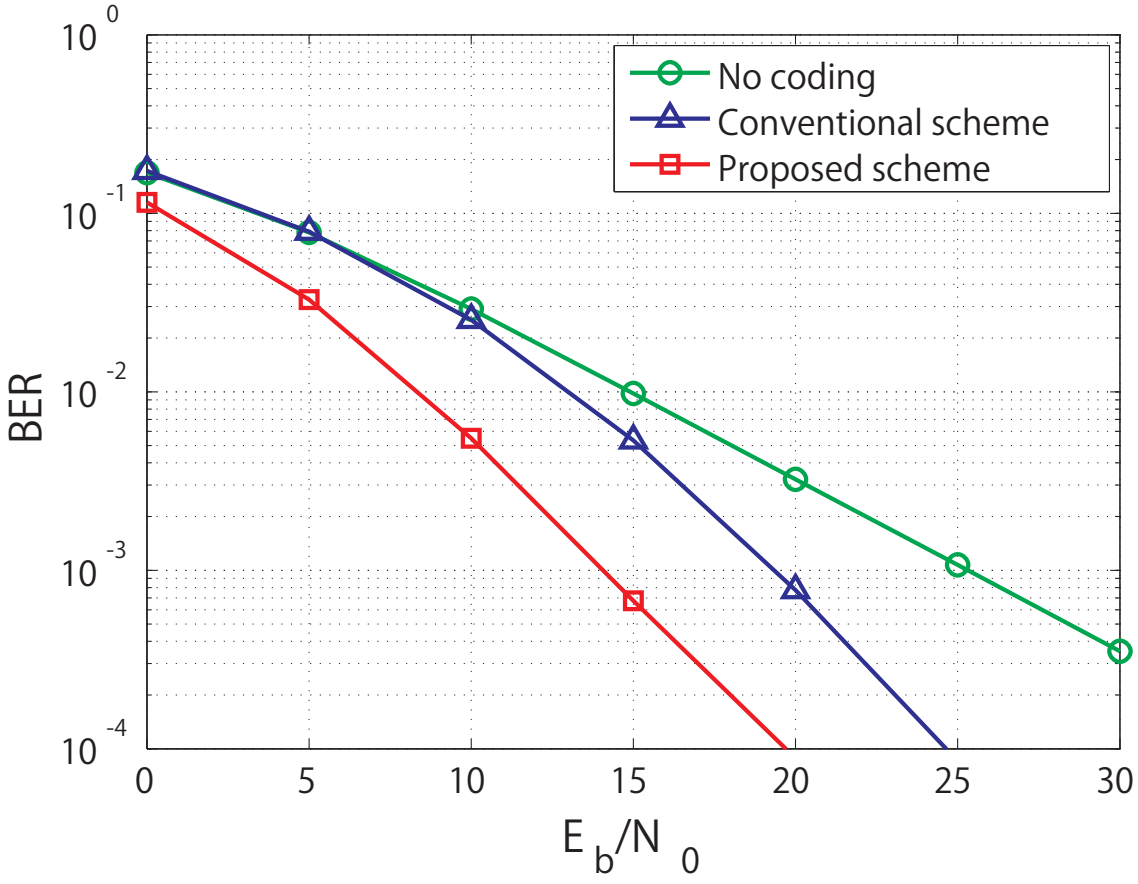

Figure 3.3: BER vs. E_b/N_0 ($\tau_d = \frac{1}{4}T_s$)

The BER performance curves with $\tau_d = \frac{1}{4}T_s$ are shown in Fig. 3.3. The proposed

scheme achieves the second order diversity in this figure. This is expected in Eq. (3.22). On the other hand, the conventional scheme can also achieve transmit path diversity. However, its BER performance is inferior to that of the proposed scheme by about 5[dB] at BER $= 10^{-4}$. It is because the IPI within one OFDM symbol limits the BER performance of the conventional scheme.

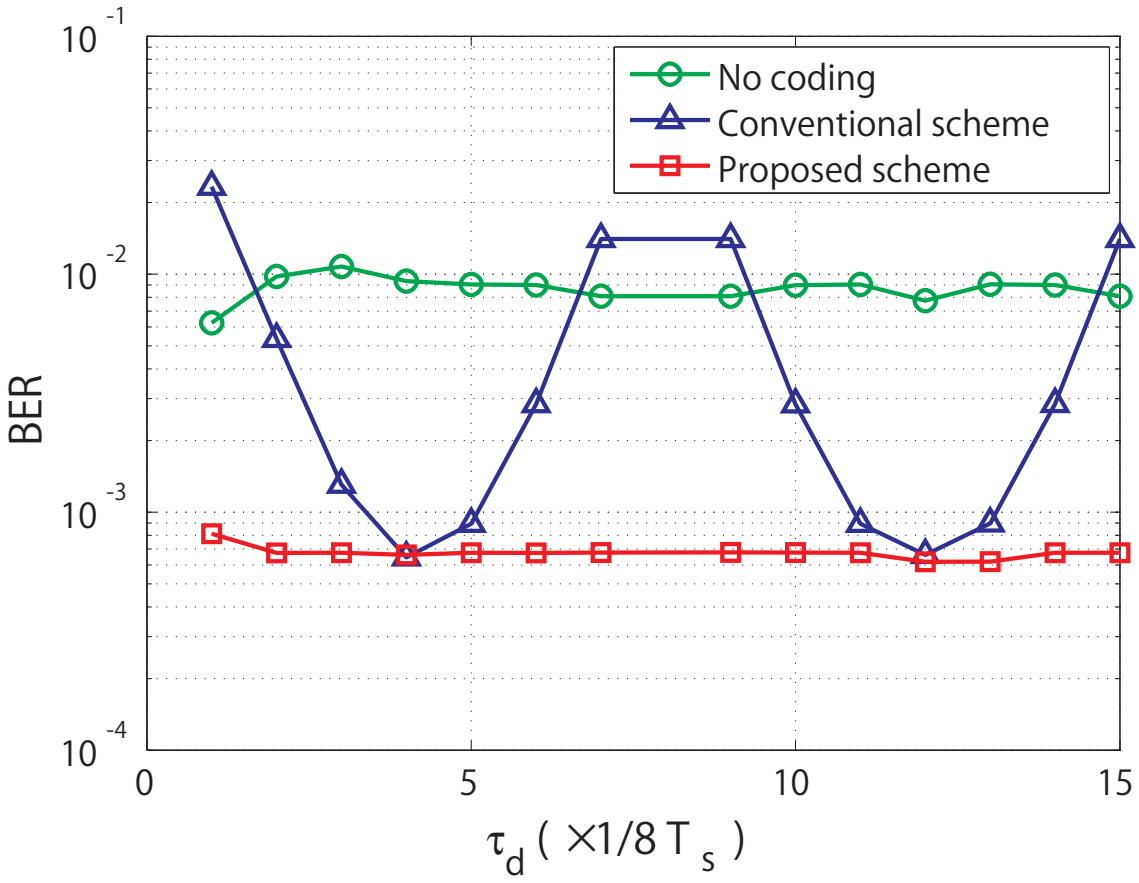

Figure 3.4: BER vs. τ_d ($E_b/N_0 = 15$[dB])

Figure 3.4 shows the BER vs. τ_d with $E_b/N_0 = 15$[dB]. From this figure, the BER performance of the proposed scheme is independent of τ_d. It shows that the proposed scheme can remove IPI completely for any τ_d. On the other hand, that of the conventional scheme is dependent on τ_d. On this channel model, the normalization factors, ν_c and ν_p, are given as following equations. Suppose $\mathbf{R}[k]$ is expressed as

$$\mathbf{R}[k] = \begin{bmatrix} 1 & \psi[k] \\ \psi^*[k] & 1 \end{bmatrix}.$$

The frequency response of the channel expressed in Eq. (3.13) is given as follows:

$$\begin{aligned} H_c[k] &= \sqrt{\frac{1}{\nu_c}}\boldsymbol{\alpha}^H \mathbf{R}[k]\boldsymbol{\alpha} \\ &= \sqrt{\frac{1}{\nu_c}} \begin{bmatrix} \alpha_0^* & \alpha_1 \end{bmatrix} \begin{bmatrix} 1 & \psi[k] \\ \psi^*[k] & 1 \end{bmatrix} \begin{bmatrix} \alpha_0 \\ \alpha_1 \end{bmatrix} \\ &= \sqrt{\frac{1}{\nu_c}} \left\{ \underbrace{|\alpha_0|^2 + |\alpha_1|^2}_{\text{desired signal}} + \underbrace{\psi^*[k]\alpha_0\alpha_1^* + \psi[k]\alpha_0^*\alpha_1}_{\text{IPI within one OFDM symbol}} \right\}. \end{aligned}$$

Then, ν_c is calculated as

$$\nu_c = |\alpha_0|^2 + |\alpha_1|^2 + |\psi^*[k]\alpha_0\alpha_1^*| + |\psi[k]\alpha_0^*\alpha_1|. \tag{3.23}$$

By using Eq. (3.22), ν_p is obtained as

$$\nu_p = |\alpha_0|^2 + |\alpha_1|^2. \tag{3.24}$$

Therefore, the SNR of the conventional scheme and the proposed scheme, ρ_c and ρ_p, is

$$\begin{aligned} \rho_c[k] &= \frac{|\boldsymbol{\alpha}^H \mathbf{R}[k]\boldsymbol{\alpha}|^2}{\nu_c}\frac{E_b}{N_0}, \\ &= \frac{||\alpha_0|^2 + |\alpha_1|^2 + \psi^*[k]\alpha_0\alpha_1^* + \psi[k]\alpha_0^*\alpha_1|^2}{|\alpha_0|^2 + |\alpha_1|^2 + |\psi^*[k]\alpha_0\alpha_1^*| + |\psi[k]\alpha_0^*\alpha_1|}\frac{E_b}{N_0}, \qquad (3.25) \\ \rho_p[k] &= \frac{|\mathbf{w}^T[k]\mathbf{R}[k]\boldsymbol{\alpha}|^2}{\nu_p}\frac{E_b}{N_0} \\ &= \left(|\alpha_0|^2 + |\alpha_1|^2\right)\frac{E_b}{N_0}. \qquad (3.26) \end{aligned}$$

From Eq. (3.25), it can be shown that the performance of the conventional scheme is dependent on τ_d. On the other hand, Eq. (3.26) shows that the proposed scheme can remove the IPI within one OFDM symbol completely and achieve path diversity. This also explains why the performance of the proposed scheme is independent of τ_d. Comparing Eq. (3.25) with Eq. (3.26), the following inequality can be induced

$$\rho_c[k] \leqslant \rho_p[k]. \tag{3.27}$$

The equality holds when $\tau_d = \frac{T_s}{2} + nT_s$ $(n = 0, 1, \ldots)$. Therefore, the performance of the proposed scheme is the best of the three on this channel model.

In this paragraph, computational complexity of the proposed scheme at the receiver side is investgated by comparing with that of the FS-OFDM with oversampling ratio, $G = 2$, on this channel model [45]. Figure 3.5 shows the comparison of the two system models. The upper figure is the FS-OFDM and the lower one is the proposed scheme. From this figure, "OFDM MODULATION (DFT)", "NOISE-WHITENING" and "DIVERSITY COMBINING (maximal ratio combining)" can be shifted from the receiver

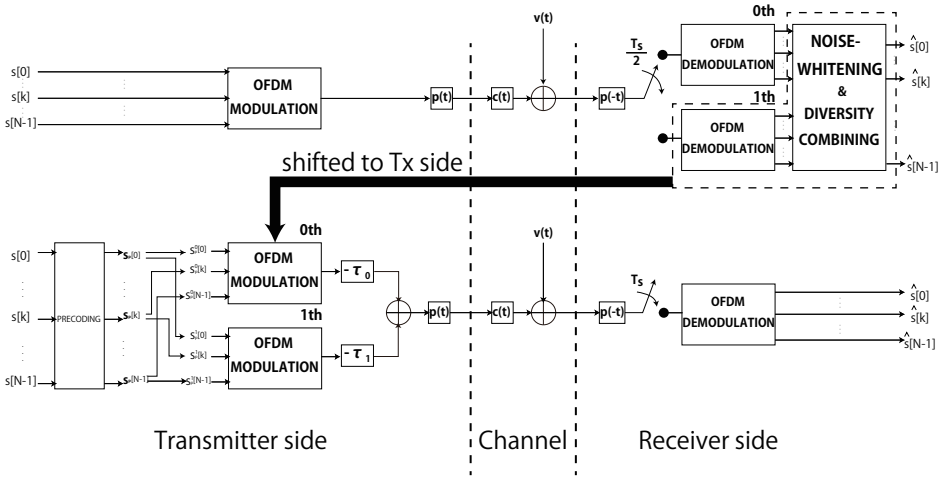

Figure 3.5: Comparison of the systems (upper: FS-OFDM, lower: Precoded FS-OFDM).

to the transmitter by using the proposed scheme. The computational complexity of these signal processings in terms of the number of multiplications are given in Table 3.2 [64]. The total amount of the computational complexity per one OFDM symbol at the receiver in FS-OFDM ($G = 2$) is

$$\begin{aligned} GN\log_2 N + G^2 + G &= 2 \cdot 128 \log_2 2^7 + 2^2 + 2 \\ &= 1798. \end{aligned} \tag{3.28}$$

The amount of reduced computational complexity per one OFDM symbol through the proposed scheme is calculated as follows:

$$\begin{aligned} N\log_2 N + G^2 + G &= 128 \log_2 2^7 + 2^2 + 2 \\ &= 902. \end{aligned} \tag{3.29}$$

From Eqs. (3.28) and (3.29), a large part of the signal processing burden has been shifted from the receiver to the transmitter.

Table 3.2: Computational complexity.

	Number of Multiplications
DFT	$N\log_2 N$
NOISE-WHITENING	G^2
MRC	G

The BER performances on CM1-4 are investigated in Figs. 3.6-3.9, respectively. Figure 3.6 shows the simulation results on CM1. The conventional scheme can achieve transmit path diversity, however the performance is worse than that of the proposed

scheme by about 1[dB] at BER = 10^{-2}. This is because of the degradation due to $|\ \boldsymbol{\alpha}^H \mathbf{R}[k]\boldsymbol{\alpha}\ |$. It is the same in the case of CM2. Compared with "No precoding" at BER = 10^{-2}, the proposed scheme improves the BER performance about 2[dB] on CM1, about 1[dB] on CM2 and about 3[dB] on CM3. From Figs. 3.6-3.8, more path diversity gain can be obtained when the number of multipath components increases. In Fig. 3.9, the BER performance of the proposed scheme is significantly deteriorated. It is due to the large delay spread on CM4. Figure 3.10 shows the example of the impulse response of a channel output including the prerake. As shown in Fig. 3.10, the impulse response of the channel with the proposed scheme exceeds the GI and ISI deteriorates the BER performance of the proposed scheme.

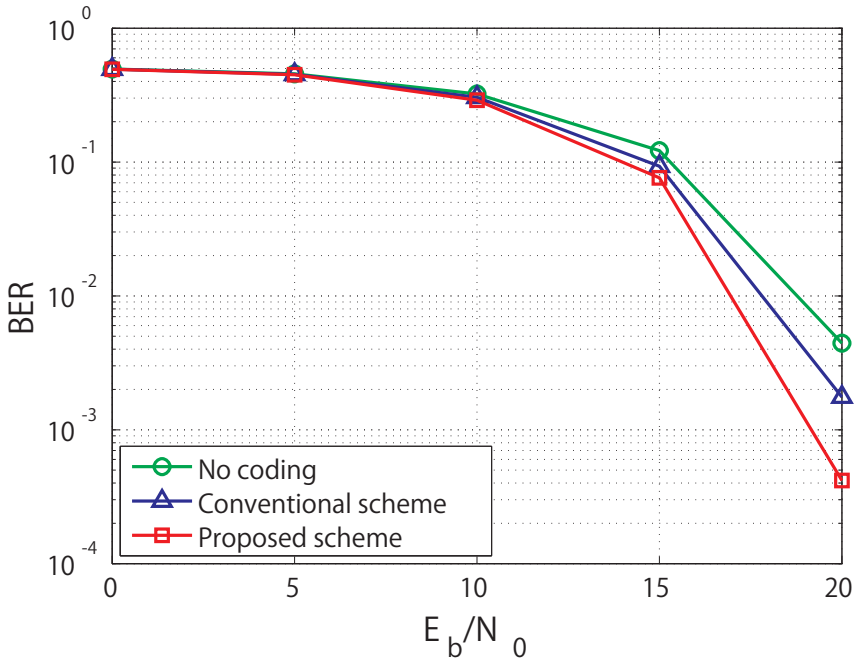

Figure 3.6: BER vs. E_b/N_0 (CM1)

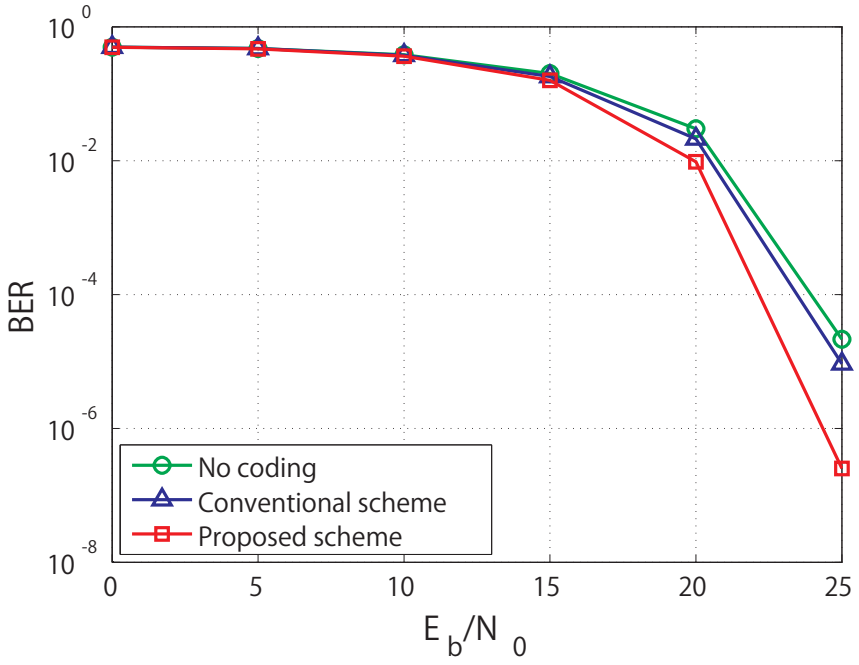

Figure 3.7: BER vs. E_b/N_0 (CM2)

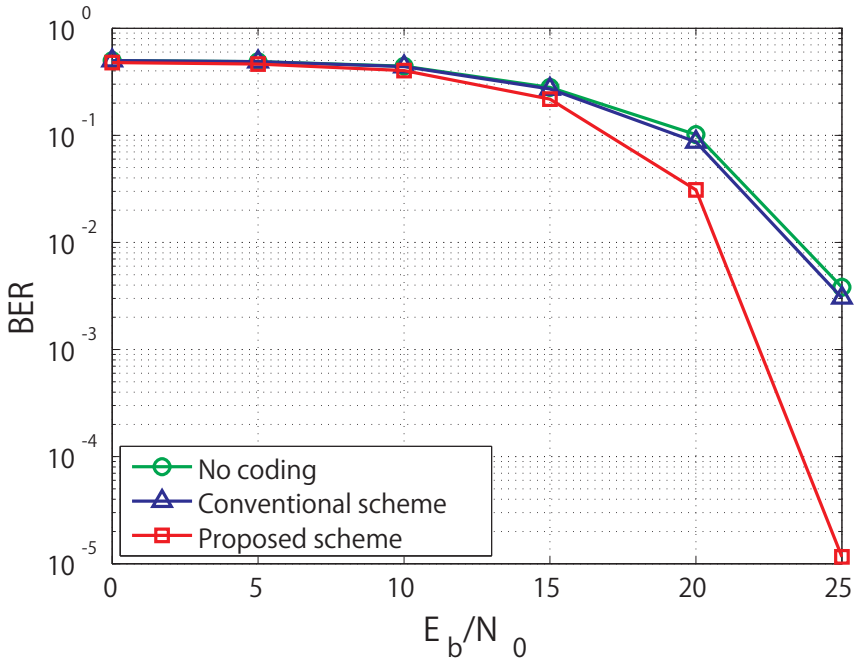

Figure 3.8: BER vs. E_b/N_0 (CM3)

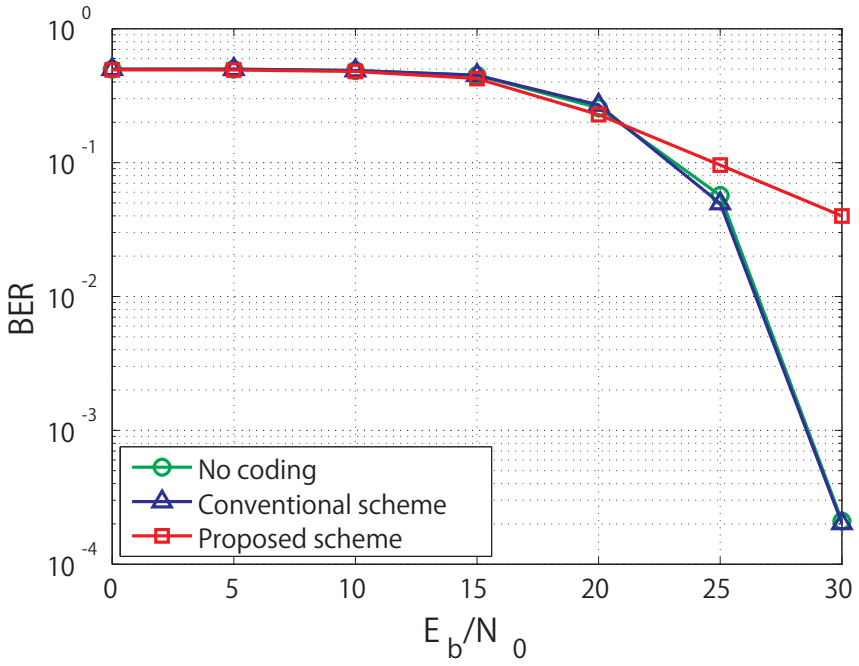

Figure 3.9: BER vs. E_b/N_0 (CM4)

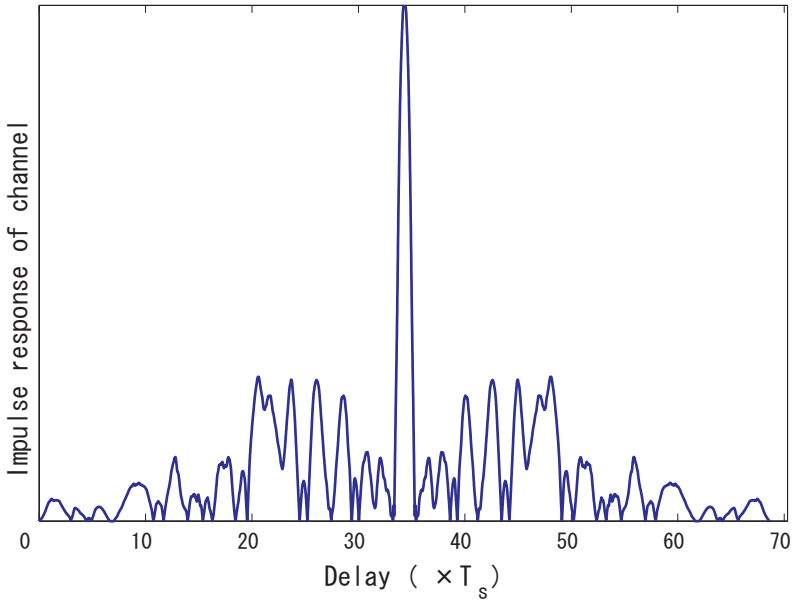

Figure 3.10: Example of impulse response of channel output (CM4)

Here, PAPR of the three signals ("No precoding", "Conventional scheme" and "Proposed scheme") is evaluated on CM2. The PAPR is defined as [81]

$$PAPR = \frac{\max\limits_{0 \leqslant t \leqslant NT_s} |x(t)|^2}{\frac{1}{NT_s}\int_0^{NT_s} |x(t)|^2 \, dt}. \tag{3.30}$$

In this thesis, the effect of non-linear distortion due to the clipping is also evaluated. The clipped signal, $\tilde{x}(t)$, is defined as

$$\tilde{x}(t) = \begin{cases} x(t) & (x(t) \leqslant A_{max}) \\ A_{max} & (x(t) > A_{max}) \end{cases} \tag{3.31}$$

where ϕ is phase of $x(t)$ and A_{max} is maximal permissible amplitude, which is defined as

$$A_{max} := \gamma_{clip} \sqrt{\frac{1}{NT_s}\int_0^{NT_s} |x(t)|^2 \, dt} \tag{3.32}$$

where γ_{clip} is clipping ratio [81,82]. Figures 3.11 and 3.12 show that the performances of PAPR and BER with a variable γ_{clip}. The both transmit precoding schemes have high PAPR. When these signal are clipped at the transmitter, their BER performances are highly deteriorated. Especially, the BER performance of the proposed scheme is the worst of the three. It means that the proposed scheme requires high dynamic range power amplifier (PA). However, it does not matter because the proposal is used in UWB systems, where power spectrum mask is limited to at most -41.6 [dBm/MHz] set by Federal Communications Commission (FCC), and because it is used only in UL and mobile terminal does not need to implement the high dynamic range PA.

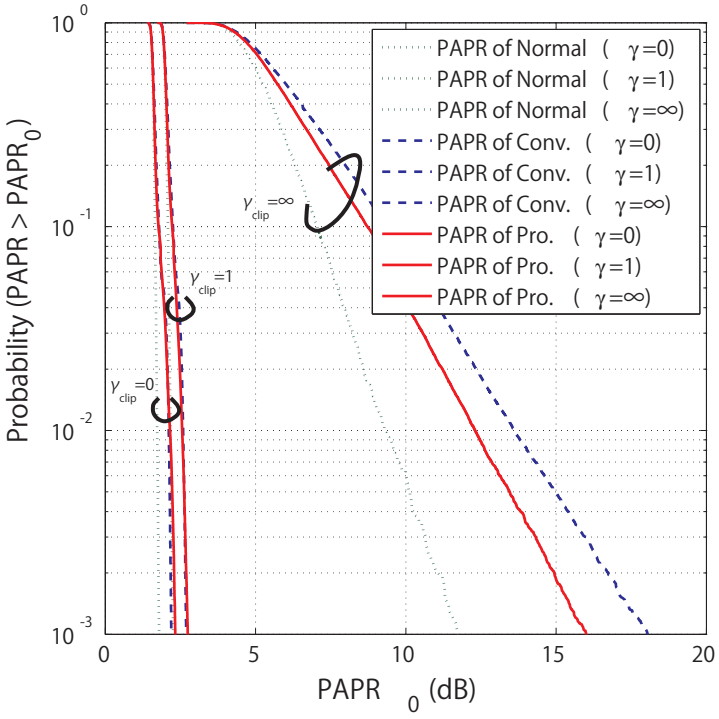

Figure 3.11: PAPR of the clipped signal (CM2)

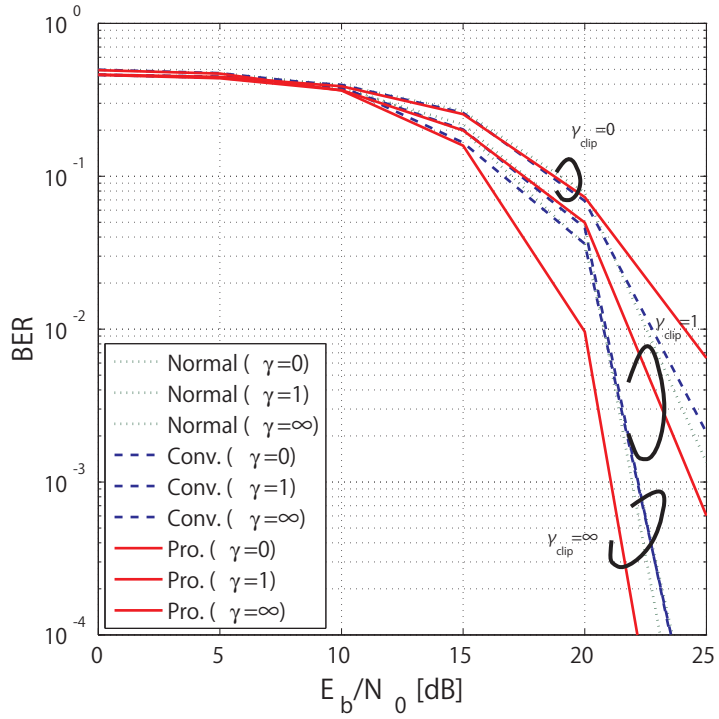

Figure 3.12: BER perfomance of the clipped signal (CM2)

3.1.4. Conclusion

In this chapter, the precoded transmit path diversity scheme in the OFDM system has been proposed. In the proposed scheme, the information symbols are precoded to remove the IPI by using the correlation matrix $\mathbf{R}[k]$ and can achieve path diversity without oversampling the received signal. On the two path Rayleigh fading model, it is clarified that the proposed scheme can achieve path diversity and its BER performance is independent of the path delay. The proposed scheme can also reduce about 50% of the computational complexity at the receiver side compared with FS-OFDM ($G = 2$). Furthermore, the proposed scheme has been evaluated on UWB channel models. On CM1-3, the path diversity can be achieved. However, on CM4, ISI deteriorates the BER performance of the proposed scheme.

3.2. Precoding on Time Variant Channels

3.2.1. Introduction

In DS/SS or Impulse radio (IR) UWB communications, a rake receiver has been proposed to resolve multipath components and achieve path diversity [57–59]. In this scheme, the receiver needs to perform channel estimation and diversity combining, etc. These signal processing increases computational complexity in the receiver.

Prerake has been proposed to shift these signal processing tasks from the receiver to a transmitter [29, 60–63]. In some circumstances the UWB tranmitter has more signal processing capability than the receiver. In this case, the transmitter sends the signal generated by convolution between the transmit symbols and the FIR filter whose coefficients are generated through reverse and conjugate operations of the impulse response of the channel known at the transmitter side. The same as the rake scheme, prerake can achieve path diversity without combining at the receiver side. In [60], a prerake combining scheme is proposed when a pulse interval is smaller than a path interval and the impulse response of the channel is independent and Rayleigh distributed in an IR-UWB system. [61, 62] have proposed precombining schemes which tackle an IPI problem when the pulse interval is longer than the path interval. The precoding scheme on time varying channels has been proposed in [63]. However, it implements multiple antenna elements at the transmitter side and does not achieve path diversity.

On the other hand, in an OFDM system, FS has been investigated to achieve path diversity with a single antenna [45, 50–52, 64–66]. However, in the FS-OFDM system, it is necessary to oversample a received signal and it leads to large power consumption in a small terminal. [53] has proposed a precoded transmit path diversity scheme in an

OFDM system. [53] makes use of the impulse response of the channel with the resolution of the FS interval and can achieve path diversity without oversampling the received signal. On time varying channels, however, the precoded transmit path diversity scheme has not been proposed yet. On this channel, ICI deteriorates the BER performance of the system proposed in [53].

In this chapter, the precoding for both ICI suppression and path diversity combining at the transmitter has been proposed. The proposed scheme has designed the precoding matrix in order to minimize MSE of received symbols. It can achieve ICI suppression and path diversity without any specific signal processing at the receiver.

3.2.2. System Model

3.2.2.1. Precoding on Time Invariant Channels

In this subsection, the existing prerake scheme is applied to the OFDM system [60–62]. The transmitted prerake signal, $x_e(t)$, is given as

$$\begin{aligned} x_e(t) &= c^*(-t) \star x(t) \\ &= \left(\sum_{m=0}^{L-1} \alpha_m^* \delta(t+\tau_m) \right) \star x(t) \\ &= \sum_{m=0}^{L-1} \alpha_m^* x(t+\tau_m). \end{aligned} \tag{3.33}$$

Therefore, the total impulse response of the channel including the prerake combining is expressed as

$$\begin{aligned} h_e(t) &= c^*(-t) \star p(t) \star c(t) \star p(-t) \\ &= \sum_{m=0}^{L-1} \sum_{l=0}^{L-1} \alpha_m^* \alpha_l p_2(t+\tau_m-\tau_l). \end{aligned} \tag{3.34}$$

With the sampled version of $h_e(t)$, $h_e[n] = h_e(nT_s)$, the frequency response of the channel, $H_e[k]$, is given as

$$\begin{aligned} H_e[k] &= \mathrm{DFT}\left[h_e[n]\right] \\ &= \sum_{m=0}^{L-1} \sum_{l=0}^{L-1} \sum_{n=0}^{N-1} \alpha_m^* \alpha_l p_2(nT_s+\tau_m-\tau_l) e^{-j\frac{2\pi kn}{N}}. \end{aligned} \tag{3.35}$$

By using a multipath coefficient vector, $\boldsymbol{\alpha} = [\alpha_0 \cdots \alpha_{L-1}]^T$, Eq. (3.35) is expressed as

$$H_e[k] = \boldsymbol{\alpha}^T \mathbf{R}[k] \boldsymbol{\alpha}^* \tag{3.36}$$

where $\mathbf{R}[k]$ is the path correlation matrix of size $L \times L$ and its $(m,\ l)$th component is expressed as

$$[\mathbf{R}[k]]_{m,l} = \sum_{n=0}^{N-1} p_2(nT_s + \tau_m - \tau_l) e^{-j\frac{2\pi kn}{N}}. \tag{3.37}$$

Then, the received symbols are expressed as

$$\begin{aligned} \mathbf{Y} &= \mathbf{HS} + \mathbf{V} \\ &= \mathbf{ARA}^H\mathbf{S} + \mathbf{V} \\ \mathbf{A} &= \text{diag}\left(\boldsymbol{\alpha}^T \cdots \boldsymbol{\alpha}^T\right) \\ \mathbf{R} &= \text{diag}\left(\mathbf{R}[0]\ \mathbf{R}[1] \cdots \mathbf{R}[k] \cdots \mathbf{R}[N-1]\right) \end{aligned} \tag{3.38}$$

where the sizes of the matrices, $\mathbf{A}$ and $\mathbf{R}$, are $L \times LN$ and $LN \times LN$, respectively.

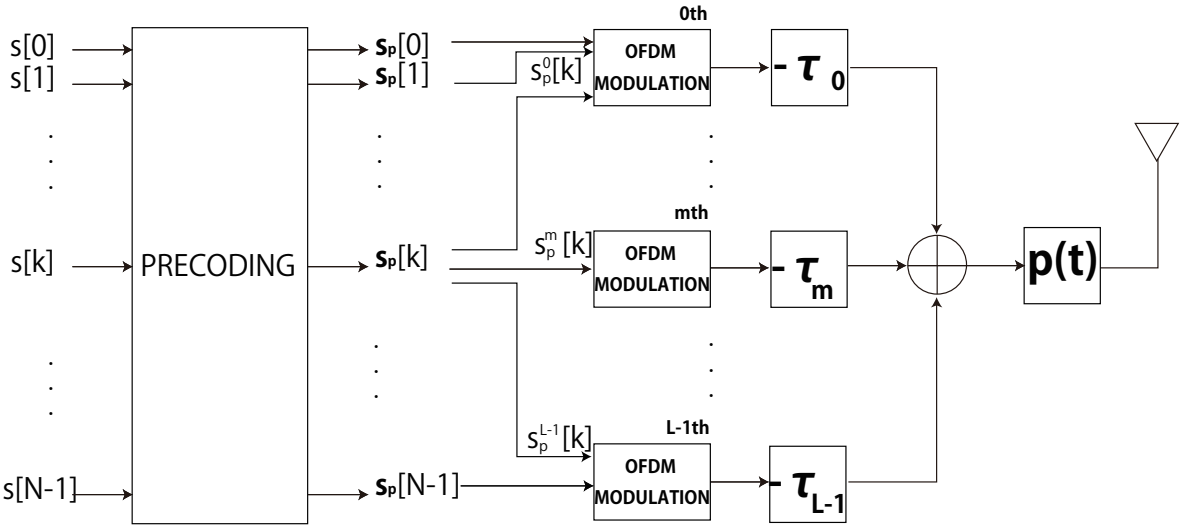

Figure 3.13: Block diagram of precoding system.

The block diagram of the conventional scheme is shown in Fig. 3.13. The conventional scheme precodes the information symbols on the kth subcarrier that is expressed as $S[k]$ $(k = 0, \ldots, N-1)$. The precoded information symbol vector of size $L \times 1$, $\mathbf{S}_{c_1}[k]$ $(k = 0, \ldots, N-1)$, is given as the following equation:

$$\mathbf{S}_{c_1}[k] = \begin{bmatrix} S_{c_1}^0[k] \\ S_{c_1}^1[k] \\ \vdots \\ S_{c_1}^{L-1}[k] \end{bmatrix} = \mathbf{R}^{-1}[k]\boldsymbol{\alpha}^* S[k]. \tag{3.39}$$

The precoded information symbols, $\mathbf{S}_{c_1}[k]$, are input to the OFDM demodulators in parallel. The mth OFDM symbol $(m = 0, \ldots, L-1)$, $x_{c_1}^m[n]$, and the baseband signal,

$x_{c_1}^m(t)$, are expressed by the following equations, respectively.

$$x_{c_1}^m[n] = \sqrt{\frac{1}{N}} \sum_{k=0}^{N-1} S_{c_1}^m[k] e^{j\frac{2\pi nk}{N}}, \tag{3.40}$$

$$x_{c_1}^m(t) = \sum_{n=-N_{\mathrm{GI}}}^{N-1} x_{c_1}^m[n] p(t - nT_s). \tag{3.41}$$

The transmitted signal is generated by

$$x_{c_1}(t) = \sum_{m=0}^{L-1} x_{c_1}^m(t + \tau_m). \tag{3.42}$$

Thus, the received symbols are expressed by the following equations:

$$\begin{aligned} \mathbf{Y} &= \mathbf{HS} + \mathbf{V} \\ &= \mathbf{ARR}^{-1}\mathbf{A}^H\mathbf{S} + \mathbf{V} \\ &= \mathbf{AA}^H\mathbf{S} + \mathbf{V}, \end{aligned} \tag{3.43}$$

$$\begin{aligned} \mathbf{AA}^H &= \begin{bmatrix} \boldsymbol{\alpha}^T\boldsymbol{\alpha}^* & & 0 \\ & \ddots & \\ 0 & & \boldsymbol{\alpha}^T\boldsymbol{\alpha}^* \end{bmatrix} \\ &= \begin{bmatrix} \sum_{l=0}^{L-1} \mid \alpha_l \mid^2 & & 0 \\ & \ddots & \\ 0 & & \sum_{l=0}^{L-1} \mid \alpha_l \mid^2 \end{bmatrix}. \end{aligned} \tag{3.44}$$

By precoding the information symbols, the IPI is removed and path diversity is achieved on time invariant channels [53].

3.2.2.2. Precoding on Time Varying Channel

On time varying channels, the received signal is distorted due to ICI as well as IPI. The received signal is expressed as

$$y(t) = \sum_{-N_{\mathrm{GI}}}^{N-1} x\left[n\right] h\left(t,\ t - nT_s\right) + v\left(t\right) \tag{3.45}$$

where $h\left(t,\ \tau\right)$ is the impulse response of the channel given as

$$h\left(t,\ \tau\right) = p(t) \star c(t,\ \tau) \star p(-t) \tag{3.46}$$

where $c(t,\ \tau)$ is the impulse response of the physical channel.

Suppose the multipath channel model as shown in Fig. 3.14, $c(t,\ \tau)$ is expressed as

$$c(t,\ \tau) = \sum_{l=0}^{L-1} \alpha_l(t)\delta(\tau - \tau_l) \tag{3.47}$$

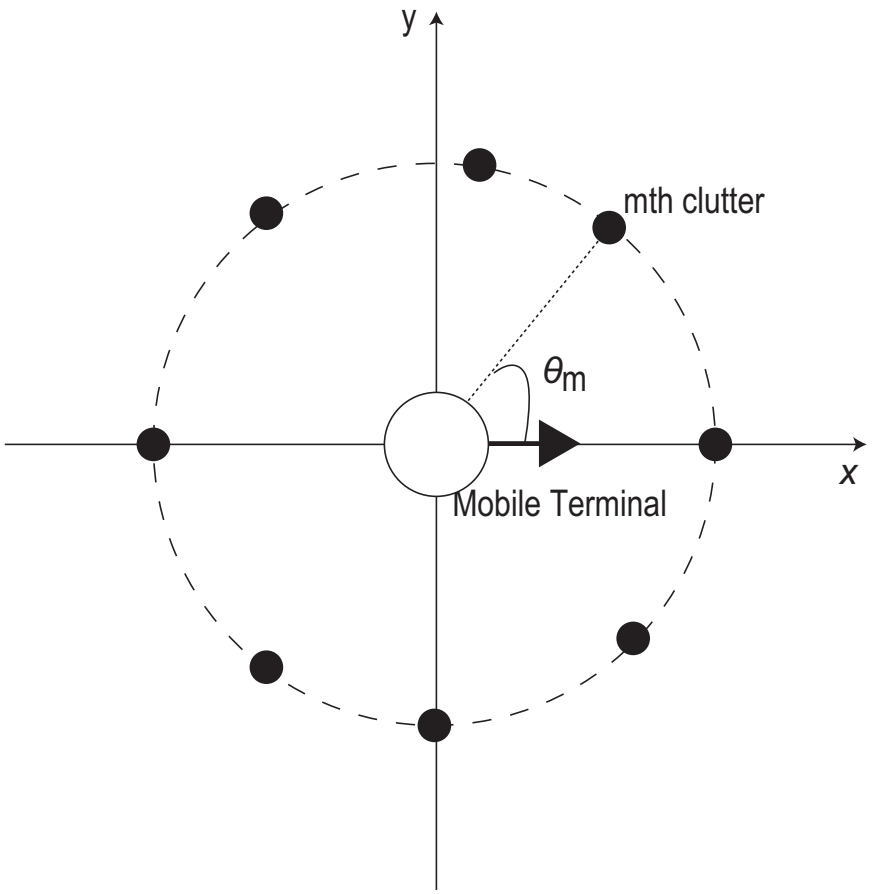

Figure 3.14: Time varying channel model.

where

$$\alpha_l(t) = \sqrt{\frac{2}{L_l}} \sum_{m=0}^{L_l-1} \exp\left(2\pi \left(f_c + f_D \cos\theta_m\right) t + \phi_m\right) \tag{3.48}$$

where $L_l,\ f_D,\ \theta_m,\ \phi_m$ are the number of the clutter of the lth delay path, the maximum Doppeer frequency, the angle of arrival of the mth clutter and the initial phase of the mth clutter, respectively [83]. In the precoding system, the received symbols are expressed as

$$\mathbf{Y} = \mathbf{ARWA}^H\mathbf{S} + \mathbf{V}. \tag{3.49}$$

In this channel model, the path matrix, $\mathbf{A}$, is expressed as follows:

$$\mathbf{A} = \begin{bmatrix} A_{0,0\cdot L+0} & \cdots & A_{0,0\cdot L+1} & \cdots & A_{0,(m-1)\cdot l} & \cdots & A_{0,(L-1)\cdot L+l} \\ A_{1,0} & & & & A_{1,(m-1)\cdot l} & \cdots & A_{1,(L-1)\cdot L+l} \\ \vdots & \ddots & & & & & \\ & & & & A_{k,(m-1)\cdot l} & & \\ & & & & & & \\ A_{N-1,0} & & & & & & A_{N-1,(L-1)\cdot L+l} \end{bmatrix},$$

$$A_{k,(m-1)\cdot L+l} = \frac{1}{NT_s}\int_0^{NT_s} \alpha_l(t) e^{-j2\pi(k-m)\Delta f t} dt \tag{3.50}$$

where $\Delta f = \frac{1}{NT_s}$ is the subcarrier spacing. The precoded information vectors, $\mathbf{S}_{c_1}$ and $\mathbf{S}_p$, are given as

$$\begin{aligned} \mathbf{S}_{c_1} &= \left[\mathbf{S}_{c_1}^T[0]\, \mathbf{S}_{c_1}^T[1] \cdots \mathbf{S}_{c_1}^T[k] \cdots \mathbf{S}_{c_1}^T[N-1]\right]^T \\ &= \mathbf{W}_{c_1}\mathbf{A}^H\mathbf{S}, \end{aligned} \tag{3.51}$$

$$\begin{aligned} \mathbf{S}_p &= \left[\mathbf{S}_p^T[0]\, \mathbf{S}_p^T[1] \cdots \mathbf{S}_p^T[k] \cdots \mathbf{S}_p^T[N-1]\right]^T \\ &= \mathbf{W}_p\mathbf{A}^H\mathbf{S}, \end{aligned} \tag{3.52}$$

and they are input to the OFDM modulator and combined as shown in Eqs. from Eq. (3.39) to Eq. (3.42). In the following subsections, the precoding matrices, $\mathbf{W}_{c1}$ and $\mathbf{W}_p$, are designed.

In the conventional scheme, the precoding matrix, $\mathbf{W}_{c_2}$, is designed to remove the IPI as discussed in Subsection 3.2.2.1. Therefore, $\mathbf{W}_{c_2}$ is given as

$$\mathbf{W}_{c_2} = \mathbf{R}^{-1}. \tag{3.53}$$

The received symbols are expressed as

$$\begin{aligned} \mathbf{Y} &= \mathbf{HS} + \mathbf{V} \\ &= \mathbf{ARW}_{c_2}\mathbf{A}^H\mathbf{S} + \mathbf{V} \\ &= \mathbf{ARR}^{-1}\mathbf{A}^H\mathbf{S} + \mathbf{V} \\ &= \mathbf{AA}^H\mathbf{S} + \mathbf{V} \end{aligned} \tag{3.54}$$

where

$$\begin{aligned}
\mathbf{A}\mathbf{A}^H &= \sum_{k_1=0}^{N-1}\sum_{k_2=0}^{N-1}\sum_{m=0}^{N-1}\sum_{l=0}^{L-1} A_{k_1,(m-1)L+l} A^*_{k_2,(m-1)L+l} \\
&= \underbrace{\sum_{k=0}^{N-1}\sum_{m=0}^{N-1}\sum_{l=0}^{L-1} \mid A_{k,(m-1)L+l} \mid^2}_{\text{Desired signal}} \\
&+ \underbrace{\sum_{\substack{k_1=0 \\ k_1\neq k_2}}^{N-1}\sum_{k_2=0}^{N-1}\sum_{m=0}^{N-1}\sum_{l=0}^{L-1} A_{k_1,(m-1)L+l} A^*_{k_2,(m-1)L+l}}_{\text{Inter-carrier interference}} . \qquad (3.55)
\end{aligned}$$

According to these equations, the ICI remains in the received signal. In the proposed scheme, the precoding matrix is designed to suppress the effect of the ICI. In this subsection, $\mathbf{W}_p$ is calculated to suppress the effect of the ICI as following:
The cost function is given as

$$\begin{aligned}
CF(\mathbf{W}_p) &= \mathrm{E} \parallel \mathbf{S} - \left(\mathbf{A}\mathbf{R}\mathbf{W}_p\mathbf{A}^H\mathbf{S} + \mathbf{V}\right) \parallel^2 \\
&= N\sigma_s^2 \cdot (1 - F_1 - F_2 + F_3) + N\sigma_v^2 \qquad (3.56) \\
F_1 &= \mathrm{tr}\left\{\mathbf{A}\mathbf{R}\mathbf{W}_p\mathbf{A}^H\right\} \qquad (3.57) \\
F_2 &= \mathrm{tr}\left\{\mathbf{A}\mathbf{W}_p^H\mathbf{R}^H\mathbf{A}^H\right\} \qquad (3.58) \\
F_3 &= \mathrm{tr}\left\{\mathbf{A}\mathbf{W}_p^H\mathbf{R}^H\mathbf{A}^H\mathbf{A}\mathbf{R}\mathbf{W}_p\mathbf{A}^H\right\} \qquad (3.59)
\end{aligned}$$

$$\frac{\partial CF(\mathbf{W}_p)}{\partial \mathbf{W}_p^*} = N\sigma_s^2 \cdot \frac{\partial}{\partial \mathbf{W}_p^*} \cdot (-F_1 - F_2 + F_3) \qquad (3.60)$$

$$\frac{\partial CF(\mathbf{W}_p)}{\partial \mathbf{W}_p^*} = 0 \qquad (3.61)$$

from which we can derive the following equation [84]:

$$\mathbf{W}_p = \mathbf{R}^{-1}\left(\mathbf{A}^H\mathbf{A}\right)^\dagger\left(\mathbf{A}^H\mathbf{A}\right)\left(\mathbf{A}^H\mathbf{A}\right)^\dagger . \qquad (3.62)$$

The solution of Eqs. (3.56) and (3.61) are explained in Appendices 4.2 and 4.2, respectively.

3.2.3. Numerical Results

3.2.3.1. Simulation Conditions

Simulation conditions are presented in Table 3.3. Modulation parameters are following the MB-OFDM standard [79]. A convolutional code with the coding rate of

Table 3.3: Simulation conditions.

Modulation	1st: QPSK 2nd: OFDM
Channel	Two path Rayleigh Fading IEEE802.15.3a CM1
Channel Estimation	Ideal
Coding	Convolutional coding
Coding rate	1/2
Constraint length(K)	7
Points of FFT	128
Number of subcarriers	128
OFDM Symbol Duration	312.5 [ns]
Cyclic Prefix	60.61 [ns]
Decoder	Soft decision Viterbi

1/2 and the constraint length of 7 is used for forward error correction. QPSK and OFDM are used for the first and second modulations. The number of subcarriers, N, is 128. The OFDM symbol duration is 312.5 nsec and the cyclic prefix is 60.61 nsec. At the receiver side, soft decision Viterbi decoder is employed. The impulse response of a channel is assumed to be constant during one OFDM packet and known at the transmitter side. The total response of the transmitter and receiver filters is assumed to be truncated sinc pulse with the duration of T_s. Assumed channel models are two path Rayleigh fading with uniform delay profile and UWB channel models (CM1 – 4). Regarding the two path Rayleigh fading model, BER performance is evaluated when the delay between the paths, $\tau_d = \mid \tau_0 - \tau_1 \mid$, is $\frac{T_s}{4}$. CM1 is a LOS channel within a distance between 0m and 4m. CM2 is a NLOS channel within a distance between 0m and 4m. CM3 is a NLOS channel within a distance between 4m and 10m. CM4 is a dense multipath NLOS channel. For the UWB channel models, 100 impulse responses are generated. It is expected that all the impulse responses are tested. Then, the best 90 BERs are averaged [79,80]. In the transmitter, all of the path components are used for the precoding transmit diversity. In this simulation, the normalized Doppler frequency is assumed to be $f_D N T_s = f_D T_B = 1.0 \times 10^{-5}$ or 1.0×10^{-4}. In the figures, "NORMAL" means the BER curves without diversity combining at either the transmitter or the receiver. "CONV" is the BER curves of the conventional precoding scheme which is expressed in Eq. (3.33). "PRO" indicates the BER curves of the proposed precoding scheme in which the precoded information symbols are generated by Eq. (3.39).

3.2.3.2. Simulation Results

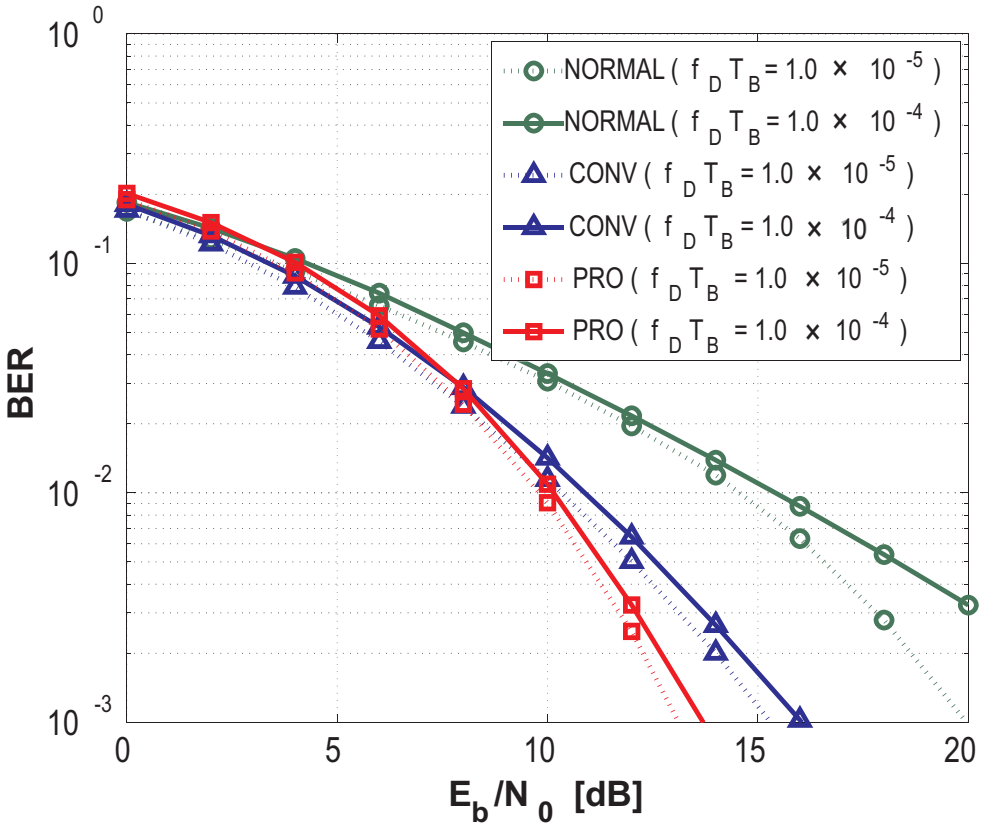

Figure 3.15: Two path Rayleigh fading model.

The BER performance on the two path Rayleigh fading model is shown in Fig. 3.15. The performance of the conventional scheme is improved compared with "NORMAL". However, the performance is inferior to that of the proposed scheme, "PRO". It is because the performance of the conventional scheme is deteriorated by the ICI expressed in Eq. (3.55). On the other hand, the proposed scheme can achieve ICI suppression and path diversity.

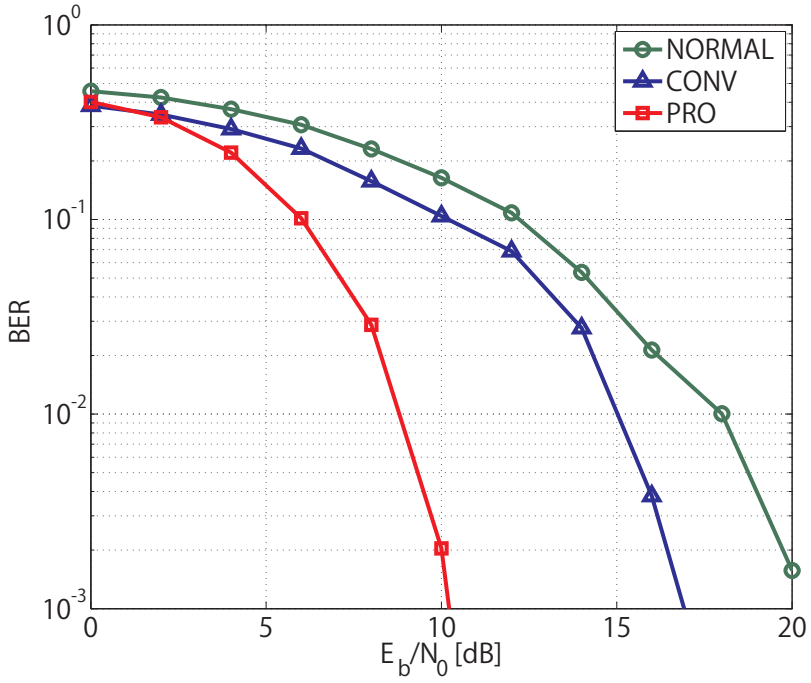

Figure 3.16: CM1 ($f_D T_B = 1.0 \times 10^{-4}$).

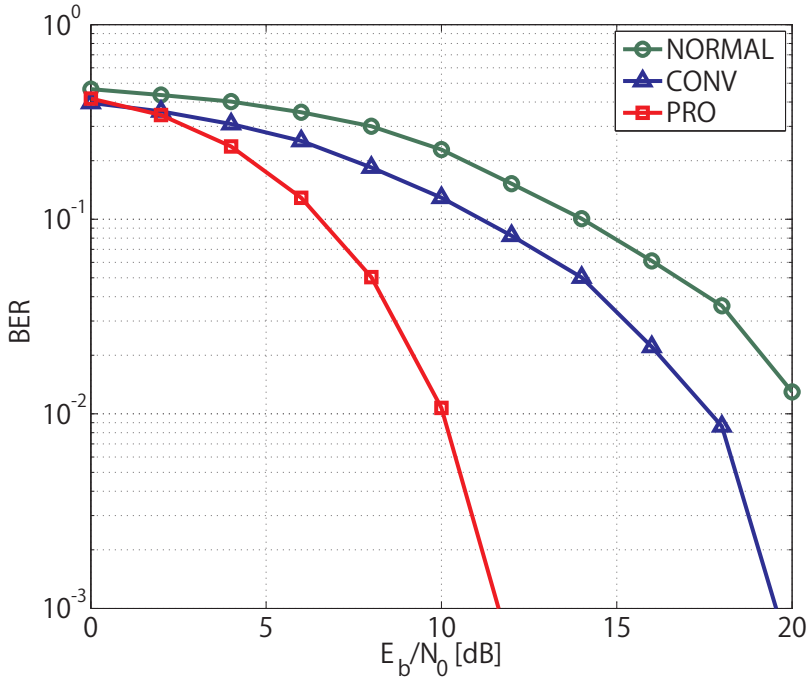

Figure 3.17: CM2 ($f_D T_B = 1.0 \times 10^{-4}$).

Figures 3.16-3.19 show the BER curves on CM1-4, respectively. As shown in Fig. 3.15, the BER performance of the proposed scheme is about 1 [dB] better than that of

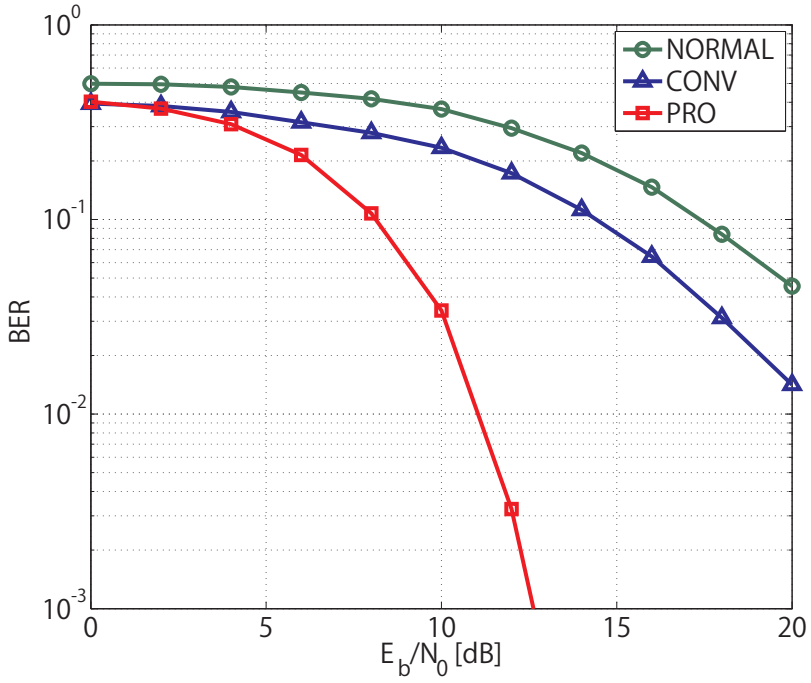

Figure 3.18: CM3 ($f_D T_B = 1.0 \times 10^{-4}$).

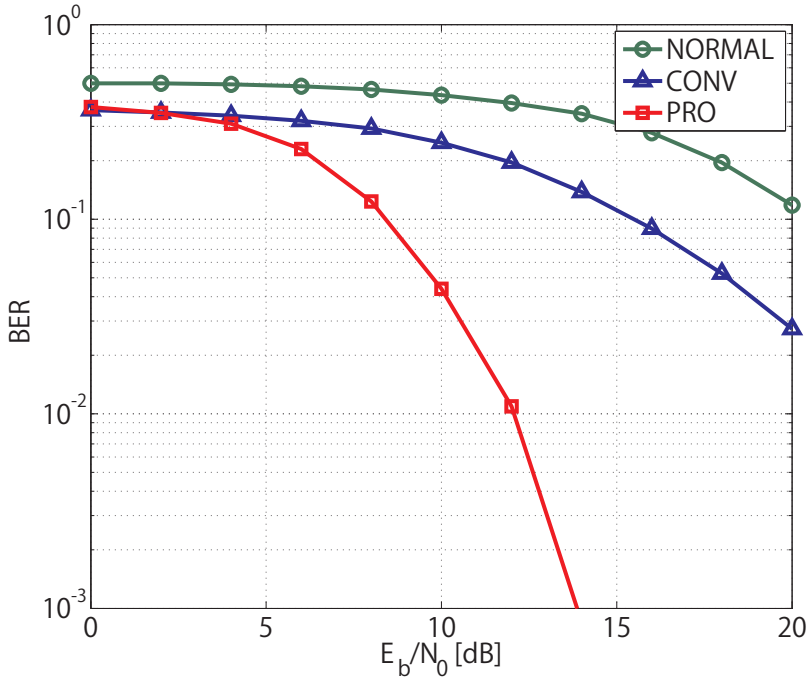

Figure 3.19: CM4 ($f_D T_B = 1.0 \times 10^{-4}$).

the conventional scheme on the two path Rayleigh fading channel model. At BER = 10^{-2} in Figs. 3.16-3.19, compared with the conventional scheme, the performance of

the proposed scheme is better by about 7[dB] on CM1, 8[dB] on CM2, 9[dB] on CM3, and more than 10[dB] on CM4. It is because that the amount of the ICI induced by the conventional scheme is proportional to the number of multipaths and that the proposed scheme can suppress the ICI which is given as in Eq. (3.55).

3.2.4. Conclusions

In this chapter, the precoding scheme for ICI suppression and path diversity in FS-OFDM has been proposed. In the conventional scheme, a precoded transmit path diversity scheme on time invariant channels has been proposed. On time varying channels, however, the precoded transmit path diversity scheme has not been proposed yet. The ICI due to the Doppler spread distorts the received signal in the conventional scheme. The proposed scheme has designed the precoding matrix in order to minimize the MSE of the received symbols to suppress the ICI. The numerical results through computer simulation show that both the proposed scheme and the conventional scheme can achieve path diversity on the time variant channels without oversampling the received signal at the receiver. On the two path Rayleigh fading model, the BER performance of the proposed scheme is better than that of the conventional scheme by about 1[dB] at BER $= 10^{-2}$. On UWB channels, the performance of the proposed scheme is better by about 7-10[dB] at the BER of 10^{-2}. The effect of the ICI suppression is more significant as the number of the multipath is larger. It is because the amount of the ICI induced by the conventional scheme is proportional to the number of multipaths and the proposed scheme can suppress the ICI. Therefore, the proposed scheme can achieve ICI suppression and path diversity without any specific signal processing at the receiver.

Chapter 4

Overall Conclusions

A FS scheme in OFDM has been proposed to achieve diversity with a single antenna. In the FS scheme, a received baseband signal is sampled with a rate higher than the baud rate and combined to achieve path diversity on each subcarrier. Though the FS achieves diversity, it increases power consumption of the receiver. In this dissertation, the author has mainly proposed two path diversity schemes to overcome the effect of signal fading in a multipath environment. To obtain path diversity gain and maintain the battery life at small terminal, the author has proposed reduction of the computational complexity for diversity combining in receiver side and shifts the signal processing burden from the receiver to transmitter.

4.1. Path Diversity Schemes in Receiver

Although the FS achieves diversity, it increases power consumption of the receiver. In some channel conditions, the energy of the received signal may be large enough with baud rate sampling. In this dissertation, the digital signal processing schemes for path diversity for the purpose of downsizing and longer battery life of the receiver are proposed and investigated. Chapter 2 introduces the methods to reduce the computational complexity at receiver.

In section 2.1, SRS scheme has been proposed. SRS selects the oversampling ratio according to frequency response of channel to reduce the number of OFDM demodulators for signal detection. The most of the bit error occurs on the subcarrier with low frequency response. Thus, the oversampling ratio, G, should be chosen in order to increase the power of the received signal on the subcarrier with the lowest frequency response. In the selection, there is a trade off between the BER performance and the computational complexity. The selection of the coefficient for each oversampling ratio depends on the channel models and required performance in terms of BER and power consumption. With the proposed scheme, the power consumption can be re-

duced significantly if the delay spread is small. When the delay spread is large, the BER performance can be improved while the power consumption is still saved with the proposed sampling rate selection scheme.

To achieve more reduction of the computational complexity, it is required that more path diversity should be obtained with the same oversampling ratio. Section 2.2 has proposed SPS scheme. In the conventional scheme, the interval between the sampling points is fixed to $\frac{T_S}{G}$ and it cannot extract the multipath which arrive non-uniformly in the delay domain. In this section, non-uniform sampling point selection has been proposed. In this scheme, the interval between the sampling points is not fixed. It then improves diversity gain by about 2 [dB] when the oversampling rate is 2. However, it actually deteriorates the performance when the oversampling rate is 4. This is due to the correlation of the noise samples. In addition as the oversampling rate increases, the complexity for the sampling point selection grows exponentially. Therefore, this section has also proposed the low-complexity sampling point selection scheme to eliminate the specific sets of the sampling points which lead to large noise correlation. In the low-complexity non-uniform sampling point selection scheme, the complexity for the sampling point selection with $G = 2$ has been reduced by about 70% of the original one while it maintains the equivalent BER. As compared to the fixed sampling point selection scheme, the total complexity including the demodulation of 100 symbols decreases by a factor of 2. The proposed scheme with $G = 2$ achieves slightly better BER than the fixed sampling point scheme with $G = 4$ when the RMS delay spread is larger than 40 [ns] for imperfect CE. Therefore, both path diversity and complexity reduction have been achieved with the proposed scheme.

4.2. Path Diversity Scheme in Transmitter

Chapter 2 has proposed SRS/SPS and achieved the reduction of the computational complexity at receiver while obtaining the path diversity gain. However, they still require the high computational complexity and many OFDM demodulators. To provide low power consumption and small sized mobile terminal, circuit size must be small. In this chapter, transmit path diversity schemes have been introduced to shift the signal processing burden from receiver to transmitter.

Section 3.1 introduces the transmit path diversity scheme on time invariant channels. When the conventional prerake scheme [60–62] is applied to the OFDM system, effect of the path diversity is limited. This is because IPI within one OFDM symbol is generated at the receiver side. In the proposed scheme, the information symbols are precoded to remove the IPI by using the correlation matrix $\mathbf{R}[k]$ and can achieve path diversity without oversampling the received signal. On the 2 path Rayleigh fading model, it is

clarified that the proposed scheme can achieve path diversity and its BER performance is independent of the path delay. The proposed scheme can also reduce about 50% of the computational complexity at the receiver side compared with FS-OFDM ($G = 2$). Furthermore, the proposed scheme has been evaluated on UWB channel models.

Section 3.2 introduces the transmit path diversity scheme on time variant channels. In this section, the precoding scheme for ICI suppression and path diversity in FS-OFDM has been proposed. In the conventional scheme, a precoded transmit path diversity scheme on time invariant channels has been proposed. On time varying channels, however, the precoded transmit path diversity scheme has not been proposed yet. On time variant channels, Doppler spread causes ICI and it deteriorate the communication quality. The ICI due to the Doppler spread distorts the received signal in the conventional scheme. The proposed scheme has designed the precoding matrix in order to minimize the MSE of the received symbols to suppress the ICI. The numerical results through computer simulation show that both the proposed scheme and the conventional scheme can achieve path diversity on the time variant channels without oversampling the received signal at the receiver. On the two path Rayleigh fading model, the BER performance of the proposed scheme is better than that of the conventional scheme by about 1[dB] at BER $= 10^{-2}$. On UWB channels, the performance of the proposed scheme is better by about 7-10[dB] at the BER of 10^{-2}. The effect of the ICI suppression is more significant as the number of the multipath is larger. It is because the amount of the ICI induced by the conventional scheme is proportional to the number of multipath and the proposed scheme can suppress the ICI. Therefore, the proposed scheme can achieve ICI suppression and path diversity without any specific signal processing at the receiver.

References

[1] J. Winters, "On the Capacity of Radio Communication Systems with Diversity in a Rayleigh Fading Environment," *IEEE Journal on Selected Areas in Commun.*, vol. 5, no. 5, pp. 871 – 878, June 1987.

[2] L. Zheng and D. Tse, "Diversity and Multiplexing: A Fundamental Tradeoff in Multiple-antenna Channels," *IEEE Transa. on Information Theory*, vol. 49, no. 5, pp. 1073 – 1096, May 2003.

[3] T. Hattori and M. Fujioka, *Wireless Broadband Textbook Vol.2 (in Japanese)*. Impress, 2006.

[4] M. Rahnema, "Overview of the GSM System and Protocol Architecture," *IEEE Commun. Mag.*, vol. 31, no. 4, pp. 92 –100, April 1993.

[5] E. Dahlman, B. Gudmundson, M. Nilsson, and A. Skold, "UMTS/IMT-2000 Based on Wideband CDMA," *IEEE Commun. Mag.*, vol. 36, no. 9, pp. 70 –80, Sept. 1998.

[6] P. Chaudhury, W. Mohr, and S. Onoe, "The 3GPP Proposal for IMT-2000," *IEEE Commun. Mag.*, vol. 37, no. 12, pp. 72 –81, Dec. 1999.

[7] K. Zheng, L. Huang, G. Li, H. Cao, W. Wang, and M. Dohler, "Beyond 3G Evolution," *IEEE Vehi. Tech. Mag.*, vol. 3, no. 2, pp. 30 –36, June 2008.

[8] D. Astely, E. Dahlman, A. Furuskar, Y. Jading, M. Lindstrom, and S. Parkvall, "LTE: the Evolution of Mobile Broadband," *IEEE Commun. Mag.*, vol. 47, no. 4, pp. 44 –51, April 2009.

[9] M. H. Ng, S.-D. Lin, J. Li, and S. Tatesh, "Coexistence Studies for 3GPP LTE with Other Mobile Systems," *IEEE Commun. Mag.*, vol. 47, no. 4, pp. 60 –65, April 2009.

[10] K. Safjan, V. D'Amico, D. Bultmann, D. Martin-Sacristan, A. Saadani, and H. Schoneich, "Assessing 3GPP LTE-advanced as IMT-advanced Technology: the WINNER+ Evaluation Group Approach," *IEEE Commun. Mag.*, vol. 49, no. 2, pp. 92 –100, Feb. 2011.

[11] I.-R. M.2134, "Requirements Related to Technical Performance for IMT-Advanced Radio Interface(s)," Tech. Rep., 2008.

[12] B. Crow, I. Widjaja, L. Kim, and P. Sakai, "IEEE 802.11 Wireless Local Area Networks," *IEEE Commun. Mag.*, vol. 35, no. 9, pp. 116 –126, Sep. 1997.

[13] Y.Sanada and M.Ikehara, *Multimedia Communication (in Japanese).* Baihukan, 2002.

[14] *IEEE 802.11a-Part 11: Wireless LAN Medium Access Control (MAC) and Physical Layer (PHY) Specifications; Highspeed Physical Layer in the 5GHz Band.*, Std., 2000.

[15] *IEEE Standard for Information Technology–Telecommunications and information Exchange Between Systems–Local and Metropolitan Area Networks–Specific Requirements Part 11: Wireless LAN Medium Access Control (MAC) and Physical Layer (PHY) Specifications Amendment 5: Enhancements for Higher Throughput*, Std., 29 2009.

[16] E. Perahia, "IEEE 802.11n Development: History, Process, and Technology," *IEEE Commun. Mag.*, vol. 46, no. 7, pp. 48 –55, July 2008.

[17] *IEEE Standard for Information Technology - Telecommunications and Information Exchange Between Systems - Local and Metropolitan Area Networks - Specific Requirements. - Part 15.1: Wireless Medium Access Control (MAC) and Physical Layer (PHY) Specifications for Wireless Personal Area Networks (WPANs)*, Std., 2005.

[18] J. Karaoguz, "High-rate Wireless Personal Area Networks," *IEEE Commun. Mag.*, vol. 39, no. 12, pp. 96 –102, Dec. 2001.

[19] G. Aiello and G. Rogerson, "Ultra-wideband Wireless Systems," *IEEE Microwave Mag.*, vol. 4, no. 2, pp. 36 – 47, June 2003.

[20] A. Goldsmith, *Wireless Communications.* Cambridge University Press, 2005.

[21] P. Flikkema, "Spread-spectrum Techniques for Wireless Communication," *IEEE Signal Processing Mag.*, vol. 14, no. 3, pp. 26 –36, May 1997.

[22] S. Weinstein and P. Ebert, "Data Transmission by Frequency-Division Multiplexing Using the Discrete Fourier Transform," *IEEE Trans. on Commun. Tech.*, vol. 19, no. 5, pp. 628 –634, Oct. 1971.

[23] W. Zou and Y. Wu, "COFDM: An Overview," *IEEE Transactions on Broadcasting*, vol. 41, no. 1, pp. 1 –8, Mar. 1995.

[24] J. Bingham, "Multicarrier Modulation for Data Transmission: an Idea Whose Time Has Come," *IEEE Commun. Mag.*, vol. 28, no. 5, pp. 5 –14, May 1990.

[25] A. Peled and A. Ruiz, "Frequency Domain Data Transmission Using Reduced Computational Complexity Algorithms," in *in Proc. the IEEE International Conference on ICASSP*, vol. 5, April 1980, pp. 964 – 967.

[26] R. Price and P. Green, "A Communication Technique for Multipath Channels," *Proceedings of the IRE*, vol. 46, no. 3, pp. 555 –570, March 1958.

[27] G. Turin, "Introduction to Spread-spectrum Antimultipath Techniques and Their Application to Urban Digital Radio," *Proc. of the IEEE*, vol. 68, no. 3, pp. 328 – 353, Mar. 1980.

[28] R. Esmailzadeh and M. Nakagawa, "Pre-RAKE Diversity Combination for Direct Sequence Spread Spectrum Mobile Communications Systems," *IEICE Trans. on Commun.*, vol. E76-B, no. 8, pp. 1008–1015, 1993.

[29] R. Esmailzadeh, E. Sourour, and M. Nakagawa, "PreRAKE Diversity Combining in Time-division Duplex CDMA Mobile Communications," *IEEE Trans. on Vehi. Tech.*, vol. 48, no. 3, pp. 795 –801, May 1999.

[30] R. Murch and K. Letaief, "Antenna Systems for Broadband Wireless Access," *IEEE Commun. Mag.*, vol. 40, no. 4, pp. 76 –83, April 2002.

[31] R. Vaughan and J. Andersen, "Antenna Diversity in Mobile Communications," *IEEE Trans. on Vehi. Tech.*, vol. 36, no. 4, pp. 149 – 172, Nov. 1987.

[32] G. J. Foschini and M. J. Gans, "On Limits of Wireless Communications in a Fading Environment When Using Multiple Antennas," *Wireless Personal Communications*, vol. 6, pp. 311–335, 1998.

[33] G. J. Foschini, "Layered Space-time Architecture for Wireless Communication in a Fading Environment When Using Multi-element Antennas," *Bell Labs Technical Journal*, vol. 1, no. 2, pp. 41–59, 1996. [Online]. Available: http://doi.wiley.com/10.1002/bltj.2015

[34] E. Telatar, "Capacity of Multi-antenna Gaussian Channels," *European Transactions on Telecommunications*, pp. 10(6):585–596, 1999.

[35] Y. Zhang, J. Cosmas, M. Bard, and Y.-H. Song, "Diversity Gain for DVB-H by Using Transmitter/Receiver Cyclic Delay Diversity," *IEEE Trans. on Broadcasting*, vol. 52, no. 4, pp. 464 –474, Dec. 2006.

[36] S. Alamouti, "A Simple Transmit Diversity Technique for Wireless Communications," *IEEE Journal on Selected Areas in Commun.*, vol. 16, no. 8, pp. 1451 –1458, Oct. 1998.

[37] V. Tarokh, N. Seshadri, and A. Calderbank, "Space-time Codes for High Data Rate Wireless Communication: Performance Criterion and Code Construction," *IEEE Trans. on Information Theory*, vol. 44, no. 2, pp. 744 –765, Mar. 1998.

[38] J.-C. Guey, M. Fitz, M. Bell, and W.-Y. Kuo, "Signal Design for Transmitter Diversity Wireless Communication Systems over Rayleigh Fading Channels," *IEEE Trans. on Commun.*, vol. 47, no. 4, pp. 527 –537, April 1999.

[39] S. Sandhu, R. Heath, and A. Paulraj, "Space-time Block Codes Versus Space-time Trellis Codes," in *in Proc. IEEE International Conference on Communications*, vol. 4, 2001, pp. 1132 –1136 vol.4.

[40] V. Tarokh, H. Jafarkhani, and A. Calderbank, "Space-time Block Codes from Orthogonal Designs," *IEEE Trans. on Information Theory*, vol. 45, no. 5, pp. 1456 –1467, July 1999.

[41] J. Tan and G. Stuber, "Multicarrier Delay Diversity Modulation for MIMO Systems," *IEEE Trans. on Wireless Commun.*, vol. 3, no. 5, pp. 1756 – 1763, Sept. 2004.

[42] A. Assalini, "Maximizing Outage Capacity of OFDM Transmit Diversity Systems," *IEEE Trans. on Vehi. Tech.*, vol. 58, no. 9, pp. 4786 –4794, Nov. 2009.

[43] G. Bauch and J. Malik, "Cyclic Delay Diversity with Bit-interleaved Coded Modulation in Orthogonal Frequency Division Multiple Access," *IEEE Trans. on Wireless Commun.*, vol. 5, no. 8, pp. 2092 –2100, Aug. 2006.

[44] G. Rangaraj, D. Jalihal, and K. Giridhar, "Exploiting Multipath Diversity in Multiple Antenna OFDM Systems with Spatially Correlated Channels," *IEEE Trans. on Vehi. Tech.*, vol. 54, no. 4, pp. 1372 – 1378, July 2005.

[45] C. Tepedelenlioglu and R. Challagulla, "Low-complexity Multipath Diversity Through Fractional Sampling in OFDM," *IEEE Trans. on Signal Processing*, vol. 52, no. 11, pp. 3104 – 3116, Nov. 2004.

[46] S. Haykin, *An Introduction to Analog and Digital Communications.* Wiley, 1989.

[47] A. Papoulis and S. Pillai, *Probability, Random Variables, and Stochastic Processes*, ser. McGraw-Hill electrical and electronic engineering series. McGraw-Hill, 2002.

[48] S. Thoen, L. Van der Perre, B. Gyselinckx, and M. Engels, "Performance Analysis of Combined Transmit-SC/Receive-MRC," *IEEE Trans. on Commun.*, vol. 49, no. 1, pp. 5 –8, Jan. 2001.

[49] R. Nakamura and Y. Sanada, "Experimental Investigation of IEEE802.11n Reception with Fractional Sampling," in *in Proc. IEEE International Symposium on Personal, Indoor and Mobile Radio Communications*, Sept. 2010, pp. 1044 –1048.

[50] H. N. T. Shinkai and Y. Sanada, "Improvement on Diversity Gain with Filter Bandwidth Enlargement in Fractional Sampling OFDM Receiver," *IEICE Trans. on Communication*, vol. E93-B, pp. 1526–1533, June 2010.

[51] T. Shinkai, H. Nishimura, M. Inamori, and Y. Sanada, "Effect of Baseband Filter Bandwidth in Fractional Sampling Orthogonal Frequency Division Multiplexing on Indoor Channel Model with Measured Impulse Responses," *IET Trans. on Commun.*, vol. 4, no. 16, pp. 1934 –1941, Nov. 2010.

[52] M. I. H. Nishimura and Y. Sanada, "Sampling Rate Selection for Fractional Sampling in OFDM," *IEICE Trans. on Communications*, vol. E91-B, pp. 2876–2882, 2008.

[53] Y. S. H. Nishimura, M. Inamori and M. Ghavami, "Precoded Transmit Path Diversity in FS-OFDM on UWB Channels," *submitted to Wireless Personal Communications.*

[54] ——, "Transmit Precoding Scheme for ICI Suppression and Path Diversity in FS-OFDM," in *the 8th International Symposium on Wireless Communication Systems, Aachen*, Nov. 2011.

[55] M. I. H. Nishimura and Y. Sanada, "Initial Sampling Point Selection in OFDM Receiver with Fractional Sampling," in *in Proc. International Workshop on Vision, Communications and Circuits*, Nov. 2008.

[56] K. Saito, T. Shinkai, H. Nishimura, and Y. Sanada, "Experiment Investigation of Sampling Point Selection in Fractional Sampling OFDM Receiver," in *in Proc. IEEE Pacific Rim Conf. Commun., Comput., and Signal Proces.*, Aug. 2009, pp. 820 –825.

[57] M. Win, R. Scholtz, and M. Barnes, "Ultra-wide Bandwidth Signal Propagation for Indoor Wireless Communications," in *in Proc. IEEE International Conference on Communications*, vol. 1, June 1997, pp. 56 –60 vol.1.

[58] M. Win and R. Scholtz, "Ultra-wide Bandwidth Time-hopping Spread-spectrum Impulse Radio for Wireless Multiple-access Communications," *IEEE Trans. on Commun.*, vol. 48, no. 4, pp. 679 –689, April 2000.

[59] ——, "Characterization of Ultra-wide Bandwidth Wireless Indoor Channels: A Communication-theoretic View," *IEEE Journal on Selected Areas in Commun.*, vol. 20, no. 9, pp. 1613 – 1627, Dec. 2002.

[60] K. Usuda, H. Zhang, and M. Nakagawa, "Pre-Rake Performance for Pulse Based UWB System in a Standardized UWB Short-range Channel," in *in Proc. IEEE Wireless Communications and Networking Conference 2004*, vol. 2, Mar. 2004, pp. 920 – 925 Vol.2.

[61] S. Zhao and H. Liu, "On the Optimum Linear Receiver for Impulse Radio Systems in the Presence of Pulse Overlapping," *IEEE Commun. Lett.*, vol. 9, no. 4, pp. 340 – 342, April 2005.

[62] ——, "Transmitter-Side Multipath Preprocessing for Pulsed UWB Systems Considering Pulse Overlapping and Narrow-Band Interference," *IEEE Trans. on Vehi. Tech.*, vol. 56, no. 6, pp. 3502 –3510, Nov. 2007.

[63] D. Reynolds, X. Wang, and K. Modi, "Interference Suppression and Diversity Exploitation for Multiantenna CDMA with Ultra-low Complexity Receivers," *IEEE Trans. on Signal Processing*, vol. 53, no. 8, pp. 3226 – 3237, Aug. 2005.

[64] H. Nishimura, M. Inamori, Y. Sanada, and M. Ghavami, "Non-uniform Sampling Point Selection in Orthogonal Frequency Division Multiplexing Receiver with Fractional Sampling," *IET Trans.on Commun.*, vol. 5, no. 4, pp. 554 –562, Mar. 2011.

[65] H. N. T. Kobayashi and Y. Sanada, "Sampling Point Selection Scheme for Fractional Sampling-OFDM Receivers on Fast Time-Varying Multipath Channels," *IEICE Trans. on Fundamentals*, vol. E93-A, pp. 2122–2129, 2010.

[66] M. Inamori, H. Nishimura, Y. Sanada, and M. Ghavami, "Correlated Noise Cancellation in Fractional Sampling Orthogonal Frequency and Code Division Multiplexing with Alternative Spreading Code," *IET Trans. on Commun.*, vol. 4, no. 10, pp. 1217 –1225, July 2010.

[67] I. Mitola, L., "Technical Challenges in the Globalization of Software Radio," *IEEE Commun. Mag.*, vol. 37, no. 2, pp. 84 –89, Feb. 1999.

[68] K. Muhammad, D. Leipold, B. Staszewski, Y.-C. Ho, C. Hung, K. Maggio, C. Fernando, T. Jung, J. Wallberg, J.-S. Koh, S. John, I. Deng, O. Moreira, R. Staszewski, R. Katz, and O. Friedman, "A Discrete-time Bluetooth Receiver in a 0.13 mu;m Digital CMOS Process," in *ISSCC Dig. Tech. Papers*, Feb. 2004, pp. 268 – 527 Vol.1.

[69] A. Matsuzawa, "Analog IC Technologies for Future Wireless Systems," *IEICE Trans. on Electron*, vol. 89-C, pp. 446–454, April 2006.

[70] S. Goto, T. Yamada, N. Takayama, and H. Yasuura, "A Design for a Low-power Digital Matched Filter Applicable to W-CDMA," in *Digital System Design, 2002. Proceedings. Euromicro Symposium*, Sept. 2002, pp. 210 – 217.

[71] J. Proakis, *Digital communications*, ser. McGraw-Hill series in electrical and computer engineering. McGraw-Hill, 2001. [Online]. Available: http://books.google.co.jp/books?id=aUp2QgAACAAJ

[72] *IEEE 802.11g-Part 11: Wireless LAN Medium Access Control (MAC) and Physical Layer (PHY) Specifications; Highspeed Physical Layer in the 2.4GHz Band.*, Std.

[73] M. Anderson, K. Norling, A. Dreyfert, and J. Yuan, "A Reconfigurable Pipelined ADC in 0.18 mu;m CMOS," in *2005 Symposium on VLSI Circuits Digest of Technical Papers*, June 2005, pp. 326 – 329.

[74] *Joint Technical Committee of Committee T1 R1P1.4 and TIA TR46.3.3/TR45.4.4 on Wireless Access, "Draft Final Report on RF Channel Characterization", Paper no. JTC(AIR)/94.01.17-238R4, Jan. 17, 1994.*

[75] A. Maltsev, R. Maslennikov, A. Sevastyanov, A. Lomayev, A. Khoryaev, A. Davydov, and V. Ssorin, "Characteristics of Indoor Millimeter-wave Channel at 60 GHz in Application to Perspective WLAN System," in *Antennas and Propagation (EuCAP), 2010 Proceedings of the Fourth European Conference on*, april 2010, pp. 1 –5.

[76] A. M. A. Davydov and A. Sadri, "Saleh-Valenzuela Channel Model Parameters for Library Environment," *IEEE document 802.15-06-0302-02-003c.*, July 2006.

[77] *IEEE 802.16e–Part 16: Air Interface for Fixed and Mobile Broadband Wireless Access Systems–Amendment for Physical and Medium Access Control Layers for Combined Fixed and Mobile Operation in Licensed Bands (Amendment and Corrigendum to IEEE Std 802.16-2004).*, Std.

[78] M. Inamori, N. Haruki, Y. Sanada, and M. Ghavami, "Fractional Sampling OFCDM with Alternative Spreading Code," in *in Proc. the 11th IEEE International Conference on Commun. Systems*, Nov. 2008, pp. 1394 –1398.

[79] *Multi-band OFDM Physical Layer Proposal for IEEE 802.15 Task Group 3a*, IEEE P802.15-04/0493r1 Std.

[80] A. Molisch, J. Foerster, and M. Pendergrass, "Channel Models for Ultrawideband Personal Area Networks," *IEEE Wireless Commun.*, vol. 10, no. 6, pp. 14 – 21, Dec. 2003.

[81] S. H. Han and J. H. Lee, "An overview of peak-to-average power ratio reduction techniques for multicarrier transmission," *IEEE Commun. Mag.*, vol. 12, no. 2, pp. 56 – 65, April 2005.

[82] H. Ochiai and H. Imai, "Performance Analysis of Deliberately Clipped OFDM Signals," *IEEE Trans. on Commun.*, vol. 50, no. 1, pp. 89 –101, Jan. 2002.

[83] C. Xiao, Y. Zheng, and N. Beaulieu, "Second-order Statistical Properties of the WSS Jakes' Fading Channel Simulator," *IEEE Trans. on Commun.*, vol. 50, no. 6, pp. 888 –891, June 2002.

[84] D. Brandwood, "A Complex Gradient Operator and its Application in Adaptive Array Theory," *IEE Proceedings - Part F: Commun., Radar and Signal Processing*, vol. 130, no. 1, pp. 11 –16, Feb. 1983.

List of Achievements

Journal Publications

1. H. Nishimura, M. Inamori, and Y. Sanada, "Sampling Rate Selection for Fractional Sampling in OFDM," IEICE Trans. on Communications, vol.E91-B, no.9, pp.2876-2882, Sept. 2008.

2. H. Nishimura, M. Inamori, Y. Sanada, and M. Ghavami, "Non-uniform Sampling Point Selection in OFDM Receiver with Fractional Sampling," IET Trans. on Communications, vol.5, iss.4, pp.554-562, April 2011.

3. H. Nishimura, M. Inamori, Y. Sanada, and M. Ghavami, "Precoded Transmit Path Diversity in FS-OFDM on UWB Channels," accepted to Wireless Personal Communications.

Other Journal Publications

1. M. Inamori, T. Kawai, T. Kobayashi, H. Nishimura, and Y. Sanada, "Effect of Pulse Shaping Filters on a Fractional Sampling OFDM System with Subcarrier-Based Maximal Ratio Combining," IEICE Trans. on Communication, vol.E92-B, no.5, pp.1484-1494, May 2009.

2. T. Shinkai, H. Nishimura, and Y. Sanada, "Improvement on Diversity Gain with Filter Bandwidth Enlargement in Fractional Sampling OFDM Receiver," IEICE Trans. on Communication, vol.E93-B, no.6, pp.1526-1533, June 2010.

3. M. Inamori, H. Nishimura, Y. Sanada, and M. Ghavami, "Correlated Noise Cancellation in Fractional Sampling OFCDM with Alternative Spreading Code," IET Communications, vol.4, Issue 10, pp.1217-1225, July 2010.

4. T. Kobayashi, H. Nishimura, and Y. Sanada, "Sampling Point Selection Scheme for Fractional Sampling-OFDM Receivers on Fast Time-Varying Multipath Channels," IEICE Trans. on Fundamentals, vol.E93-A, no.11, pp.2122-2129, Nov. 2010.

5. T. Shinkai, H. Nishimura, M. Inamori, and Y. Sanada, "Effect of Baseband Filter Bandwidth in Fractional Sampling OFDM on Indoor Channel Model with Measured Impulse Responses," IET Communications, vol.4, issue 16, pp.1934-1941, Nov. 2010.

Conference Publications

1. H. Nishimura, M. Inamori, and Y. Sanada, "Sampling Rate Selection for Fractional Sampling in OFDM," in Proc. the 18th Annual International Symposium on Personal Indoor and Mobile Radio Communications, Athens, Sept. 2007.

2. H. Nishimura, M. Inamori, and Y. Sanada, "Initial Sampling Point Selection in OFDM Receiver with Fractional Sampling," in Proc. International Workshop on Vision, Communications and Circuits, Xi'an, China, Nov. 2008.

3. H. Nishimura, M. Inamori, Y. Sanada, and M. Ghavami, "Non-uniform Sampling Point Selection in OFDM Receiver with Fractional Sampling," in Proc. 2009 IEEE Pacific Rim Conference on Communications, Computers and Signal Processing, pp.837-842, Victoria, Aug. 2009.

4. H. Nishimura, M. Inamori, Y. Sanada, and M. Ghavami "Precoded Transmit Path Diversity in FS-OFDM," in Proc. IEEE International Symposium on Access Spaces, Yokohama, June 2011.

5. H. Nishimura, M. Inamori, Y. Sanada, and M. Ghavami, "Transmit Precoding Scheme for ICI Suppression and Path Diversity in FS-OFDM," the 8th International Symposium on Wireless Communication Systems, Aachen, Nov. 2011.

Other Conference Publications

1. T. Kobayashi, H. Nishimura, and Y. Sanada, "MMSE Combining Scheme with Subblock Noise Covariance Matrix for Fractional Sampling-OFDM Receivers," in Proc. the 19th Annual International Symposium on Personal Indoor and Mobile Radio Communications, Cannes, France, Sept. 2008.

2. H. Higuchi, H. Nishimura, and Y. Sanada, "Antenna/Sampling Point Selection Algorithm in Fractional Sampling-MIMO-OFDM," in Proc. the Eleventh IEEE International Conference on Communications Systems, pp.411-416, Guangzhou, China, Nov. 2008.

3. T. Shinkai, H. Nishimura, M. Inamori, and Y. Sanada, "Experimental Investigation of Fractional Sampling in IEEE802.11a WLAN System," in Proc. the

Eleventh IEEE International Conference on Communications Systems, pp.1368-1373, Guangzhou, China, Nov. 2008.

4. M. Inamori, H. Nishimura, Y. Sanada, and M. Ghavami, "Fractional Sampling OFCDM with Alternative Spreading Code," in Proc. the Eleventh IEEE International Conference on Communications Systems, pp.1394-1398, Guangzhou, China, Nov. 2008.

5. M. Inamori, T. Kawai, T. Kobayashi, H. Nishimura, and Y. Sanada, "Effect of Frobenius Norm of Whitening Matrix on Fractional Sampling OFDM with Subcarrier-Based Maximal Ratio Combining," in Proc. the 2009 RISP International Workshop on Nonlinear Circuits and Signal Processing, Hawaii, U.S.A., March 2009.

6. K. Saito, T. Shinkai, H. Nishimura, and Y. Sanada, "Experiment Investigation of Sampling Point Selection in Fractional Sampling OFDM Receiver," in Proc. 2009 IEEE Pacific Rim Conference on Communications, Computers and Signal Processing, pp.820-825, Victoria, Aug. 2009.

7. T. Shinkai, H. Nishimura, and Y. Sanada, "Improvement on Diversity Gain with Filter Bandwidth Expansion in Fractional Sampling OFDM Receiver," in Proc. 2009 IEEE Pacific Rim Conference on Communications, Computers and Signal Processing, pp.832-836, Victoria, Aug. 2009.

8. M. Inamori, T. Kawai, T. Kobayashi, H. Nishimura, and Y. Sanada, "Metric Weighting Scheme on a Coded Fractional Sampling OFDM System," in Proc. the 70th IEEE Vehicular Technology Conference, Anchorage, U.S.A., Sept. 2009.

9. T. Kobayashi, H. Nishimura, and Y. Sanada, "Sampling Point Selection Scheme for Fractional Sampling-OFDM Receivers on Fast Time-Varying Multipath Channels," in Proc. the 72th IEEE Vehicular Technology Conference, Ottawa, Sept. 2010.

10. E. Sakai, H. Nishimura, M. Inamori, Y. Sanada, and M. Ghavami, "Low-Complexity Sampling Point Selection in OFDM Receiver with Fractional Sampling," in Proc. 2010 International Symposium on Information Theory and its Applications & 2010 International Symposium on Spread Spectrum Techniques and Applications, pp.662-667, Taiwan, Oct. 2010.

11. H. Osada, H. Nishimura, M. Inamori, and Y. Sanada, "Adjacent Channel Interference Cancelation in Fractional Sampling OFDM Receiver," accepted to the 74th IEEE Vehicular Technology Conference, San Francisco, Sept. 2011.

Technical Reports

1. H. Nishimura, M. Inamori, Y. Sanada, "Sampling Rate Selection for Fractional Sampling in OFDM," Technical Reports of IEICE, SR2007-1, May 2007.

2. H. Nishimura, M. Inamori, Y. Sanada, "Sampling Rate Selection for Fractional Sampling in OFDM," Japan Society for Simulation Technology Conference, 11-1, June 2007.

3. H. Nishimura, M. Inamori, Y. Sanada, "Sampling Point Selection in OFDM Receiver with Fractional Sampling," Technical Reports of IEICE, SR2007-87, March 2008.

4. H. Nishimura, M. Inamori, Y. Sanada, "Sampling Point Selection in OFDM Receiver with Fractional Sampling," IEICE General Conference, BS-1-10, March 2008.

5. H. Nishimura, M. Inamori, Y. Sanada, M. Ghavami, "Non-uniform Sampling Point Selection in OFDM Receiver with Fractional Sampling," Technical Reports of IEICE, SR2008-41, Oct. 2008.

6. H. Nishimura, M. Inamori, Y. Sanada, "Complexity Reduction Scheme for Sampling Point Selection in Fractional Sampling OFDM Receiver," IEICE General Conference, B-17-23, March 2009.

7. H. Nishimura, M. Inamori, Y. Sanada, M. Ghavami, "Precoded transmit Path Diversity in FS-OFDM," Technical Reports of IEICE, CS2009-134, March 2010.

8. H. Nishimura, M. Inamori, Y. Sanada, M. Ghavami, "Performance of Precoded Transmit Path Diversity in FS-OFDM on Indoor Channels," Technical Reports of IEICE, SR2010-2, May 2010.

9. H. Nishimura, M. Inamori, Y. Sanada, M. Ghavami, "Transmit Precoding Scheme for ICI Suppression and Path Diversity in FS-OFDM ," Technical Reports of IEICE, WBS2011-2, May 2011.

Other Technical Reports

1. H. Higuchi, H. Nishimura, Y. Sanada, "Antenna/Sampling Point Selection Algorithm in Fractional Sampling-MIMO-OFDM," Technical Reports of IEICE, SR2008-6, May 2008.

2. M. Inamori, H. Nishimura, Y. Sanada, "Alternative Spreading Code for Fractional Sampling OFCDM," Technical Reports of IEICE, SR2008-12, May 2008.

3. H. Higuchi, H. Nishimura, Y. Sanada, "Antenna/Sampling Point Selection Algorithm in Fractional Sampling-MIMO-OFDM," Japan Society for Simulation Technology Conference, 6-14, June 2008.

4. T. Kobayashi, H. Nishimura, Y. Sanada, ""MMSE Combining Scheme with Subblock Noise Covariance Matrix for Fractional Sampling-OFDM Receivers," Technical Reports of IEICE, SR2008-13, May 2008.

5. T. Shinkai, H. Nishimura, M. Inamori, Y. Sanada, "Experimental Investigation of Fractional Sampling in IEEE802.11a WLAN System," Technical Reports of IEICE, SR2008-28, July 2008.

6. M. Inamori, T. Kawai, T. Kobayashi, H. Nishimura, Y. Sanada, "Effect of pulse shaping filters on fractional sampling OFDM systems with subcarrierbased maximal ratio combining," Technical Reports of IEICE, SR2008-42, Oct. 2008.

7. T. Shinkai, H. Nishimura, Y. Sanada, "Improvement on Diversity Gain with Filter Bandwidth Expansion in Fractional Sampling OFDM Receiver," Technical Reports of IEICE, SR2008-76, Jan. 2009.

8. M. Inamori, K. Takashi, T. Kobayashi, H. Nishimura, Y. Sanada, "Metric Weighting Scheme on a Fractional Sampling Coded OFDM System with Subcarrier-Based Maximal Ratio Combining," IEICE General Conference, B-17-22, March 2009.

9. K. Saito, T. Shinkai, H. Nishimura, Y. Sanada, "Experiment Investigation of Sampling Point Selection in Fractional Sampling OFDM Receiver," Technical Reports of IEICE, SR2009-22, July 2009.

10. M. Inamori, H. Nishimura, Y. Sanada, "Performance Evaluation of Fractional Sampling OFCDM System with Alternative Spreading Code in Multiuser Environment," Technical Reports of IEICE, SR2009-56, Oct. 2009.

11. E. Sakai, H. Nishimura, M. Inamori, Y. Sanada, M. Ghavami, "Low-Complexity Sampling Point Selection in OFDM Reciever with Fractional Sampling," Technical Reports of IEICE, SR2010-1, May 2010.

12. H. Osada, H. Nishimura, M. Inamori, Y. Sanada, "Adjacent Channel Interference Cancelation in Fractional Sampling OFDM Receiver," Technical Reports of IEICE, SR2010-94, March 2011.

Appendix
Correlation of Noise Samples

Correlation of Noise Samples

In this subsection, the effect of noise-whitening on the received signal is investigated. From Eq. (2.15), all the received signals on N subcarriers are expressed as

$$\mathbf{Y} = \mathbf{HS} + \mathbf{V} \tag{A-1}$$

where

$$\begin{aligned} \mathbf{Y} &= [\mathbf{Y}^T[0], \ldots, \mathbf{Y}^T[N-1]]^T, && \text{(A-2)} \\ \mathbf{H} &= \text{diag}[\mathbf{H}[0], \ldots, \mathbf{H}[N-1]], && \text{(A-3)} \\ \mathbf{S} &= [S[0], \ldots, S[N-1]]^T, && \text{(A-4)} \\ \mathbf{V} &= [\mathbf{V}^T[0], \ldots, \mathbf{V}^T[N-1]]^T. && \text{(A-5)} \end{aligned}$$

Noise vector $\mathbf{V}$ is the colored noise and expressed as

$$\mathbf{w} = \mathbf{R}_w^{\frac{1}{2}} \boldsymbol{\omega} \tag{A-6}$$

where $\mathbf{R}_w$ is the noise correlation matrix and $\boldsymbol{\omega}$ is the white noise in vector form given as follows.

$$\begin{aligned} \boldsymbol{\omega} &= [\boldsymbol{\omega}^T[0], \ldots, \boldsymbol{\omega}^T[N-1]]^T, && \text{(A-7)} \\ \boldsymbol{\omega}[k] &= [\omega_0[k], \ldots, \omega_{G-1}[k]]^T. && \text{(A-8)} \end{aligned}$$

where $\omega_g[k]$ is the gth white noise on the kth subcarrier. Through noise-whitening in Eq. (2.26), Eq. (A-1) is converted to the following equation.

$$\mathbf{R}_{ww}\mathbf{Y} = \mathbf{R}_{ww}\mathbf{HS} + \mathbf{R}_{ww}\mathbf{V} \tag{A-9}$$

where $\mathbf{R}_{ww} = \text{diag}[\mathbf{R}_w^{-\frac{1}{2}}[0], \ldots, \mathbf{R}_w^{-\frac{1}{2}}[N-1]]$. As a result, Eq. (A-9) is expressed as

$$\mathbf{Y}' = \mathbf{H}'\mathbf{S} + \mathbf{V}'. \tag{A-10}$$

where

$$\begin{aligned}\mathbf{Y}^{'} &= \mathbf{R}_{ww}\mathbf{Y} \\ &= [\mathbf{Y}^{'T}[0],\ldots,\mathbf{Y}^{'T}[N-1]]^T \qquad \text{(A-11)} \\ \mathbf{H}^{'} &= \mathbf{R}_{ww}\mathbf{H} \\ &= [\mathbf{H}^{'}[0],\ldots,\mathbf{H}^{'}[N-1]] \qquad \text{(A-12)}\end{aligned}$$

$$\begin{aligned}\mathbf{V}^{'} &= [\mathbf{V}^{'}[0],\ldots,\mathbf{V}^{'}[N-1]]^T \\ &= \mathbf{R}_{ww}\mathbf{V} \\ &= \mathbf{R}_{ww}\mathbf{R}_w^{\frac{1}{2}}\boldsymbol{\omega} \\ &= \begin{bmatrix} \mathbf{I}_G & \mathbf{R}_n[0,1] & \ldots & \mathbf{R}_n[0,N-1] \\ \mathbf{R}_n[1,0] & \mathbf{I}_G & \ddots & \vdots \\ \vdots & \ddots & \ddots & \vdots \\ \mathbf{R}_n[N-1,0] & \ldots & \ldots & \mathbf{I}_G \end{bmatrix} \\ &\times \begin{bmatrix} \boldsymbol{\omega}[0] \\ \boldsymbol{\omega}[1] \\ \vdots \\ \boldsymbol{\omega}[N-1] \end{bmatrix} \qquad \text{(A-13)}\end{aligned}$$

where $\mathbf{R}_n[k_1,k_2]$ is a $G\times G$ matrix. It corresponds to the (k_1,k_2)th subblock of the $NG\times NG$ matrix and is expressed as $\mathbf{R}_{ww}\mathbf{R}_w^{\frac{1}{2}}$. The g_1th element of $\mathbf{V}^{'}[k_1]$ is expressed as follows.

$$\begin{aligned}\mathbf{V}^{'}_{g_1}[k_1] &= \sum_{k_2=0}^{N-1}\sum_{g_2=0}^{G-1}\mathbf{R}_n[k_1,k_2]_{g_1,g_2}\omega_{g_2}[k_2] \\ &= \omega_{g_1}[k_1] + \sum_{\substack{k_2=0 \\ k_2\neq k_1}}\sum_{g_2=0}^{G-1}\mathbf{R}_n[k_1,k_2]_{g_1,g_2}\omega_{g_2}[k_2]\end{aligned} \qquad \text{(A-14)}$$

where $[\mathbf{R}_n[k_1,k_2]]_{g1,g2}$ is the (g_1,g_2)th component of $\mathbf{R}_n[k_1,k_2]$. The second term of this equation represents the noise intruded from the others subcarriers after noise-whitening. This component deteriorates the BER performance in the receiver.

To improve the BER performance, the Frobenius norm of $\mathbf{R}_n[k_1,k_2]$ must be kept small. From Eq. (A-13), $\mathbf{R}_n[k_1,k_2]$ is given as

$$\mathbf{R}_n[k_1,k_2] = \mathbf{R}_w^{-\frac{1}{2}}[k_1]\mathbf{R}_w^{\frac{1}{2}}[k_1,k_2] \qquad \text{(A-15)}$$

where $\mathbf{R}_w^{\frac{1}{2}}[k_1,k_2]$ is the (k_1,k_2)th subblock of $\mathbf{R}_w^{\frac{1}{2}}$.

Appendix
Solution of Eq. (3.61)

Proof of Eq. (3.56)

$$
\begin{aligned}
& \mathrm{E} \parallel \mathbf{S} - \left(\mathbf{A}\mathbf{R}\mathbf{W}_p\mathbf{A}^H\mathbf{S} + \mathbf{V}\right) \parallel^2 \\
= \; & \mathrm{E}\left[\left(\mathbf{S} - \left(\mathbf{A}\mathbf{R}\mathbf{W}_p\mathbf{A}^H\mathbf{S} + \mathbf{V}\right)\right)^H \left(\mathbf{S} - \left(\mathbf{A}\mathbf{R}\mathbf{W}_p\mathbf{A}^H\mathbf{S} + \mathbf{V}\right)\right)\right] \\
= \; & \mathrm{E}\left[\left(\mathbf{S}^H - \mathbf{S}^H\mathbf{A}\mathbf{W}_p^H\mathbf{R}^H\mathbf{A}^H - \mathbf{V}^H\right)\left(\mathbf{S} - \mathbf{A}\mathbf{R}\mathbf{W}_p\mathbf{A}^H\mathbf{S} - \mathbf{V}\right)\right] \\
= \; & \mathrm{E}\left[\mathbf{S}^H\mathbf{S} - \mathbf{S}^H\mathbf{A}\mathbf{R}\mathbf{W}_p\mathbf{A}^H\mathbf{S} - \mathbf{S}^H\mathbf{V}\right. \\
- \; & \mathbf{S}^H\mathbf{A}\mathbf{W}_p^H\mathbf{R}^H\mathbf{A}^H\mathbf{S} + \mathbf{S}^H\mathbf{A}\mathbf{W}_p^H\mathbf{R}^H\mathbf{A}^H\mathbf{A}\mathbf{R}\mathbf{W}_p\mathbf{A}^H\mathbf{S} \\
+ \; & \left.\mathbf{S}^H\mathbf{A}\mathbf{W}_p^H\mathbf{R}^H\mathbf{A}^H\mathbf{V} - \mathbf{V}^H\mathbf{S} + \mathbf{V}^H\mathbf{A}\mathbf{R}\mathbf{W}_p\mathbf{A}^H\mathbf{S} + \mathbf{V}^H\mathbf{V}\right]. \qquad \text{(A-1)}
\end{aligned}
$$

By using

$$
\begin{aligned}
\mathrm{E}\left[\mathbf{S}^H\mathbf{S}\right] &= N\sigma_s^2 && \text{(A-2)} \\
\mathrm{E}\left[\mathbf{S}^H\mathbf{X}\mathbf{S}\right] &= N\sigma_s^2 \cdot \mathrm{tr}\left(\mathbf{X}\right) && \text{(A-3)} \\
\mathrm{E}\left[\mathbf{V}^H\mathbf{X}\right] &= 0 && \text{(A-4)} \\
\mathrm{E}\left[\mathbf{X}^H\mathbf{V}\right] &= 0 && \text{(A-5)} \\
\mathrm{E}\left[\mathbf{V}^H\mathbf{V}\right] &= N\sigma_v^2 && \text{(A-6)}
\end{aligned}
$$

where $\mathbf{X}$ is an arbitrary vector of size $N \times 1$. The expected value of Eq. (A-1) in terms of $\mathbf{S}$ and $\mathbf{V}$ can be expressed as

$$
N\sigma_s^2 \cdot (1 - F_1 - F_2 + F_3) + N\sigma_v^2. \qquad \text{(A-7)}
$$

Solution of Eq. (3.61)

In this section, the following three formulas are used for the proof of the solution.

FORMULAS

$$\mathrm{tr}\left\{\mathbf{ABCD}\right\} = \mathrm{vec}\left(\mathbf{A}^H\right)^H \left(\mathbf{D}^H \otimes \mathbf{B}\right) \mathrm{vec}\left(\mathbf{C}\right) \tag{A-8}$$

$$\mathrm{tr}\left\{\mathbf{A}^H\mathbf{B}\right\} = \mathrm{vec}\left(\mathbf{A}\right)^H \mathrm{vec}\left(\mathbf{B}\right) \tag{A-9}$$

$$\mathrm{tr}\left\{\mathbf{ABC}\right\} = \left(\mathbf{C}^T \otimes \mathbf{A}\right) \mathrm{vec}\left(\mathbf{B}\right) \tag{A-10}$$

By using Eq. (A-8), F_1 can be expressed as (A-10)

$$F_1 = \left(\mathbf{A}^H \otimes \mathbf{AR}\right) \mathrm{vec}\left(\mathbf{W}_p\right). \tag{A-11}$$

Then,

$$\frac{\partial F_1}{\partial \mathbf{W}_p^*} = \mathbf{0}. \tag{A-12}$$

Using Eq. (A-9)

$$F_2 = \mathrm{vec}\left(\mathbf{W}_p\mathbf{A}^H\right)^H \mathrm{vec}\left(\mathbf{R}^H\mathbf{A}^H\right) \tag{A-13}$$

and using Eq. (A-10)

$$\begin{aligned} F_2 &= \left[\left\{\left(\mathbf{A}^H\right)^T \otimes \mathbf{I}\right\} \mathrm{vec}\left(\mathbf{W}_p\right)\right]^H \mathrm{vec}\left(\mathbf{R}^H\mathbf{A}^H\right) \\ &= \mathrm{vec}\left(\mathbf{W}_p\right)^H \left(\mathbf{A}^T \otimes \mathbf{I}\right) \mathrm{vec}\left(\mathbf{R}^H\mathbf{A}^H\right) \qquad \text{(A-14)} \\ &= \mathrm{vec}\left(\mathbf{W}_p\right)^H \mathrm{vec}\left(\mathbf{R}^H\mathbf{A}^H\mathbf{A}\right). \qquad \text{(A-15)} \end{aligned}$$

Then,

$$\frac{\partial F_2}{\partial \mathbf{W}_p^*} = \mathbf{R}^H\mathbf{A}^H\mathbf{A}. \tag{A-16}$$

F_3 can be expressed in the same way as F_2. By using Eqs. (A-9) and (A-10),

$$\begin{aligned} F_3 &= \mathrm{tr}\left\{\mathbf{A}\mathbf{W}_p^H\mathbf{R}^H\mathbf{A}^H\mathbf{ARW}_p\mathbf{A}^H\right\} \\ &= \mathrm{vec}\left(\mathbf{W}_p\mathbf{A}^H\right)^H \mathrm{vec}\left(\mathbf{R}^H\mathbf{A}^H\mathbf{ARW}_p\mathbf{A}^H\right) \\ &= \left[\left\{\left(\mathbf{A}^H\right)^T \otimes \mathbf{I}\right\} \mathrm{vec}\left(\mathbf{W}_p\right)\right]^H \mathrm{vec}\left(\mathbf{R}^H\mathbf{A}^H\mathbf{ARW}_p\mathbf{A}^H\right) \\ &= \mathrm{vec}\left(\mathbf{W}_p\right)^H \left(\mathbf{A}^T \otimes \mathbf{I}\right) \mathrm{vec}\left(\mathbf{R}^H\mathbf{A}^H\mathbf{ARW}_p\mathbf{A}^H\right) \\ &= \mathrm{vec}\left(\mathbf{W}_p\right)^H \mathrm{vec}\left(\mathbf{R}^H\mathbf{A}^H\mathbf{ARW}_p\mathbf{A}^H\mathbf{A}\right) \qquad \text{(A-17)} \end{aligned}$$

Then,

$$\frac{\partial F_3}{\partial \mathbf{W}_p^*} = \mathbf{R}^H \mathbf{A}^H \mathbf{A} \mathbf{R} \mathbf{W}_p \mathbf{A}^H. \tag{A-18}$$

From Eqs. (A-12), (A-16) and (A-18), Eq. (3.61) is expressed as

$$-\mathbf{0} - \mathbf{R}^H \mathbf{A}^H \mathbf{A} + \mathbf{R}^H \mathbf{A}^H \mathbf{A} \mathbf{R} \mathbf{W}_p \mathbf{A}^H \mathbf{A} = \mathbf{0} \tag{A-19}$$

$$\mathbf{W}_p = \mathbf{R}^{-1} \left(\mathbf{A}^H \mathbf{A}\right)^\dagger \left(\mathbf{A}^H \mathbf{A}\right) \left(\mathbf{A}^H \mathbf{A}\right)^\dagger \tag{A-20}$$

Acknowledgements

First, I must express my deep gratitude to my supervisor Prof. Yukitoshi Sanada for his patient instruction and encouragement throughout my research in Sanada Laboratory. Without his support, I could not yield any achievement and complete my dissertation.

I would like to express my gratitude for the referees who examined this dissertation, Prof. Sasase, Prof. Ohtsuki, Prof. Ishikuro and Prof. Ghavami. Their critical review and constructive suggestions added an extra layer of polish to this dissertation. Prof. Ghavami is my second supervisor, who has supported and given constructive advises throughout research collaboration. Thank you very much.

I am also very grateful to my colleagues in Sanada Laboratory. They are Prof. Inamori, Dr. Kizilirmak, Dr. Zhang, and so on. I really appreciate their advice about my research.

Furthermore, I would like to appreciate the financial support from the Global Center of Excellence (GCOE) for High-Level Global Cooperation for Leading-Edge Platform on Access Spaces from the Ministry of Education, Culture, Sport, Science, and Technology in Japan. With the support from GCOE, I could visit United Kingdom to do research collaboration with Prof. Ghavami.

Finally, I would like to express my deep gratitude and love to my family and friends for their understanding and support throughout my life.